Characterization and Simulation of Localized States in Optical Structures

A. Sopaheluwakan

Characterization and Simulation of Localized States in Optical Structures

Ardhasena Sopaheluwakan

ISBN 90-365-2447-4

Characterization and Simulation of Localized States in Optical Structures

Characterization and simulation of localized states in optical structures
|| Ph.D. thesis, University of Twente, The Netherlands
|| Ardhasena Sopaheluwakan

The research presented in this thesis was carried out at the group of Applied Analysis and Mathematical Physics, Faculty of Electrical Engineering, Mathematics and Computer Science, and at the MESA+ Institute for Nanotechnology, University of Twente, Enschede, The Netherlands.
The research was funded by the Extended Programme in Applied Mathematics-Industrial Mathematics of KNAW (Royal Dutch Academy of Arts and Sciences), The Netherlands.

Samenstelling promitiecommissie:

Voorzitter en secretaris:	
Prof. dr. ir. A.J. Mouthaan	University of Twente
Promotor:	
Prof. dr. ir. E.W.C van Groesen	University of Twente
Leden:	
Dr. Andonowati	Institut Teknologi Bandung
Prof. dr. K.J. Boller	University of Twente
Prof. dr. ir. E.R. Fledderus	Technische Universiteit Eindhoven
Dr. H.J.W.M. Hoekstra	University of Twente
Prof. dr. Y.H. Lee	Korean Advanced Institute of Science & Technology
Dr. R. Stoffer	University of Twente

Cover design by A. Sopaheluwakan & Aditya K. Jati.
Printed by Wohrmann Print Service, The Netherlands.

email: a.sopaheluwakan@alumnus.utwente.nl

ISBN 90-365-2447-4

CHARACTERIZATION AND SIMULATION OF LOCALIZED STATES IN OPTICAL STRUCTURES

PROEFSCHRIFT

ter verkrijging van
de graad van doctor aan de Universiteit Twente,
op gezag van de rector magnificus,
prof. dr. W.H.M. Zijm,
volgens besluit van het College van Promoties
in het openbaar te verdedigen
op donderdag 14 december 2006 om 15.00 uur

door

Ardhasena Sopaheluwakan
geboren op 1 februari 1976
te Jakarta, Indonesië

Dit proefschrift is goedgekeurd door de promotor
prof. dr. ir. E.W.C. van Groesen

this thesis is dedicated
to my *father* and *mother*
and to my *beloved wife*

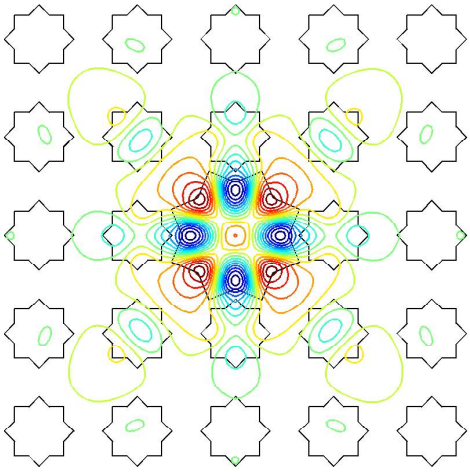

with the power and skill did We construct the firmament,
for it is We who create the vastness of space.
(Q.S. 51:47)

Contents

1 Introduction **1**
1.1 General perspective 1
1.2 Maxwell equations 2
1.3 Boundary conditions for optical problems 4
1.3.1 Transparent-influx boundary conditions 5
1.3.2 1D transmission problem 7
1.3.3 1D resonant modes 8
1.3.4 1D radiation modes 10
1.3.5 1D standing state 11
1.3.6 Integral expressions 12
1.4 Thesis outline 14
Bibliography 21

2 Finite element method and Transparent Influx Boundary Condition **23**
2.1 Variational formulation and FEM 23
2.2 DtN operators for a half space 26
2.3 DtN operators for a square 27
2.4 Implementation of the DtN operators in the FEM scheme . 28
Bibliography 31

3 Extremal characterization of band gaps in nonlinear gratings **33**
3.1 Introduction 33
3.2 Extremal characterization at normal incidence 34

3.2.1 Shift-skew symmetry of Edge states 34
3.2.2 Variational formulation 35
3.3 Oblique incidence and omni-directional band gap 38
3.3.1 Monotonicity for oblique incidence 39
3.3.2 Omni-directional band gap 40
3.4 Approximate and numerical results 41
3.4.1 Approximate field functions 42
3.4.2 FEM calculations 44
3.5 Conclusion and remarks 46
Bibliography 49

4 Direct characterization of states and modes in defect grating structures 51
4.1 Introduction 51
4.2 Optical characterization of gratings 55
4.2.1 The Optical Transfer Matrix 55
4.2.2 Grating properties 56
4.2.3 Effective Boundary conditions 59
4.2.4 States and modes 61
4.3 Defect states in grating structures 63
4.3.1 Defect states between half-infinite gratings 63
4.3.2 States for a single finite grating 65
4.3.3 States in a defect grating 66
4.4 Defect modes 67
4.4.1 Defect mode decomposed into defect states 68
4.4.2 Defect mode as superposition of defect states 68
4.5 Remarks and conclusions 71
Bibliography 74

5 Pulse loading and radiative unloading of an optical defect grating structure: low dimensional modeling and numerical simulations 75
5.1 Introduction 75
5.2 Finite Element Time Domain calculation 77
5.2.1 Wave equation, weak formulation 77
5.2.2 Space discretization of the weak formulation, FEM . 78
5.2.3 Time integration 79
5.2.4 Example 79

5.3 Defect states and leaky modes 83
5.3.1 Defect states 84
5.3.2 Leaky modes 87
5.4 Unloading and pulse loading 90
5.5 Comparison of the low dimensional model with the FETD calculation 92
5.6 Conclusion 93
Bibliography 96

6 Characterization and calculation of leaky modes in photonic crystal microcavities 97
6.1 Introduction 97
6.2 Computational approach 98
6.3 Plane wave excitation 101
6.4 Pulse excitation 103
6.5 Variational formulation for leaky modes 106
6.6 Calculating the quality factor of leaky modes 111
6.7 Conclusion 112
Bibliography 116

7 Conclusions and recommendations 117

Summary 121

Samenvatting 123

Acknowledgements 125

List of publications 127

About the author 129

Chapter

1

Introduction

1.1 General perspective

In the modern day of communication systems, electromagnetic waves play an important role. Since the invention of lasers in the 1960s as coherent light sources [1], and low loss optical fibers in the 1970s [2], optical communication and information systems have developed rapidly. Nowadays the operation of communication devices in these systems rely on electronics and photonics. For long distance communication, links between two communication nodes are mostly served by optical fibers, which carry the information via light propagation. In a communication network, these links of optical fibres are connected to nodes, where the information is routed to its designated destination. This information routing is still being done by electrical devices, but this is predicted to break down since the demand for telecommunication services is increasing exponentially. Therefore devices that can replace the routing function of the electronic devices are very much needed. One way to do, is to go via all optical processing.

One type of structure, that can serve as basic building block for optical devices is the Photonic Crystal (PC). Generally speaking, a PC is a structure of periodically arranged dielectric material. Since the photonic crystal concept was introduced for the first time [3, 4], there has been a growing interest in developing electromagnetic crystal materials. Their amazing feature is the ability of blocking the propagation of light or electromagnetic waves in a certain range of frequency. This range of frequency is called the Photonic Band Gap (PBG), analogous to the electronic band gap that is present in semiconductors. In the PBG light can not propagate

due to destructive interference of diffracted waves through the crystal.

The existence of such a PBG offers the possibility of designing many different kinds of integrated optical devices. The construction of integrated optical circuits would enable the revolutionary shift from optoelectronic to photonic technology to take place [5]. However to make the photonic crystal useful for application, we must introduce defects in the structure. There are a lot of applications already made with photonic crystals, such as waveguides with low losses [6, 7, 8, 9, 10, 11, 12], resonators and filters [13, 14, 15, 16, 17, 18]. Another application is that with 3D photonic crystal structures, mostly thin slabs, it is possible to make lasers [19, 20, 21, 22, 23] from photonic crystal point defect structures.

These individual devices have to be integrated in a circuit to be able to function as a unit. In [24, 25, 26, 27], authors have proposed ultrasmall and high-density photonic integrated circuits that combine light emitters, waveguides and functional devices based on the photonic crystal concept.

Of the above mentioned individual devices, resonators structures are in the heart of the complete functionality. Optical resonators are generally structures where a build up of electromagnetic energy can occur. Usually, it is build from components which have two essential functions, which are the cavity, where the energy will be stored in its vicinity, and a 'mirror' function where it functions to retain the energy inside the structure.

In this thesis two types of optical resonator will be studied. The first is the so-called defect grating structure. This structure is a one dimensional system of layered dielectric material. The second one is the so-called photonic crystal microcavity. The structure consists of arrays of dielectric rods placed in air. One of the rods has a different diameter, and this serves as the cavity for the structure.

1.2 Maxwell equations

The field of optics has made enormous progress from the time of Huygens in the 17^{th} century until Maxwell in the 1860s. It was Maxwell who unified Ampere's Law and Faraday's Law into one unified theory for electromagnetic phenomena. In their differential form, the Maxwell equations are the

following

$$\nabla \times \mathbf{E} = -\frac{\partial \mathbf{B}}{\partial t} \tag{1.1}$$

$$\nabla \times \mathbf{H} = \frac{\partial \mathbf{D}}{\partial t} + \mathbf{J} \tag{1.2}$$

$$\nabla \cdot \mathbf{D} = \rho \tag{1.3}$$

$$\nabla \cdot \mathbf{B} = 0 \tag{1.4}$$

where the symbols $\mathbf{E}$ and $\mathbf{H}$, are the electric and magnetic field, $\mathbf{B}$ and $\mathbf{D}$ are the magnetic and electric flux density, $\mathbf{J}$ is the electric current density and ρ is the electric charge density. These equations can be simplified for the case of electromagnetic field propagation in dielectric materials. Photonic crystals which we will study are composite material of different homogeneous dielectric materials, and there are no free charges or currents, therefore $\mathbf{J} = \rho = 0$.

Further we assume that the materials are linear and isotropic, hence the electric field and the electric flux density satisfies the constitutive relation $\mathbf{D} = \varepsilon \mathbf{E}$, where ε is the permittivity. A similar constitutive relation exist between the magnetic flux density and the magnetic field, $\mathbf{B} = \mu_0 \mu_r \mathbf{H}$, where μ_0 and μ_r are the free-space and relative permeability respectively. For dielectric materials which we consider in this thesis, the relative permeability is very close to unity, hence we have $\mathbf{B} = \mu_0 \mathbf{H}$. We also assumed that the dielectric materials are nondispersive, and lossless, hence the relative permittivity is a real number. The relative permittivity will be denoted by $\varepsilon_r = n^2$, where n is called the refractive index.

In this thesis we only consider problems in one and two dimensions (i.e. for structures with uniform properties in the other two and one space dimension respectively), and restrict ourselves to the discussion of transverse electric (TE) polarized wave. For this polarization, the electric field vector is perpendicular to the propagation direction. In one and two dimensions, the electric and magnetic field vector of TE waves have the following forms

$$\mathbf{E} = [0, E(z), 0]\,; \quad \mathbf{H} = [H_x(z), 0, 0]$$

and

$$\mathbf{E} = [0, E(x, z), 0]\,; \quad \mathbf{H} = [H_x(x, z), 0, H_z(x, z)]\,.$$

Within this restriction, the Maxwell equations reduce to scalar wave equation for the principal component $E(x, z)$

$$\Delta E(x, z) - \frac{n^2(x, z)}{c^2} \partial_t^2 E = 0 \tag{1.5}$$

where $c = 1/\sqrt{\varepsilon_0 \mu_0}$ is the speed of light in free-space. Throughout this thesis we normalized the space and time variable with the following scaling

$$(\tilde{x}, \tilde{z}) = \frac{(x, z)}{\lambda_0} \quad \text{and} \quad \tilde{t} = \frac{t \cdot c}{\lambda_0}$$

where λ_0 is the wavelength of light in free-space. With this normalization, the wave equation (1.5) simplifies to

$$\Delta E(\tilde{x}, \tilde{z}) - n^2(\tilde{x}, \tilde{z}) \partial_{\tilde{t}}^2 E = 0. \tag{1.6}$$

For simplicity of writing, we will omit the $\tilde{}$ sign from the variables in further derivations. Next we restrict solutions for the wave equation (1.6) to a class of bounded functions where the dependence on the spatial and temporal variable is assumed to be separated. So, looking for solutions in the form of $E(x, z, t) = u(x, z)T(t)$, the function $u(x, z)$ should satisfy

$$\Delta u + \omega^2 n^2(x, z) u = 0 \tag{1.7}$$

and $T(t) = e^{\pm i\omega t}$. The equation (1.7) is called the Helmholtz equation, and the function $T(t)$ is often referred as harmonic time dependence. The parameter ω is called the frequency, and throughout this thesis we choose the time dependence in the form of $e^{-i\omega t}$.

Problems on optical devices that are considered in this thesis are governed by the Helmholtz equation. In principal these problems are modelled in an unbounded domain, but often it is desirable to study the performance of the device in a bounded domain, e.g. for computational purposes. Then it is important to have boundary conditions that replace the physical effect of the exterior of the domain. In the following Section we will describe various boundary conditions for the problems that are considered in this thesis.

1.3 Boundary conditions for optical problems

A basic setup for an optical experiment in real life consists of two essential parts. First is the optical structure, and second is the light source that

is used to study the behaviour of the optical structure. Typically, light sources can be classified into two classes, continuous waves (CW) or pulse sources. To understand the behaviour of the optical structure, we have to solve the Maxwell equations. But often, especially for structures with complicated refractive index profile, analytic solutions are not available and numerical methods are required to solve them. For this purpose, a key ingredient to obtain solutions with the correct optical behaviour is an appropriate formulation of boundary conditions on the boundary of the numerical domain. This numerical window is necessarily bounded, while the physical solutions are formulated on the whole space. The boundary conditions should not change the optical fields we aim to calculate. This is difficult, since in general we do not know the effect of the internal structure (which is the reason why we want to calculate it), while this internal solution determines partly the boundary conditions. Stated differently, the solution we are after in the interior domain should be such that it can be matched with an exterior solution (which we do not want to calculate) in such a way that the common continuity conditions at the boundary are satisfied. One of these conditions is continuity of the field. Another condition is continuity of the normal derivative, since we will deal only with TE- polarized wave. This makes it clear that boundary conditions are important for modeling optical phenomena in any spatial dimensions. In this thesis, we consider optical structures in 1 and 2 dimensions only. The outline of this thesis will be presented in the last section of this chapter.

1.3.1 Transparent-influx boundary conditions

Suppose that there is a bounded planar domain Ω with refractive index properties determined by $n(x, z)$ in a uniform exterior Ω^c with refractive index n_0. We want to define transparent-influx boundary conditions (TIBC) on $\partial\Omega$ such that the problem in the interior

$$\Delta u + \omega^2 n^2(x, z)u = 0 \text{ in } \Omega, \text{ and TIBC on } \partial\Omega$$

is suitable for numerical calculations, for instance we will use calculations based on finite element methods in this thesis. For a given influx field u^{in}, the boundary condition should be able to prescribe the influx and at the same time should be transparent for the unknown outflux. The outflux u^{out} at the boundary is related to the numerical solution u_Ω of

the interior problem. The numerical solution u_Ω provides Dirichlet data on the boundary, $u_\Omega|_{\partial\Omega}$. From this we derive that the outgoing field u^{out} is $u^{out}|_{\partial\Omega} = u_\Omega|_{\partial\Omega} - u^{in}|_{\partial\Omega}$. By construction of the TIBCs, the interior solution u_Ω and the exterior solution

$$u_{ext} = u^{in} + u^{out} \text{ in } \Omega^{\mathrm{c}}$$

should satisfy the interface condition on $\partial\Omega$, so that the existence of a solution on the whole plane is guaranteed.

Depending on the dimensionality of the problem and numerical treatment, we will encounter two classes of TIBC's: local and nonlocal TIBC's. For 1D problems, the boundary conditions are local (since the boundary consist of separate points only), while for the 2D problems that we will consider in Chapter 6, we will use nonlocal TIBCs. The main ingredient of the nonlocal TIBCs is the Dirichlet-to-Neumann (DtN) operator which is typically exact, whereas the local TIBCs are usually approximate. If the DtN operators for the uniform exterior domain Ω^c can be found, then analytic expressions for the TIBCs can be derived.

In the following we will introduce notions for the Dirichlet-to-Neumann operators. For a given Dirichlet data g at the boundary $\partial\Omega$, we define the following operators to map the Dirichlet data to the Neumann data

$D^+(g) = \partial_n u|_{\partial\Omega}$ with u is the outgoing solution of the Helmholtz equation, with $u|_{\partial\Omega} = g$,

$D^-(g) = \partial_n u|_{\partial\Omega}$ with u is the incoming solution of the Helmholtz equation, with $u|_{\partial\Omega} = g$.

The word outgoing (incoming) refers to the outgoing (incoming) Sommerfeld radiation condition to be satisfied at infinity. In the following we will derive the formulation for the TIBC for various special solutions, all derived from the following general observations. Restricting to TE-polarization, continuity of the field and the normal derivative at $\partial\Omega$ requires that

$$\partial_n u_\Omega = \partial_n(u^{in} + u^{out}) = \partial_n u^{in} + \partial_n u^{out} \text{ on } \partial\Omega \tag{1.8}$$

and using the definitions of the DtN operators this is equivalent to

$$\partial_n u_\Omega = D^-(u^{in}) + D^+(u^{out}) \text{ on } \partial\Omega.$$

Because $D^+(u^{out})$ is unknown since u^{out} is unknown, we use continuity of the field, then we have that $u^{out} = u_\Omega - u^{in}$ at $\partial\Omega$ from which we obtain the general form of the transparent-influx boundary condition:

$$\text{TIBC: } \partial_n u_\Omega - D^+(u_\Omega) = D^-(u^{in}) - D^+(u^{in}) \text{ on } \partial\Omega. \tag{1.9}$$

In the following we will derive characterizations for solutions of various types of optical problems, where boundary conditions are essential in the formulation. As introduction, we describe below the 1D cases for which the TIBCs are local, and we will make remarks about the 2D cases that will be considered in the rest of this thesis.

1.3.2 1D transmission problem

The 1D problem involving an optical structure and a source, the so-called transmission problem, has a setting as follows. Consider an optical structure with refractive index configuration $n(z)$ defined in $\Omega = [0, L]$, placed in air with refractive index $n_0 = 1$. A given influx field $u^{in} = f$ with fixed

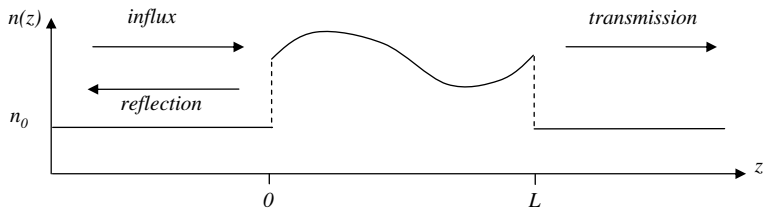

Figure 1.1: An illustration of a typical transmission problem in 1D

frequency is incident to the optical structure, and part of the influx may be transmitted or reflected back. This problem is then formulated as follows

$$\begin{aligned} \partial_z^2 u + \omega^2 n^2(z) u &= 0 \text{ in } \Omega \\ -\partial_z u - D^+(u) &= D^-(f) - D^+(f) \text{ at } z = 0, \text{ and} \qquad (1.10) \\ \partial_z u - D^+(u) &= 0 \text{ at } z = L, \qquad (1.11) \end{aligned}$$

where we have to solve the Helmholtz equation in the interior of the optical structure subject to the boundary conditions. The first boundary condition at $z = 0$ is a transparent influx boundary condition, allowing reflected

fields to pass through the boundary (it is transparent since the left hand side of the boundary condition formulation vanishes for such fields), and prescribing the incoming influx by the terms on the right hand side of the boundary condition formulation. The second boundary condition at $z = L$ is such that only outgoing fields are allowed, and no incoming fields from the right are present. These boundary conditions are derived straightforward from the general form in (1.9). For this type of setting, the *transmittance* is a parameter that is defined to measure the portion of energy that is transmitted through the optical structure. Remembering the harmonic time dependence of the field in the form of $e^{-i\omega t}$, the solution of the Helmholtz equation in the exterior of the optical structure can be written as

$$u(z) = \begin{cases} a_{inf}e^{i\omega n_0 z} + r_{ref}e^{-i\omega n_0 z}, & z < 0 \\ t_{trans}e^{i\omega n_0 z}, & z > L, \end{cases}$$

then the *transmittance* is defined as

$$T = |t_{trans}|^2/|a_{inf}|^2.$$

For transmission problems it is often found that there are frequencies for which the influx field is fully transmitted through the optical structure. Then the *transmittance* is equal to unity. We call this solution a full transmission mode or resonant mode. For example, in Figure 1.2 we show a typical transmittance curve from an optical grating. Some of the resonant modes are indicated by arrows. A plot like Figure 1.2 is obtained (numerically) by scanning through the entire range of frequencies. If we are interested, as is often the case, in special solutions, like the transmission modes, we have to find the specific frequency together with the field; hence we will have to deal with an eigenvalue problem. We will now show the special formulations of such eigenvalue problems. We remark already here that the boundary conditions (because of the presence of the DtN operators), will depend on the eigenvalue also, so these formulations in the following lead to 'nonlinear' eigenvalue problems, where 'nonlinear' refers to the nonlinear appearance of the eigenvalue to be sought.

1.3.3 1D resonant modes

We can characterize resonant modes by means of an eigenvalue problem. That is by homogenization of the boundary conditions, excluding the Dirichlet to Neumann terms of the influx field from the formulation. Observe that

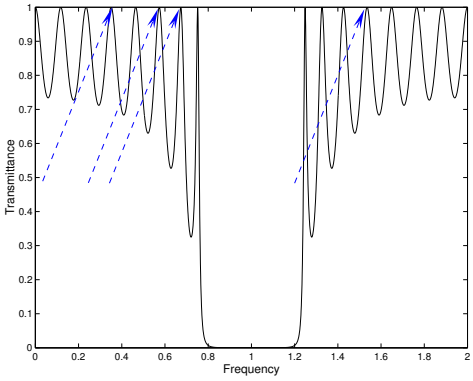

Figure 1.2: An example of a transmittance curve. Some resonant modes are pointed by arrows

the boundary condition at $z = 0$ in (1.10) can be written as

$$-\partial_z u = D^+(u - f) + D^-(f).$$

In case of no reflection, which is relevant for the transmission modes, it must hold that $D^+(u - f) = 0$, and this is true if and only if $u = f$. This last fact has a clear meaning, that the solution of the Helmholtz equation is the influx itself, and hence $D^-(u) = D^-(f)$. So for characterizing resonant fields, the problem formulation reads

$$\begin{aligned} \partial_z^2 u + \omega^2 n^2(z) u &= 0 \text{ in } \Omega \\ -\partial_z u - D^-(u) &= 0 \text{ at } z = 0, \text{ and} \\ \partial_z u - D^+(u) &= 0 \text{ at } z = L. \end{aligned}$$

In this way, we obtain only solutions of the Helmholtz equation with transmittance equal to unity. We can not generalize this problem setting for structures in higher dimensions. The notion of *transmittance* is difficult to define, since an incoming influx from one direction can have reflections in arbitrary directions. For some structures in 2D which have a disconnected boundary, for instance a structure which is extended towards infinity in one direction (e.g. a slab) and influx from one side, it is still possible to have a characterization for resonating modes (if there exist such a mode). But for finite structures in a domain, for which the exterior is a connected set, it is not possible to distinguish the reflected fields from the influx.

1.3.4 1D radiation modes

Another possible scenario is that when sources are absent. If there is a field in an optical structure, it will radiate in any possible direction, leaking its power to the surrounding neighbourhood. This type of field is called a radiation mode. The radiation mode is a solution of the Helmholtz equation with outward radiating fields in the exterior of the optical structure. Radiation modes can be formulated by the following eigenvalue problem

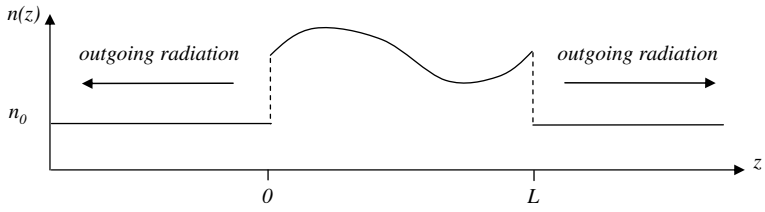

Figure 1.3: An illustration of a radiation mode for 1D optical structure

$$\begin{aligned} \partial_z^2 u + \omega^2 n^2(z) u &= 0 \text{ in } \Omega \\ -\partial_z u - D^+(u) &= 0 \text{ at } z = 0, \text{ and} \\ \partial_z u - D^+(u) &= 0 \text{ at } z = L, \end{aligned}$$

where now both boundary conditions allow only outward propagating fields. Unlike the previous eigenvalue problem described above, this formulation for radiation modes can be extended to higher dimensions. For example in 2D, if the optical structure is inside a domain of interest Ω with $\partial\Omega$ as its boundary, then the formulation is straightforward

$$\begin{aligned} \Delta u + \omega^2 n^2(x,z) u &= 0 \text{ in } \Omega \\ \partial_n u - D^+(u) &= 0 \text{ at } \partial\Omega, \end{aligned}$$

where now u is a function of (x, z).

For radiation modes, it will turn out that eigenvalues (frequencies) are complex valued. If we express the frequency as $\omega = \omega_r + i\omega_i$, then with the time dependence of the field in the form of $e^{-i\omega t}$, it is clear that the imaginary part of the frequency represent the decay (or amplification, depending on the sign) of the mode in time. Interestingly, it is possible

to describe this dynamic behaviour of the field with properties of the field itself. This will all be explained in detail in Section 1.3.6.

1.3.5 1D standing state

For 1D optical problems, there can exist another type of solution with a different time evolution behaviour. The types of solutions that we have described so far, which are the fields in the transmission problem, the resonant modes, and the radiation modes, have all propagation as a property of their time evolution. As described previously about the radiation modes, if there exist a field in an optical structure, this field will radiate to any possible directions. However, theoretically it is possible to keep the field inside the optical structure. If we give influx toward the optical structure from both directions, with the same power as what is radiated outward, it is possible to keep the field 'standing' inside the optical structure.

For this 1D case, let us assume that there are two continuous wave optical sources placed at '$\pm\infty$'. Denoting this continuous influx as u^{in}, then together with the unknown (outgoing) radiation it forms the solution of the Helmholtz equation in the exterior $u_{ext} = u^{in}+u^{out}$. To have standing states solutions it is necessary that the power flow is zero everywhere. For 1D case, the time average power flow is quantified by the Poynting quantity

$$P = \mathrm{Im}(\frac{1}{\omega} u \partial_z u).$$

If we write $u^{in} = ae^{i\omega n_0 z}$ and $u^{out} = re^{-i\omega n_0 z}$, then the general solution in the left exterior

$$u_{ext} = ae^{i\omega n_0 z} + re^{-i\omega n_0 z}, \tag{1.12}$$

has the Poynting quantity

$$P = n_0(|a|^2 - |r|^2).$$

For this to be zero it should hold that $|a| = |r|$, or equivalently $|u^{in}| = |u^{out}|$. In general the Poynting quantity will be zero if u^{in} and u^{out} differ only by a phase factor. More precisely, we can write $u^{out} = u^{in}e^{i\phi}$.

Basically, the boundary condition should be derived from the continuity requirement of the field and the normal derivative at $\partial\Omega$

$$\partial_n u = \partial_n u_{ext} = \partial_n u^{in} + \partial_n u^{out} = D^-(u^{in}) + D^+(u^{out}) \tag{1.13}$$

Since we have the relation $u^{out} = u^{in}e^{i\phi}$, it also holds that

$$D^+(u^{out}) = \partial_n u^{out} = \partial_n u^{in} e^{i\phi} = D^-(u^{in})e^{i\phi}. \tag{1.14}$$

and hence $D^-(u^{in})$ and $D^+(u^{out})$ can be expressed as

$$D^-(u^{in}) = \frac{1}{2}(D^-(u^{in}) + D^+(u^{out})e^{-i\phi}) \text{ and} \tag{1.15}$$

$$D^+(u^{out}) = \frac{1}{2}(D^+(u^{out}) + D^-(u^{in})e^{i\phi}). \tag{1.16}$$

Substituting (1.15) and (1.16) to (1.13), the condition to be satisfied on the boundary is

$$\partial_n u = \frac{1}{2}(D^-(u^{in} + u^{in}e^{i\phi})) + \frac{1}{2}(D^+(u^{out}e^{-i\phi} + u^{out})) \tag{1.17}$$

$$= \frac{1}{2}D^-(u) + \frac{1}{2}D^+(u) \tag{1.18}$$

Later in Chapter 4 we will give an example of an optical structure which has standing a state solution.

1.3.6 Integral expressions

Consider a solution of the Helmholtz equation in the domain Ω

$$\Delta u + \omega^2 n^2(x,z)u = 0 \text{ in } \Omega$$

Multiplying this equation with $\overline{u}$ (the complex conjugate of u), and integrate over the domain Ω yields the following

$$\iint_\Omega \Delta u\overline{u} + \omega^2 n^2(x,z)|u|^2 dxdz = 0,$$

or

$$\int_{\partial\Omega} \overline{u}\partial_n u dl - \iint_\Omega \{|\nabla u|^2 - \omega^2 n^2(x,z)|u|^2\}dxdz = 0,$$

after partial integration. For this equality to hold, the real and imaginary parts should vanish, giving

$$\int_{\partial\Omega} \mathrm{Re}(\overline{u}\partial_n u)dl - \iint_\Omega \{|\nabla u|^2 dxdz - \mathrm{Re}(\omega^2)n^2(x,z)|u|^2\}dxdz = 0, \tag{1.19}$$

$$\text{and } \int_{\partial\Omega} \mathrm{Im}(\overline{u}\partial_n u)dl + \iint_\Omega \mathrm{Im}(\omega^2)n^2(x,z)|u|^2 dxdz = 0. \tag{1.20}$$

It is clear that for (1.20) to hold, ω should be complex in general. Rewriting (1.19) and (1.20), we obtain

$$\mathrm{Re}(\omega^2) = \frac{\iint\limits_{\Omega} |\nabla u|^2 dxdz - \int\limits_{\partial\Omega} \mathrm{Re}(\overline{u}\partial_n u)dl}{\iint\limits_{\Omega} n^2(x,z)|u|^2 dxdz} \tag{1.21}$$

$$\mathrm{Im}(\omega^2) = \frac{-\int\limits_{\partial\Omega} \mathrm{Im}(\overline{u}\partial_n u)dl}{\iint\limits_{\Omega} n^2(x,z)|u|^2 dxdz}. \tag{1.22}$$

Below we consider two cases where the quotients (1.21) and (1.22) are useful for characterizing solutions.

- Let us turn the attention to the one dimensional standing state case. Let $\Omega = [0, p]$, for this case the quotient (1.22) is equivalent to

$$\mathrm{Im}(\omega^2) = \frac{-\mathrm{Im}(\overline{u}\partial_z u)|_0^p}{\int\limits_0^p n^2(z)|u|^2 dz}. \tag{1.23}$$

  As explained above in Subsection 1.3.5, for standing states $\mathrm{Im}(\overline{u}\partial_z u) = 0$ (Poynting quantity zero, no power flow), and so we have that $\mathrm{Im}(\omega^2) = 0$ which means that the frequency is real valued.

  In the one dimensional infinite grating case that will be considered in Chapter 3, it will be explained that for the band gap edges, the fields are 'p shift-skew symmetric' where p is the periodicity of the grating. Exploiting this fact, we can consider an interval $\Omega' = [\xi, p + \xi]$ where the field vanishes at the boundary points. Hence $\mathrm{Re}(\bar{u}\partial_z u) = 0$ and we are left with the quotient

$$\mathrm{Re}(\omega^2) = \frac{\int\limits_{\xi}^{p+\xi} |\partial_z u|^2 dz}{\int\limits_{\xi}^{p+\xi} n^2(z)|u|^2 dz}. \tag{1.24}$$

  In Chapter 3 this quotient will be exploited to characterize the band gap edges.

- For 1D or 2D radiation mode, the boundary term $\int \bar{u}\partial_n u$ does not vanish and hence the frequency is necessarily complex valued. The quotients (1.21) and (1.22) have a nice interpretation in this case, that is we find a dynamic relevance (from the expression of $\mathrm{Im}(\omega^2)$ in (1.22)), from a non-dynamic formulation of the fields. We will exploit this fact later in Chapter 5 and and in Chapter 6 for defining the quality (Q) of a mode.

1.4 Thesis outline

We start Chapter 2 by explaining the numerical schemes that we will use throughout this thesis. We will describe the Finite Element Method (FEM) with linear 'tent' basis function. We continue by describing the Transparent Influx Boundary Condition (TIBC) and its implementation with the FEM scheme.

The chapters 3,4,5 and 6 are papers that have been published or are submitted for publications. We summarize the contents below and thereby show the relation between them.

In Chapter 3 [31] we start by studying the simplest form of a photonic crystal. We consider a one dimensional optical structure built from two different linear dielectric materials. The dielectrics are arranged alternatingly with fixed thicknesses such that they form a periodic structure. This structure is called the optical grating. The optical grating that we consider in this Chapter is an infinite grating. For such a structure a band gap always exists, and our aim is to characterize the edges of the first band gap. Since the structure is linear, actually an exact solution can be written down via a Transfer Matrix Method (TMM) [29, 30] and the band gap edges can be calculated by finding zeros of the dispersion relation. However for optical gratings with smooth index variation (rather than stepsize function), or even optically nonlinear index function, it is generally not possible to do it exactly so approximations come in the picture.

Different from the TMM approach, we exploit the periodicity of the structure and apply the Floquet-Bloch theorem to the Helmholtz equation. This gives the understanding how fields behave for the edges of the band gap, and makes it possible to define an extremal characterization of the edges of the first band gap. In principle this formulation makes it possible to handle gratings with smooth index variation and also nonlinear. In our

approach we aim to obtain the band gap edges and fields simultaneously, so the extremal characterization (minimum or maximum) is in the form of an eigenvalue problem. As illustration of our approach, we consider an infinite optical grating with two different materials, such that we can compare the result with the exact one. We show that the extremum property is useful, that we can approximate, or give bounds to the band gap edges, by using a simple 'suitable' trial function with low degrees of freedom. The word 'suitable' here means that the trial function should satisfy the Helmholtz equation and also the boundary condition. As one expects, by increasing the number of degrees of freedom the accuracy of the calculation increases. More precisely, in this Chapter we choose trial functions that are a superposition of local basis 'tent' function. This is also known as the Finite Element Method. The results showed that the method is very accurate for moderate number of elements. Further we also extend the characterization to accommodate structures with a nonlinear index.

In Chapter 4 [32] we deal with an optical grating structure which is more realistic. The structure is finite and has a defect layer in it. It is known that for defect grating structure there may exist frequencies inside the band gap for which the transmittance is equal to unity. We call such frequencies as 'defect frequencies'. Defect grating structures have features that can be utilized for applications. For instance, the sharp peak of the defect frequency in a transmittance curve means that it can be used as a filter. Another important feature is that at the defect frequency the electric field is amplified in the defect layer, and this is useful for switching application when combined with nonlinear material [33].

For applications, it is important that we can find defect frequencies of a given defect grating structure. In this chapter we exploit the use of the Optical Transfer Map (OTM) to have a direct characterization of the defect frequency. Using this, we introduce the use of Effective Boundary Condition (EBC), that replaces the optical effect of a certain optical structure. Here in Chapter 4 we consider a defect grating structure which is symmetric, with one defect layer in the middle of the grating. The EBC is used to replace the optical effect of the assisting grating, and hence the problem of finding defect frequencies reduces to solving the Helmholtz equation only for the defect layer with EBC's. In this way we find two different fields for the same defect frequency which means that they are degenerate. One is amplified in the defect layer, we call this field '$S^+(z)$', and the other one

is attenuated, we call as '$S^-(z)$'. Both $S^+(z)$ and $S^-(z)$ are fields which are standing, and we call such fields as 'states'. Further in this Chapter we explain the relation between these states with the defect mode '$M(z)$', which is a propagating solution for a transmittance experiment at the defect frequency. At a first glance the amplified state $S^+(z)$ looks very much like $M(z)$, but the attenuated state $S^-(z)$ is essential for the construction of $M(z)$.

In Chapters 3 and 4 we assumed that there is a continuous flux of field and we assumed that the dependence in time is harmonic such that time can be ruled out from the governing equation. In Chapter 5 [34] we move on to a more realistic scenario, that influx from sources is time limited. We consider the same defect grating structure as in Chapter 5, but now the influx is a pulse. We consider a pulse with spectral components inside the bandgap. We developed a Finite Element Time Domain (FETD) scheme to simulate the problem, where we used Finite Element Method to handle the space discretization and Newmark scheme for the time discretization. Essential for the numerical scheme is the use of exact time domain Transparent Influx Boundary Conditions (TIBC). The results show that the defect grating is loaded in a relatively short time (proportional to the duration of the influx pulse), and the 'trapped' field stays inside the defect grating much longer. The existing field then decays in time and unloads its energy toward the exterior of the structure, and we want to understand this decay in terms of the properties of the defect grating. We do this by using a low dimensional model for the loading and the unloading phenomenon, where we assumed that it is sufficient to consider only a single frequency component to describe the phenomenon. More precisely, we describe two leaky modes based on the amplified $S^+(z)$ and the attenuated state $S^-(z)$ solution, and it effectively replaces the complete loading and unloading phenomenon. Using this model we are able to quantify the build up of the field during the loading phase and the decay of the field during the unloading phase in terms of the energy content of the field. This also provides an expression for the so called quality factor (Q) of the leaky modes. We compare the result from the low-dimensional model with the FETD calculation, and the result shows a very good agreement.

In Chapter 6 [35] we consider a finite two dimensional photonic crystal with defect. The same as for the one dimensional defect grating, for the two dimensional structure defect modes can also exist. The photonic crys-

tal considered in this Chapter consists of a square lattice of dieletric rods placed in air as background. One of the rods has a different diameter, forming the defect of the structure. Our aim here is to characterize the leaky (defect) modes in the form of a nonlinear eigenvalue problem. We use a two dimensional Finite Element Method as calculation tool, equipped with Transparent Influx Boundary Condition (TIBC) [28]. Prescribing symmetries in the structure, we reduce the computational domain and we obtain several modes. Using the properties of the mode, were able do describe the decay of the leaky modes as well as the quality factor (Q). As well as in the 1D case in Chapter 5, we also simulate pulses as influx. The spectral components of the pulses are centered around each defect frequency. The simulation results show that the excited modes decay in time and leak their energy toward the exterior. We compare this decay in time of the energy with the result of the eigenvalue problem, which shows a good agreement.

Finally, in Chapter 7 we summarize the results of the thesis.

Bibliography

[1] T. H. Maiman, Stimulated optical radiation in ruby, *Nature* **187**, 493, 1960.

[2] F. P. Kapron, D. B. Deck and R. D. Maurer, Radiation losses in glass optical waveguide, *Applied Physics Letters* **17**, 423, 1970.

[3] E. Yablonovitch, Inhibited spontaneous emission in solid-state physics and electronics, *Physical Review Letters* **58**, 2059, 1987.

[4] S. John, Strong localization of photons in certain disordered dielectric superlattices, *Physical Review Letters* **58**, 2486, 1987.

[5] E. Yablonovitch, Photonic crystals, *Journal of Modern Optics* **41**, 173-194, 1994.

[6] R. D. Meade, A. Devenyi, J. D. Joannopoulos, O. L. Allerhand, D. A. Smith and K. Kash, Novel applications of photonic band gap materials: low-loss bends and high Q cavities, *Journal of Applied Physics* **75**, 4753, 1994.

[7] T. Baba, N. Fukaya, and J. Yonekura, Observation of light propagation in photonic crystal optical waveguides with bends, *Electronics Letters* **35**, 654, 1999.

[8] A. Chutinan and S. Noda, Waveguides and waveguide bends in two-dimensional photonic crystal slabs, *Physical Review* **B 62**, 4488, 2000.

[9] N. Fukaya, D. Ohsaki dan T. Baba, Two-dimensional photonic crystal waveguides with 60° bends in a thin slab structure, *Japanese Journal of Applied Physics* **39**, 2619, 2000.

[10] M. Loncar, D. Nedeljkovic, T. Doll, J. Vukovic, A. Scherer and T. P. Pearsall, Waveguiding in planar photonic crystals, *Applied Physics Letters* **77**, 1937, 2000.

[11] S. G. Johnson, P. R. Villeneuve, S. Fan and J. D. Joannopoulos, Linear waveguides in photonic-crystal slabs, *Physical Review* **B 62**, 8212, 2001.

[12] S. Fan, S. G. Johnson, J. D. Joannopoulos, C. Manolatou and H. A. Haus, Waveguide branches in photonic crystals, *Journal of the Optical Society of America* **B 18**, 162, 2001.

[13] S. Fan, P. R. Villeneuve, J. D. Joannopoulos and H. A. Haus, Channel Drop Tunneling through Localized States, *Physical Review Letters* **80**, 960, 1996.

[14] S. Fan, P. R. Villeneuve, J. D. Joannopoulos, M. J. Khan, C. Manolatou and H. A. Haus, Theoretical analysis of channel drop tunneling processes, *Physical Review* **B 59**, 15882, 1999.

[15] D. Labilloy, H. Benisty, C. Weisbuch, T. F. Krauss, V. Bardinal, and U. Oesterle, Demonstration of cavity mode between two-dimensional photonic-crystal mirrors, *Electronics Letters* **33**, 1978, 1997.

[16] H. Benisty, C. Weisbuch, D. Labilloy, M. Rattier, C. J. M. Smith, T. F. Krauss, R. M. De La Rue, R. Houdre, U. Oesterle, C. Jouanin and D. Cassagne, Optical and confinement properties of two-dimensional photonic crystals, *Journal of Lightwave Technology* **17**, 2063, 1999.

[17] A. Chutinan, M. Mochizuki, M. Imada and S. Noda, Surface-emitting channel drop filters using single defects in two-dimensional photonic crystal slabs , *Applied Physics Letters* **79**, 2690, 2001.

[18] J. Vuckovic, M. Loncar, H. Mabuchi and A. Scherer, Design of photonic crystal microcavities for cavity QED, *Physical Review* **E 65**, 016608, 2002.

[19] H. Hirayama, T. Hamano and Y. Aoyagi, Novel surface emitting laser diode using photonic band-gap crystal cavity, *Applied Physics Letters* **69**, 791, 1996.

[20] J. O'Brien, O. Painter, R. Lee, C. C. Cheng, A. Yariv and A. Scherer, Lasers incorporating 2D photonic bandgap mirrors, *Electronics Letters* **32**, 2243, 1996.

[21] R. K. Lee, O. J. Painter, B. Kitzke, A. Scherer and A. Yariv, Photonic bandgap disk laser, *Electronics Letters* **35**, 569, 1999.

[22] J. K. Hwang, H. Y. Ryu, D. S. Song, I. Y. Han, H. W. Song, H. K. Park, Y. H. Lee, and D. H. Jang, Room-temperature triangular-lattice two-dimensional photonic band gap lasers operating at 1.54 μm , *Applied Physics Letters* **76**, 2982, 2000.

[23] T. Yoshie, J. Vuckovic, A. Scherer, H. Chen and D. Deppe, High quality two-dimensional photonic crystal slab cavities, *Applied Physics Letters* **79**, 4289, 2001.

[24] J. D. Joannopoulos, P. R. Villeneuve and S. Fan, Photonic crystals: Putting a new twist on light, *Nature* **386**, 143, 1997.

[25] H. Kosaka, T. Kawashima, A. Tomita, M. Notomi, T. Tamamura, T. Sato and S. Kawakami, Photonic crystals for micro lightwave circuits using wavelength-dependent angular beam steering, *Applied Physics Letters* **74**, 1370, 1999.

[26] A. R. McGurn, Photonic crystal circuits: A theory for two- and three-dimensional networks, *Physical Review* **B 61**, 13235, 2000.

[27] A. R. McGurn, Photonic crystal circuits: Localized modes and waveguide couplers, *Physical Review* **B 65**, 075406, 2002.

[28] J. B. Nicolau and E. van Groesen, Hybrid analytic-numeric method for light through a bounded planar dielectric structure, *Journal of Nonlinear Optical Physics and Materials* **14**, 161, 2005.

[29] P. Yeh. *Optical Waves in Layered Media*. Wiley-Interscience, 1988.

[30] J. Lekner. *Theory of Reflection of Electromagnetic and Particle Waves*. Nijhoff, Dordrecht, 1987.

[31] E. van Groesen and A. Sopaheluwakan, Extremal characterization of band baps in nonlinear gratings, *Journal of Nonlinear Optical Physics and Materials* **12**, 135, 2003.

[32] E. van Groesen,A. Sopaheluwakan and Andonowati, Direct characterization of states and modes in defect grating structures, *Journal of Nonlinear Optical Physics and Materials* **13**, 155, 2004.

[33] A. Suryanto, E. van Groesen and M. Hammer, Finite element analysis of optical bistability in one-dimensional nonlinear photonic band gap structures with a defect, *Journal of Nonlinear Optical Physics and Materials* **12**, 187, 2003.

[34] A. Sopaheluwakan and E. van Groesen, Pulse loading and radiative unloading of an optical defect grating structure: low dimensional modeling and numerical simulations , *Submitted to Optics Communications*, 2006.

[35] A. Sopaheluwakan and E. van Groesen, Characterization and calculation of leaky modes in photonic crystal microcavities, *In preparation for submission*, 2006.

Chapter

2 Finite element method and Transparent Influx Boundary Condition

In this Chapter we will explain the Finite Element Method used in this thesis. The two dimensional and one dimensional Finite Element Method (FEM) numerical schemes used in this thesis are all obtained using linear 'tent' basis functions. Below we will only explain the case for the 2D FEM, and leave out the 1D scheme since it is a special case of the 2D scheme.

Since we deal with influx and reflection of fields interacting with optical structures, it is important to have proper boundary conditions that represent the correct physical properties of the exterior of the computational domain. Boundary conditions should be able to prescribe influx and allow reflected fields to propagate through the boundary without reflection. Below we will describe the Transparent Influx Boundary Condition (TIBC) outlined in reference [1]. This boundary condition is different then other transparent boundary condition [2, 3, 4, 5, 6] since they are all local approximate boundary conditions. As we will see later, this boundary condition is nonlocal, in the sense that all points at the boundary are coupled through an integral operator. An advantage of using this boundary condition is that no additional computational domain is needed, hence it is cheaper then the Perfectly Matched Layer [7] which is widely used in computations of optical structures. A more fundamental advantage is that 'spurious' modes are not introduced by the TIBCs we consider there.

2.1 Variational formulation and FEM

By using the variational formulation of the Helmholtz equation it is possible to derive consistent numerical discretizations by approximating u as a su-

perposition of chosen basis functions. More precisely, consider the following functional

$$\mathcal{L}(u) := \frac{1}{2}\iint\limits_{\Omega}\left[(\nabla u)^2 - \omega^2 n^2(x,z)u^2\right]dxdz - \frac{1}{2}B(u)$$

where $B(u)$ denotes the boundary term. Then the critical point is found via the standard reasoning from the vanishing of the first variation

$$\delta\mathcal{L}(u,v) = \iint\limits_{\Omega}\left[\nabla u\cdot\nabla v - \omega^2 n^2(x,z)uv\right]dxdz - \frac{1}{2}\delta B(u,v) = 0 \qquad (2.1)$$

where $v(x,z)$ is an arbitrary variation. Assuming that the variation of the boundary term can be written as $\delta B(u,v) = \int \delta B(u)vdl$, after partial integration of the first term we obtain

$$\delta\mathcal{L}(u,v) = \int\limits_{\partial\Omega}(\partial_n u)vdl - \iint\limits_{\Omega}[\Delta u + \omega^2 n^2(x,z)u]vdxdz - \frac{1}{2}\int\limits_{\partial\Omega}\delta B(u)vdl = 0.$$

Since this should vanish for any variation v, we obtain the Helmholtz equation

$$\Delta u + \omega^2 n^2(x,z)u = 0 \quad \text{in} \quad \Omega$$

with the boundary condition

$$\partial_n u - \frac{1}{2}\delta B(u) = 0.$$

The first variation of the functional $\mathcal{L}$ written in (2.1) is often called the weak form of the Helmholtz equation, in the sense that if we multiply the Helmholtz equation with an arbitrary test function v, and integrate the result, we obtain (2.1). The word 'weak' means that instead of requiring u to be at least twice differentiable, by using the weak form we only require it to be at least once differentiable.

To have the general form of the TIBC (1.9) incorporated in the formulation, the boundary term should be written in the following form

$$B(u) = uD^+(u) - 2D^-(u^{in})u + 2D^+(u^{in})u,$$

where the meaning of the notion $D^{\pm}(u)$ was explained in Subsection 1.3.1. Substituting this into (2.1) gives the weak form

$$\begin{aligned} \delta\mathcal{L}(u,v) &= \iint_{\Omega} \left[\nabla u \cdot \nabla v - \omega^2 n^2(x,z) uv\right] dxdz \\ &- \int_{\partial\Omega} [D^+(u) - D^-(u^{in}) + D^+(u^{in})] v dl = 0. \end{aligned} \tag{2.2}$$

To arrive at the numerical scheme, we must choose a set of basis function and discretize the domain. Throughout this thesis, we use the set of piecewise linear 'tent' basis function, denoted by $\{\phi_i(x,z)\}_{i=1}^N$. Figure 2.1 illustrates the discretization of the domain Ω in a triangular mesh, and examples of linear basis elements. Then we seek the solution in the form of

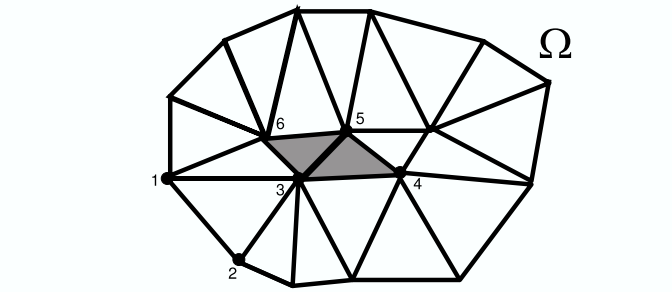

(a). Finite element triangular mesh with global numbering

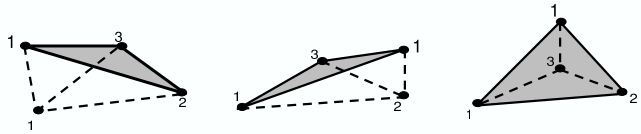

(b). Examples of linear basis functions with local numbering

Figure 2.1: (a). Illustration of the discretized domain Ω. (b). Examples of linear basis functions

$$u(x,z) \approx \sum_{i=1}^{N} \tilde{u}_i \phi_i(x,z).$$

The basis functions ϕ_i are defined by piecewise linear interpolation between the nodal values $\phi_i(x_j, z_k)$, with the property

$$\phi_i(x_j, z_k) = \delta_{i,j,k}, \quad i = 1, .., N$$

where $\delta_{i,j,k}$ is the Kronecker delta and N is the number of nodal points (x_j, z_k). For the interior of Ω, the entries of the finite element stiffness (S) matrix related to $\iint (\nabla u)^2 dxdz$ and the mass (M) matrix related to $\iint n^2 u^2 dxdz$ are evaluated as follows

$$\mathrm{S}_{i,j} = \iint\limits_{\Omega} \nabla\phi_i \nabla\phi_j ds \quad \text{and} \quad \mathrm{M}_{i,j} = \iint\limits_{\Omega} n^2(x,z)\phi_i\phi_j ds.$$

2.2 DtN operators for a half space

To express the DtN operators D^+ and D^-, and solutions in a half plane, we will use plane wave decomposition. We start by considering a uniform Western half plane $(x, z < 0)$ with index n_0. Let $g_W(x)$ be a Dirichlet boundary value given at $z = 0$, decomposed as

$$g_W(x) = \int \widehat{g_W}(k) e^{ikx} dk$$

then the outgoing solution in the exterior $z < 0$ expressed as a plane wave decomposition is given by

$$u^{out}(x, z) = \int \widehat{g_W}(k) e^{i(kx - \beta(k)z)} dk$$

where we define

$$\begin{aligned} \beta(k) &= \sqrt{\omega^2 n_0^2 - k^2}, \quad \text{if} \quad |k| < \omega n_0 \\ &= i\sqrt{k^2 - \omega^2 n_0^2}, \quad \text{if} \quad |k| > \omega n_0. \end{aligned}$$

The solution u^{out} consist of combination of translating plane waves (for $|k| < \omega n_0$) and evanescent waves (for $|k| > \omega n_0$). This form of outgoing solution leads to the Dirichlet-to-Neumann operator D^+ for the boundary value g_W

$$D^+(g_W) = \partial_n u^{out}(x, 0) = \int i\beta(k)\widehat{g_W}(k) e^{ikx} dk.$$

We can also derive the DtN operator D^- for an incoming field in the same way as we derive the operator D^+, and in fact

$$D^-(g_W) = -D^+(g_W).$$

2.3 DtN operators for a square

Suppose now that we have a square computational domain with length L_x, and the boundary function $g_0(x)$ on the interval $[0, L_x]$. We further extend the function $g_0(x)$ to the function $\tilde{g}(x)$ defined as

$$\tilde{g}(x) = \begin{cases} g_0(x), & x \in [0, L_x] \\ 0, & \text{elsewhere.} \end{cases}$$

such that it is defined on the whole real line. We represent this function on the interval $[0, \alpha L_x]$, $\alpha > 1$, by Fourier series representation

$$g(x) = \sum_{m=-\infty}^{\infty} \hat{g}(m) e^{imh_x x}, \quad \text{with} \quad h_x = \frac{2\pi}{\alpha L_x} \tag{2.3}$$

where its Fourier inverse is given by

$$\hat{g}(m) = \frac{1}{\alpha L_x} \int_0^{L_x} \tilde{g}(x) e^{-imh_x x} dx.$$

Note that the functions $\{e^{-imh_x x}\}_{m=-\infty}^{\infty}$ form an orthogonal system of functions on the interval $[0, \alpha L_x]$. The parameter α is added to prevent numerical errors as follows. If $\alpha = 1$, then function $\tilde{g}$ on the boundary is represented by a periodic series with period L_x. Then in this case, fields from outside the basic interval $[0, L_x]$ may enter the numerical window and disturb the solution being sought. Therefore we should take $\alpha > 1$ which effectively means that we set the periodic continuation of the function $\tilde{g}(x)$ (i.e. the period of the function $g(x)$) to be faraway from the basic interval $[0, L_x]$. This choice of periodic continuation will not affect the numerical window which will be supplied with boundary conditions that do not allow any influx from the other sides of the domain.

If the given function g at the Western boundary (2.3) corresponds to an outgoing field, then outside the boundary ($z < 0$) this field is given by

$$u^{out}(x,z) = \sum_{m=-\infty}^{\infty} \hat{g}(m) e^{i(mh_x x - \beta(mh_x)z)} \tag{2.4}$$

which leads to the DtN operator at the Western boundary

$$D_W^+(g) = \partial_n u^{out}(x,0) = \sum_{m=-\infty}^{\infty} i\beta(mh_x)\hat{g}(m)e^{imh_x x}.$$

The DtN operators for incoming fields at the boundary can be found in a similar manner, and in fact

$$D_W^-(g) = -D_W^+(g).$$

Remark

Observe that by the choice of the field representation in (2.4), the number of translating plane waves representing the outgoing (or incoming) field is directly related to the choice of the parameter α. For a given fixed frequency ω and index n_0, the series representation of the field in (2.4) has plane wave components if $|mh_x| < \omega n_0$. This means that the maximum number of translating plane wave taken for the field representation is

$$m_{max} = \frac{\omega n_0 \alpha L_x}{2\pi}.$$

In practice, this means that to have a sufficiently large number of plane waves in the representation, the value of α should be chosen to be large enough since we don't want to increase the window size L_x.

2.4 Implementation of the DtN operators in the FEM scheme

Having derived explicit expressions of the DtN operators above, now we show how the DtN operators can be implemented in a FEM scheme. As explained above, we chose a Fourier series representation of the function along the boundary, where we have the DtN operator

$$D_W^+(g) = \sum_{-\mathcal{M}}^{\mathcal{M}} i\beta(mh_x)\hat{g}(m)e^{imh_x x}$$

where the value $\mathcal{M}$ is taken to be finite for numerical purposes.

To evaluate the boundary integral in (2.2) on the Western boundary, we express the test function v in terms of expansion of the basis function $v = \sum_{p=1}^{N} v_p \phi_p$, and we also approximate the function $g(x)$ along the boundary in terms of the basis function $g(x) \cong \sum_{p=1}^{N} g_p \phi_p(x,0)$. Then the discrete version D_W of the D_W^+ operator takes the form

$$\int_0^{L_x} v D_W^+(g) dl \cong \frac{1}{\alpha L_x} \sum_{p,q}^{N} v_p g_p \left(\sum_{-\mathcal{M}}^{\mathcal{M}} i\beta(mh_x) \hat{\tau}_{qm} \tau_{pm} \right) \tag{2.5}$$

where $\hat{\tau}_{qm} = \int_0^{L_x} \phi_q(x,0) e^{-imh_x x} dx$, $\tau_{pm} = \int_0^{L_x} \phi_p(x,0) e^{imh_x x} dx$ and $\mathcal{M}$ is a positive integer.

By doing the same procedure for other boundaries east (D_E), north (D_N) and south (D_S), this results in the full matrix system

$$(S - M + D_W + D_E + D_N + D_S)\vec{u} + \vec{F} = 0$$

where $\vec{F}$ is the discrete version of the incoming field $D^-(u^{in}) - D^+(u^{in})$. Observe that this boundary operator is nonlocal in the sense that all points at the boundary are coupled through the integral operator.

This FEM scheme with transparent influx boundary condition was successfully implemented, and the results of Chapter 6 are based on this scheme. Simplified versions are used in Chapter 5 where specific information will be provided.

Bibliography

[1] J. B. Nicolau and E. van Groesen, Hybrid analytic-numeric method for light through a bounded planar dielectric structure, *Journal of Nonlinear Optical Physics and Materials* **14**, 161, 2005.

[2] B. Engquist and A. Majda, Radiation boundary conditions for acoustic and elastic wave calculations, *Communications on Pure and Applied Mathematics* **32**, 313, 1979.

[3] A. Bayliss and E. Turkel, Radiation boundary conditions for wave-like equations, *Communications on Pure and Applied Mathematics* **33**, 707, 1980.

[4] R. L. Higdon, Numerical absorbing boundary conditions for the wave equation, *Mathematics of Computations* **49**, 65 ,1987.

[5] D. Givoli, Non-reflecting boundary conditions, *Journal of Computational Physics* **94**, 1 ,1991.

[6] D. Givoli, I. Patlashenko and J. Keller, High-order boundary conditions and finite elements for infinite domains, *Computer Methods in Applied Mechanics and Engineering* **143**, 13 ,1997.

[7] J. P. Berenger, A perfectly matched layer for the absorption of electromagnetic waves, *Journal of Computational Physics* **114**, 185 ,1994.

Chapter

3

Extremal characterization of band gaps in nonlinear gratings

Abstract[†]. In this paper we present an explicit extremal characterization of the edges of the lowest (first) band gap in gratings; we restrict here to the case of TE-modes, but the TM case can be treated similarly. The characterization is valid for linear and Kerr-nonlinear gratings, for smooth as well as for step-variations of the index and the coefficient of nonlinearity. The variational characterization allows one to derive monotonicity properties of the band gap edges by using simple comparison arguments. For instance, the monotonic shift of the band gap as a function of the angle of oblique incidence is proved, leading to a simple criterion for omni-directionally for the band gap. Rough estimates of the band gaps can be obtained by substituting suitable trial fields in the governing functionals, while the same formulation can also be used to design a Finite Element scheme for accurate calculations.

3.1 Introduction

In this paper we will characterize for 1D gratings the precise values of the edges of the band gaps. To simplify the notation and reduce the number of formulae, we will only consider the lowest band gap. Furthermore, we will restrict to TE-modes, remarking that TM-modes can be studied similarly. On the other hand, we will allow arbitrary (periodic) index profiles and third order nonlinearity with a spatially dependent (periodic) coefficient. Then for time harmonic fields, and normal incidence, the governing

[†]This Chapter is adapted from: E. van Groesen & A. Sopaheluwakan, *Journal of Nonlinear Optical Physics and Materials*, Vol. 12, pp. 135-148, 2003.

equation for the spatially dependent amplitude E reads

$$\partial_z^2 E + \omega^2 \left[n^2(z) + \gamma(z)|E|^2 \right] E = 0. \tag{3.1}$$

Here ω is the normalized frequency (the velocity of light has been normalized to unity), $n(z)$ and $\gamma(z)$ are the index of refraction and the coefficient of nonlinearity, respectively. Special cases such as step-wise index variations and linear gratings are included. The period of the grating will be denoted by p in the following.

Studying (3.1) for varying ω leads to (nonlinear variants of) Bragg dispersion outside the band gap, and full reflection inside the band gaps. In this paper we will characterize the edges of the first band gap by giving a variational (extremal) characterization for the corresponding values of ω, i.e. we will deal with (3.1) as a (nonlinear) eigenvalue problem.

The extremal formulation will make it possible to study the dependence of the position of the band gap on the physical parameters n and γ, and will make it possible to find estimates for the band gap by comparison with simpler structures. For instance, for oblique incidence from a uniform half-space with index n_0 under an angle θ, in which case the governing equation is

$$\partial_z^2 E + \omega^2 \left[(n^2(z) - n_0^2 \sin^2\theta) + \gamma(z)|E|^2 \right] E = 0, \tag{3.2}$$

the extremal characterization will immediately give the result that the band gap shifts monotonically as a function of θ. By its nature, the extremal characterization can also be applied to obtain numerical approximations for the values of the band gap without the necessity to calculate the corresponding field profiles accurately. We will show that the use of simple field profiles suffices to obtain reasonably good approximations, with accuracy of second order in the difference of the field profiles. When more precise numerical values are desired, the formulation leads the way to simple numerical procedures for accurate calculations; by way of example we will describe this for a Finite Element Method.

3.2 Extremal characterization at normal incidence

3.2.1 Shift-skew symmetry of Edge states

For linear, infinitely long gratings the first band gap is the smallest interval of frequencies for which there is no propagating fields. Reviewing Floquet's

(Bloch's) theorem [8,9], this happens at the end of the first Brillouin zone which consists of solutions that modulate a p-periodic function $v(z)$ with a z-harmonic modulation $E = v(z)e^{iK(\omega)z}$; in the band gap, the 'wave number' $K(\omega)$ is complex, with $\mathrm{Re}(K(\omega)) = \pi/p$ and the imaginary part is the exponential growth (decay) of the solution inside the band gap. At the edges of the band gap, $\mathrm{Im}(K(\omega)) = 0$, and the solution is of the form $E = v(z)e^{i\pi z/p}$. This shows that the edge states satisfy

$$E(z+p) = -E(z)$$

which we will call 'shift-skew (ss)-symmetric'; of course this implies these states are $2p$-periodic. The edges of the band gap are the values of ω for which such a ss-symmetric solution exists. This shows that we consider (3.1) as a (nonlinear) eigenvalue problem for the set of ss-symetric functions. We can reduce this problem to a problem on an interval of one period by observing that the edge states vanish at some point, say at $z = \xi$:

$$E(\xi) = E(\xi + p) = 0,$$

which at first sight reduces the problem to a simple Dirichlet boundary value problem (DBVP). However, the precise position of the interval is not known in advance, i.e. ξ is unknown. Having a solution on the specified interval, a smooth, i.e. differentiable, ss-symmetric continuation is possible only if the derivatives at the endpoints are related according to:

$$\partial_z E(\xi) = -\partial_z E(\xi + p).$$

This additional condition should be added to the DBVP. An arbitrary choice of ξ will not lead to a solution that satisfies this condition, but in the following we will see that for a suitable ξ this condition can be satisfied.

3.2.2 Variational formulation

The linear DBVP, $\gamma = 0$, is a standard linear eigenvalue problem for which eigenvalues ω^2 and eigenfunctions can be found in a well known variational way [1] as the critical values and points of the Rayleigh quotient. Briefly, if u is a critical point of the quotient $R(u) = Q(u)/\, N_{lin}(u)$, where

$$Q(u) = \int_{\xi}^{\xi+p} (\partial_z u)^2 \, dz, \quad N_{lin}(u) = \int_{\xi}^{\xi+p} n^2(z) u^2 dz,$$

and satisfies the Dirichlet conditions, then u satisfies (3.1) with ω^2 given by the value of this quotient at the solution. The quadratic homogeneity of the functionals implies that any of the functionals can be taken as constraint for variations of the other functional; the constraint prescribes the norm of the solution to be found. For the linear problem, the value of the constraint is irrelevant, but it is the constrained formulation that can be generalized to the nonlinear problem, in contrast to the formulation with the Rayleigh quotient. This generalization will now be described.

To include the nonlinearity, define the functional

$$N(u) = \int_{\xi}^{\xi+p} \left[n^2(z)u^2 + \frac{1}{2}\gamma(z)u^4 \right] dz$$

and consider the constrained maximization problem

$$\max_u \ \{ \ N_\xi(u) \mid \ Q(u) = A, \quad u(\xi) = u(\xi + p) = 0 \ \}.$$

Then, Lagrange's multiplier rule applies and states that for some multiplier λ the maximizer U satisfies the Euler Lagrange equation

$$n^2(z)U + \gamma U^3 = -\lambda \partial_z^2 U,$$

the constraint condition, and the Dirichlet boundary conditions. Provided λ is positive, for $\omega^2 = 1/\lambda$ this is precisely (3.1). By multiplying this equation by U, and integrating over the interval, shows that λ is given by $\lambda = \int \left[n^2U^2 + \gamma U^4 \right] / \, Q(U)$; for positive γ this is positive, but it is also positive for negative γ provided the nonlinearity is not too large.
The maximizer U found in this way is not yet an acceptable field distribution E since the additional boundary condition still has to be satisfied. And, preferably, a more explicit characterization of the multiplier. To that end, we investigate the dependence of the value of the minimization problem on the position of the interval and the value of the constraint:

$$V(A, \xi) = \max_u \ \{ \ N(u) \mid \ Q(u) = A, \quad u(\xi) = u(\xi + p) = 0 \ \}$$

and denote for given ξ the maximizing solution by U and the multiplier by λ. Then we have both desired results as follows.

Claim 1 *For any ξ, the multiplier is the derivative with respect to the constraint of the value function:*

$$\lambda = \frac{d}{dA} V(A, \xi).$$

For given A, let $\bar{\xi}$ be a critical point of the value function $V(A, \xi) : \partial_\xi V(A, \bar{\xi}) = 0$. Then the corresponding solution $U(\bar{\xi})$ satisfies the additional boundary condition and is an actual physical field distribution E.

The proof of the claims is based on standard reasoning from the Calculus of Variations and will therefore not be given here.

Of course, at fixed A, the value function over one period has a maximum and a minimum value, at which points the required additional boundary condition will be satisfied; the corresponding solutions and multipliers will correspond to the edges of the band gap. Based on this, we can now finish this section with a summary. At the same time we make a simplification of the notation which is handy for the following. First it is convenient to transform to a problem on a fixed interval and to replace the shift of the interval by a shift of the inhomogeneous terms in the functionals. Taking $[0, p]$ as the interval, the functionals are then given by

$$Q(u) = \int_0^p (\partial_z u)^2 \, dz, \qquad N_\xi(u) = \int_0^p \left[n^2(z+\xi) u^2 + \frac{1}{2} \gamma(z+\xi) u^4 \right] dz.$$

The formulae for the lower and the upper edge of the band gap are then

$$\begin{pmatrix} \omega^{-2} \\ \Omega^{-2} \end{pmatrix} (A) = \begin{pmatrix} \max_\xi \\ \min_\xi \end{pmatrix} \frac{d}{dA} \, V(A, \xi) \, ,$$

$$\text{with} \quad V(A, \xi) := \max_u \ \{ \, N_\xi(u) \mid Q(u) = A, \quad u(0) = u(p) = 0 \, \} \, .$$

Note that for linear gratings, with $\gamma = 0$, the value function is linear in the constraint A and the differentiation to find the multiplier can be avoided by normalizing $A = 1$.

For nonlinear gratings a similar simplification can be achieved as follows. In fact, exploiting the fact that we are dealing with integrands in the functionals that are just polynomials, and in particular that the

functional Q is quadratic, the value of the constraint can be normalized, leading to

$$V(A,\xi) := \max_u \ \{N_{\xi,A}(u) \mid Q(u) = 1, \quad u(0) = u(p) = 0\}; \tag{3.3}$$

with

$$N_{\xi,A}(u) = \int_0^p An^2(z+\xi)u^2 + \frac{1}{2}A^2\gamma(z+\xi)u^4 \, dz \tag{3.4}$$

This is the final formulation, valid for linear and nonlinear gratings, that will be used in numerical calculations in the following.

Remark 2 *For step-gratings, with steps at z_{step}, note that $\partial_\xi n^2(z+\xi) = \Sigma_{steps}\left[\pm\delta_{Dirac}(z - z_{step})\right]$, with plus or minus sign for a positive, resp. negative step. From this it follows that in a two-step grating, the values of the field at each side of a layer are either the same or opposite. The field at the lower edge is the same at the edges of the high-index material, while the field at the upper edge of the band gap is the same at the edges of the low-index region. For gratings that also have stepwise changes in the nonlinearity, additional symmetry conditions arise.*

3.3 Oblique incidence and omni-directional band gap

An immediate consequence of the extremizing formulation above is the possibility to derive inequalities. For instance, if for the same γ, the index is changed, say decreased at each point, for each trial function u, and each ξ, the functional $N_{\xi,A}(u)$ will decrease, while $Q(u)$ remains unaltered, leading to a decrease of $\frac{d}{dA}V(A,\xi)$, and then a decrease of both $\max_\xi \frac{d}{dA}V(A,\xi)$ and $\min_\xi \frac{d}{dA}V(A,\xi)$. which will correspond to an increase of the values for the band gap. We will now exploit this to investigate the omni-directionality of the band gap.

An omni-directional band gap is a range of frequency ω such that under all incident angle $\theta \in [0, \pi/2)$ there are no propagating solutions for (3.2), or total reflection. The existence of omni-directional band gap in periodic structures has also been discussed in several publications [2-5] using the transfer matrix approach. Here we use extremal characterization which will give the possibility for direct calculation of the band gap edges for arbitrary periodic index profile.

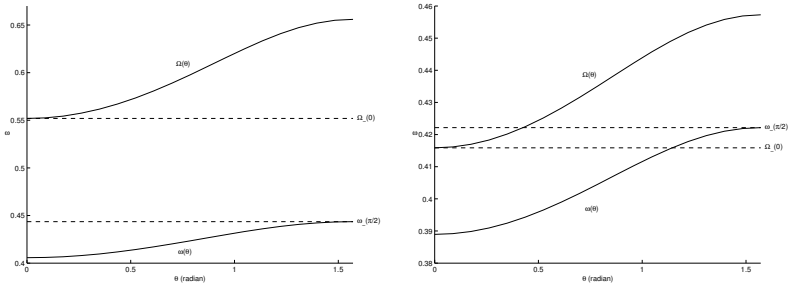

(a) Parameters: $n_0 = 1$, $n_a = 1.544 \hookrightarrow SiO_2$, $n_b = 2.616 \hookrightarrow TiO_2$, and the width of each cell: $a = b = \pi/2$.

(b) Parameters: $n_0 = 1$, $n_a = 2.354 \hookrightarrow ZnS$, $n_b = 2.616 \hookrightarrow TiO_2$, and the width of each cell: $a = b = \pi/2$.

Figure 3.1: Examples of band gap edges from structure with omni-directional band gap (a), and without omni-directional band gap (b). Parameters for these (half infinite) linear grating with step-wise varying index are as indicated above.

3.3.1 Monotonicity for oblique incidence

For oblique incidence to a linear grating ($\gamma = 0$), the index of refraction in the governing equation and in the functional $N_{\xi,A}(u)$ is replaced by the effective index $n^2 - n_0^2 \sin^2(\theta)$ with θ the angle with the normal. Hence the index decreases monotonically with increasing $\theta \in [0, \pi/2)$ to a lowest value $n^2 - n_0^2$ at grazing incidence. Assuming $n^2 - n_0^2$ to be positive, the above reasoning applies and we conclude that both band gap edges $\omega(\theta)$ and $\Omega(\theta)$ are monotonically increasing functions of θ. Examples are given in Figures 3.1.a and 3.1.b for a linear grating with step-wise varying index. Figure 3.2 shows the same pattern for a harmonic change of the index; this case cannot be solved explicitly and the plot has been produced using the numerical method to be explained below.

For a linear grating the value function is linear in the constraint A, and has nonzero derivative for each A. For small nonlinearity, the monotonicity in θ will therefore not be disturbed; an example is shown in Figure 3.3.

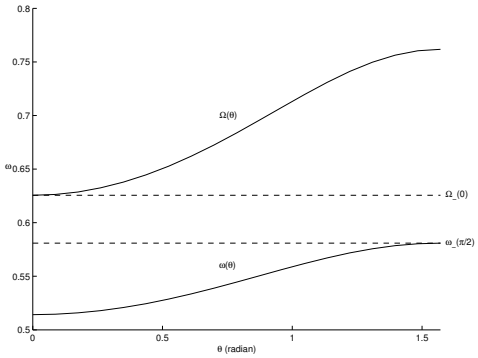

Figure 3.2: Band gap edges for (half infinite) linear grating with harmonic index profile $n(z) = \bar{n}(1 + \varepsilon \cos(z))$. Here $\bar{n} = 1.923 \hookrightarrow \mathrm{ZrSiO_4}$, and $\varepsilon = 0.2$.

3.3.2 Omni-directional band gap

Omni-directional reflectance will be present when the lower edge at grazing incidence is smaller than the upper edge value at normal incidence

$$\omega(\pi/2) < \Omega(0)$$

A sufficient condition could be obtained from an upperbound for $\omega(\pi/2)$ and a lowerbound for $\Omega(0)$. An upperbound for $\omega(\pi/2)$ has been constructed above. A lowerbound for $\Omega(0)$ can be obtained from the saddle point character: in each neighbourhood there are functions with a lower value. Explicit functions can be found as follows. Suppose $U_\zeta(z)$ is the solution corresponding to

$$U_\zeta(z) \in \min_\xi \frac{d}{dA} V(A, \xi)$$

which reaches the minimal value at $\bar{\zeta}$:

$$\Omega^{-2}(0) = N_{\bar{\zeta},A}(U_{\bar{\zeta}}, 0)$$

Then a lower value is attained for each U_ζ with ζ close to $\bar{\zeta}$. In a numerical procedure that searches for this minimum, such functions will be easily found.

Remark 3 *More fundamentally, it can be found by observing that it is a function in the tangent direction:* $U_{\bar{\zeta}} + \varepsilon W$ *with* $W = \partial_\zeta U_\zeta(z)|_{\zeta=\bar{\zeta}}$. *For*

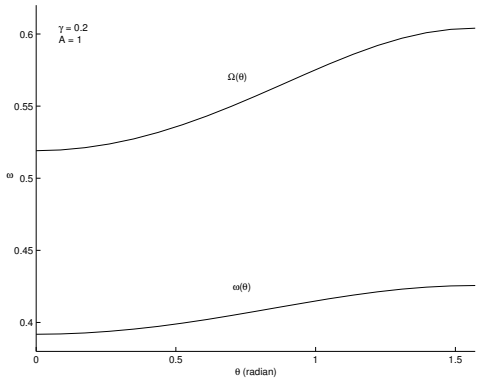

Figure 3.3: Band gap edges for (half infinite) nonlinear grating with step-wise varying index. Parameters: $n_0 = 1$, $n_a = 1.544 \hookrightarrow \mathrm{SiO}_2$, $n_b = 2.616 \hookrightarrow \mathrm{TiO}_2$, and the width of each cell: $a = b = \pi/2$. Furthermore $\gamma = 0.2$ and $A = 1$.

linear gratings, W satisfies the same equation (but with different boundary conditions: $W(\bar{\zeta}) = -W(\bar{\zeta} + p) \neq 0$). Hence it is the solution adjoint to $U_{\bar{\zeta}}$ that can be expressed in a standard way for second order equations, explicitly:

$$W(z) = U_{\bar{\zeta}}(z) \int^z \frac{dz'}{U_{\bar{\zeta}}(z')^2}$$

Hence, having found an approximation for $U_{\bar{\zeta}}(z)$ an approximation for W can thus be derived and a shift in this direction will produce a lower bound, provided the approximation is sufficiently accurate.

For nonlinear gratings, W will satisfy the linearized equation and a similar reasoning applies.

3.4 Approximate and numerical results

In the previous section we have shown the applicability of the extremal characterization to obtain monotonicity properties about the dependence on the angle of incidence. Now we show that as another consequence of the formulation we can derive simple approximations for the band gap, or, alternatively, design a simple FEM code with which accurate calculations can be performed.

3.4.1 Approximate field functions

Just as the minimum value of a function can be estimated above by its value at *any* point, we can take an 'arbitrary' function (or a parameterized family of trial functions) in the variational formulation and find bounds for the value function and then the band gap edge. Of course, the accuracy of the bound depends on the choice of the trial function.

To show this in some detail, for instance to approximate the lower edge, take a function W that satisfies the Dirichlet boundary conditions and then find the optimal value of the index-shift. With the normalization $Q(W) = 1$, for each ξ

$$V(A, \xi) := \max_u \ \{ \ N_{\xi,A}(u) \mid \ Q(u) = 1, \ \} \geq N_{\xi,A}(W)$$

and hence $\max_\xi V(A, \xi) \geq N_{\xi,A}(W)$ and then

$$\max_\xi V(A, \xi) \geq \max_\xi N_{\xi,A}(W)$$

For a linear problem (take $A = 1$) this implies we have an immediate upperbound for the lower edge:

$$\omega^{-2} \geq \max_\xi N_{\xi,A}(W)$$

and similarly for the upper edge for a trial function V:

$$\Omega^{-2} \geq \min_\xi N_{\xi,A}(V).$$

with rhs that can be computed directly.

With respect to the quality of the upperbound depending on the choice of W and V, it should be noted that 'first order' accuracy of the field will lead to second accuracy in the determination of the critical values, owing to the fact that the first order terms vanish because of the critical point property.

Below in Figure 3.4 we show the resulting graphs for the choice $W(z) = V(z) = \sin(z\pi/p)$ for each θ; this function is known to be exact when there is no index variation, and hence can be expected to be accurate for shallow gratings.

For nonlinear gratings, as an example, we calculate the band gap edges using the trial function $W(z)$ as above, $p = \pi$.

$$\begin{aligned}\begin{pmatrix} \omega^{-2} \\ \Omega^{-2} \end{pmatrix}(A) &= \begin{pmatrix} \max\limits_{\xi} \\ \min\limits_{\xi} \end{pmatrix} \frac{d}{dA} N_{\xi,A}(W) \\ &= \begin{pmatrix} \max\limits_{\xi} \\ \min\limits_{\xi} \end{pmatrix} \int_0^{\pi} (n^2(z+\xi) - n_0^2 \sin^2(\theta)) \sin^2 z \; dz \\ &+ A\gamma \int_0^{\pi} \sin^4 z \; dz\end{aligned}$$

Evaluating the integral above results in an explicit function of ξ for the band gap edges

$$\begin{pmatrix} \omega^{-2} \\ \Omega^{-2} \end{pmatrix}(A) = \begin{pmatrix} \max\limits_{\xi} \\ \min\limits_{\xi} \end{pmatrix} \frac{1}{2}(n_b^2 - n_a^2)\sin(2\xi) + \frac{\pi}{4}(n_b^2 + n_a^2) - \frac{\pi}{2} n_0^2 \sin^2\theta + A\gamma\frac{3\pi}{8}$$

Clearly, ω^{-2} and Ω^{-2} is obtained if $\xi = \pi/4$ and $\xi = 3\pi/4$ respectively. We show the resulting band gap edges in Figure 3.6.a for various values of γ.

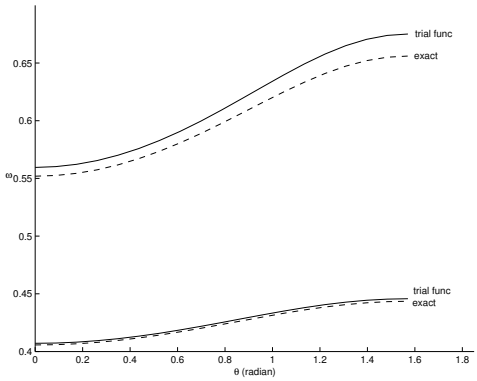

Figure 3.4: Band gap edges approximation using trial function $W(z) = sin(z\pi/p)$ (solid line) as indicated above and the exact result (dashed line), for (half infinite) linear grating with step-wise varying index. Parameters: $n_0 = 1$, $n_a = 1.544 \hookrightarrow SiO_2$, $n_b = 2.616 \hookrightarrow TiO_2$, and the width of each cell: $a = b = \pi/2$.

3.4.2 FEM calculations

Above we took a simple harmonic function as trial function. Another way, to obtain more accurate results, is to approximate a function as a superposition of base function, and optimize with respect to the choice of the expansion coefficients. If the base functions are taken to be local spline functions this leads to the Finite Element Method. We will now briefly describe this. For a given grid, $(z_0, z_1, ..., z_N, z_{N+1})$, with $z_0 = 0, z_{N+1} = p$, take piecewise linear base functions: φ_m with $\varphi_m(z_m) = 1$, and vanishing at other grid points. For a given function write $u(z) = \Sigma_{m=1}^{N} u_m \varphi_m(z) \equiv \vec{u} \cdot \vec{\varphi}(z)$ with $u_m = u(z_m)$. Then 'discretize' the functionals by restriction to such expansions, obtaining functions of $\vec{u}$:

$$\hat{Q}(\vec{u}) := Q(\vec{u} \cdot \vec{\varphi}(z)), \quad \hat{N}_{\xi,A}(\vec{u}) := N_{\xi,A}(\vec{u} \cdot \vec{\varphi}(z))$$

The corresponding extremal problem then leads, for fixed ξ, to the Euler Lagrange equation for $\vec{u}$:

$$\nabla \hat{N}_{\xi,A}(\vec{u}) = \mu \nabla \hat{Q}(\vec{u}),$$

where ∇ consists of differentiation with respect to the vector $\vec{u}$. In more detail, the equation contains matrices F_ξ, G and a matrix $R(\vec{u})$ depending quadratically on $\vec{u}$ such that

$$\left[AF_\xi + A^2 R(\vec{u})\right] \vec{u} = \mu G \vec{u}.$$

For linear problems, $R = 0$, this is a standard eigenvalue problem, for which the largest eigenvalue is sought, say $\mu(\xi)$. Then $\max_\xi \mu(\xi)$ leads to an approximation for the lower edge, and $\min_\xi \mu(\xi)$ for the upper edge of the band gap.

When the problem is nonlinear, an iteration method is required to deal with the nonlinearity; a simple way is to take the nonlinear term at a previous iterate:

$$\left[AF_\xi + A^2 R(\vec{u}^{(j)})\right] \vec{u}^{(j+1)} = \mu^{(j+1)} G \vec{u}^{(j+1)}, \quad Q(u^{(j+1)}) = 1.$$

When converged, the computed largest eigenvalue $\mu(\xi)$ gives the value function $V(A, \xi)$ for a fixed value of A. Then a central difference scheme is used to calculate the derivative of the value function, which leads just as above to the approximations of the lower and upper edge.

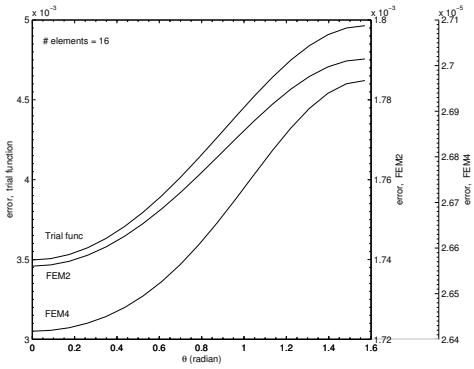

(a) In the figure above, 16 elements is used for both FEM2 and FEM4.

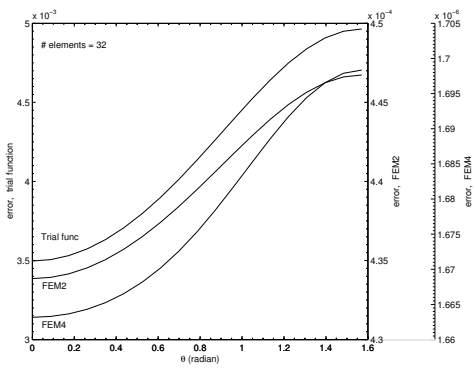

(b) In the figure above, 32 elements is used for both FEM2 and FEM4.

Figure 3.5: Errors of using trial function, FEM2 and FEM4, for (half infinite) linear grating with step-wise varying index. Parameters: $n_0 = 1$, $n_a = 1.544 \hookrightarrow SiO_2$, $n_b = 2.616 \hookrightarrow TiO_2$, and the width of each cell: $a = b = \pi/2$.

The method described above is second order accurate, say FEM2. When taking a uniform mesh, with an even number of points, a simple method known as Richardson extrapolation [6] can be used to arrive at a fourth order scheme: FEM4. We have used this method to obtain the previous figures when no exact solution was possible.

Below we show the performance in a linear case with step-index for which the exact band gap can be calculated with matrix transfer technique: in Figure 3.5.a and 3.5.b we present the error for the lower edge of the band gap, defined as

$$error = \frac{|\omega_{appr} - \omega_{exact}|}{\omega_{exact}}$$

for three different methods: the trial function $\sin(\pi z/p)$, FEM2 and FEM4 for 16 and 32 elements.

In Figure 3.6.a and 3.6.b, the results for a nonlinear grating with a trial function and FEM4 are shown. The finite elements calculations were implemented using MATLAB. Each set of computations, such as the graphs in Figure 3.6 takes less than two seconds on a regular PC.

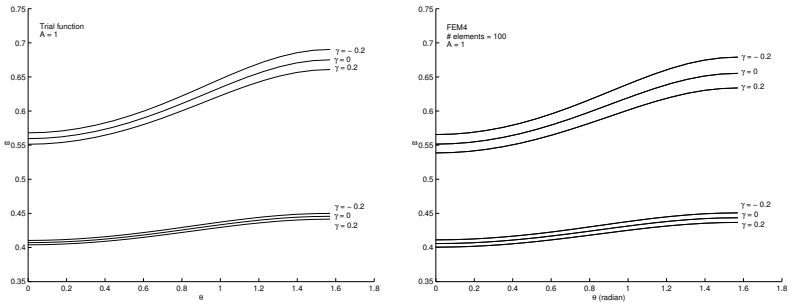

(a) Band gap edges for nonlinear grating using the trial function $W(z) = sin(z\pi/p)$.

(b) Band gap edges for nonlinear grating using FEM4 with 100 elements.

Figure 3.6: Result of using the trial function (a) and FEM4 (b), for (half infinite) nonlinear grating with step-wise varying index. Here we take $A = 1$ and the values of $\gamma = -0.2$, 0, and 0.2. Parameters: $n_0 = 1$, $n_a = 1.544 \hookrightarrow SiO_2$, $n_b = 2.616 \hookrightarrow TiO_2$, and the width of each cell: $a = b = \pi/2$.

3.5 Conclusion and remarks

In this paper we have characterized the edges of the first band gap in a variational way. Essential for that is that we can use the fact that the corresponding fields vanish at the end points of an interval of length equal to the period of the grating. Would the interval have been known in advance, a standard eigenvalue problem, extended to nonlinear case, would have resulted. Since the fields have to be extendable to $2p$-periodic skew-symmetric fields, the interval had to be chosen appropriately, which could also be formulated in a variational way. For the lower-edge a double maximization formulation resulted, while for the upper-edge a mini-max formulation makes the saddle point character explicit. This can be interpreted that the sine and cosine solutions of the Helmholtz equation that exist when the index is constant and the gap is closed, bifurcate into the two branches parameterized by the index difference.

Simple comparison arguments were used to show that the extremal characterizations lead to the conclusion that the band gaps shift monotonically with increasing angle of incidence.

The extremal characterization makes it possible to express the value

of the band gap without the necessity to calculate the edge fields in all details. Taking simple trial functions for the fields at the edges, good predictions of the band gap were found, both for linear and nonlinear gratings. For more accurate quantitative results, a numerical calculation scheme based on the FEM was designed and showed good results, fourth order of accuracy when Richardson extrapolation was applied.

The FE-scheme is used here for the approximate solution of the (nonlinear) eigenvalue problem; a comparable scheme has been used in Ref. [7] to calculate the transmittance properties, and to study the bi-stablity near band gap edges, for a grating of finite length (without and with defects; see also the references in that paper to relevant literature). This problem can also be studied qualitatively by using variational methods as will be shown in a forthcoming paper. An extension of the methods of this paper to more space dimensions seems also possible, in particular for planar photonic periodic structures.

Bibliography

[1] R. Courant and D. Hilbert. *Methods of Mathematical Physics, vol 1.* Interscience Publishers, 1953.

[2] D. N. Chigrin, A. V. Lavrinenko, D. A. Yarotsky and S. V. Gaponenko, Observation of total omnidirectional reflection from a one-dimensional dielectric lattice, *Applied Physics* **A 68**, 25, 1999.

[3] D. N. Chigrin, A. V. Lavrinenko, D. A. Yarotsky and S. V. Gaponenko, All-dielectric one-dimensional periodic structures for total omnidirectional reflection and patial spontaneous emission control, *Journal of Lightwave Technology* **17**, 2018, 1999.

[4] J. Lekner, Omnidirectional reflection by multilayer dielectric mirrors, *Journal of Optics* **A 2**, 349, 2000.

[5] A. Iskandar and J. Prawiharjo, Understanding dielectric mirror, in *Proceedings of Symposium on Modern Optics and Periodic Optical Systems*, Bandung, 2002.

[6] H. P. Uranus, H. J. W. M. Hoekstra and E. van Groesen, Fourth-order variational mode solving for anisotropic planar structures, *Journal of Nonlinear Optical Physics and Materials* **12**, 247, 2003.

[7] A. Suryanto, E. van Groesen, M. Hammer and H. J. W. M. Hoekstra, A simple finite element scheme to study the nonlinear respons of a finite grating without and with defects, *Optical and Quantum Electronics* **35**, 313, 2003.

[8] C. Kittel. *Introduction to Solid State Physics.* Wiley, New York, 1996.

[9] J.K. Hale. *Ordinary Differential Equations.* Wiley-Interscience, 1969.

Chapter

4

Direct characterization of states and modes in defect grating structures

Abstract[†]. For one dimensional optical structures consisting of gratings surrounding a defect region, optical field solutions inside the bandgap are investigated that are steady states or fully transmitted modes. The observation that a mode is a suitable combination of two states, and that each state is a resonant phenomenon, implies that an accidental degeneracy condition has to be satisfied in order that two states occur at the same frequency. Finding the conditions, and thereby the required design-parameters of the structure, makes it possible to characterize the modes without the necessity to scan the whole bandgap for transmission properties. The mathematical formulation is based on the optical transfer map and leads to a non-standard, not well-studied, eigenvalue problem on the defect region with effective boundary conditions that simulate the surrounding gratings.

Keywords: Optical defect grating structures, bandgap states and modes, optical transfer map, non-standard eigenvalue problem.

4.1 Introduction

In this paper we consider the transmission through one-dimensional grating structures that consist of a 'defect' region that is positioned between two infinite gratings or between two finite gratings placed in an exterior uniform medium. In particular we will address the problem of the direct

[†]This Chapter is adapted from: E. van Groesen, A. Sopaheluwakan and Andonowati, *Journal of Nonlinear Optical Physics and Materials*, Vol. 13, pp. 155-173, 2004.

characterization of so-called defect modes (DM) that can be observed to appear for specific defect frequencies (DF) in the bandgap (BG) of certain finite defect grating structures. This appearance is remarkable since in a uniform grating without defect the bandgap is the interval of wavelengths for which the structure acts like an almost perfect mirror. In Figure 4.1 (left) the transmittance curve of a uniform periodic grating is depicted, and we can see that there is an interval of frequency where the transmittance is zero (BG). When the periodicity of the grating is broken by a defect layer, then a DM appear inside the BG with a transmittance value equal to unity, see Figure 4.1 (right). The field profile of such a DM is illustrated in Figure 4.2.

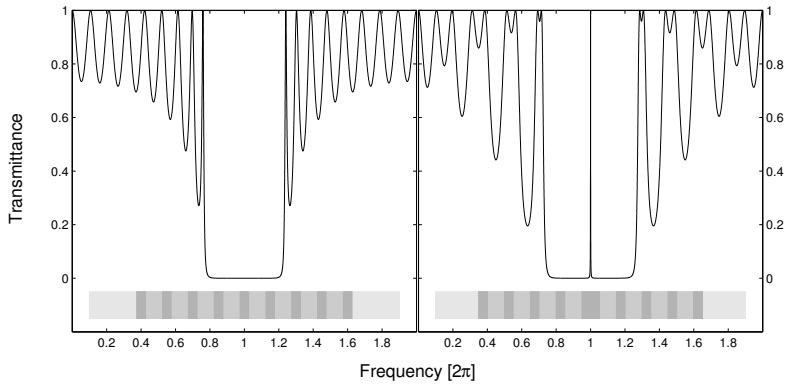

Figure 4.1: *Left:* relative optical transmittance $|T|^2$ versus the frequency, for perpendicular plane wave incidence on a multilayer stack of transparent dielectric materials. The symmetric, finite periodic grating consists of 17 inner layers, alternating with low refractive index $n_1 = 1.25$ and high refractive index $n_2 = 2.5$, with their thicknesses satisfying $n_1 l_1 = n_2 l_2 = 1/4$ (quarter-wavelength stack). The outermost layers are of the high index material; we assume the structure to be surrounded by air (refractive index $n_0 = 1.0$). *Right:* analogous to the one on the left, for a grating, where the central, high refractive index layer is twice as thick as the neighboring layers with high refractive index. Observe the additional transmission maximum at the design frequency $\omega = 1 \cdot 2\pi$.

For several applications and for fundamental understanding of the resonance phenomenon, it is desirable to characterize the DF and DM in a

direct way, avoiding the necessity to scan with transmittance experiments the whole frequency range in the BG. Except when transfer matrix techniques (TMT) can be used, which is restricted to linear materials with step-wise index structures, no analytic ways to tackle this problem seem to exist. This will be the aim and contribution of this paper: to characterize in a direct way the DF and DM. The formulation will in principle be applicable for arbitrary material properties within the defect region, even if it is inhomogeneous or nonlinear. Further it is possible, to design simple numerical programs, Finite Element for instance, that use only the defect region as calculational domain. First the problem for defect states (DS) will be addressed. This DS is the solution of an eigenvalue problem in the frequency ω, which problem is, for Kerr-type of nonlinear materials, of the form

$$\partial_z^2 u + \omega^2 \left[n_d^2(z) + \chi \left| u \right|^2 \right] u = 0, \quad \text{for } z \in (-L, L) \tag{4.1}$$
$$\partial_z u = \kappa_\pm(\omega) u \quad \text{at } z = \pm L$$

Note that the (possibly nonlinear) Helmholtz equation is dressed up with so-called 'effective' boundary conditions at the boundary $\pm L$ of the defect region; these bc's replace the optical effect of the surrounding gratings. The fact that these effective boundary conditions depend on the frequency itself makes this a *non-standard* eigenvalue problem: even when the field equation is linear ($\chi = 0$) the eigenvalue appears in a nonlinear (and non-polynomial) way in the functions $\kappa(\omega)$. Not much is known yet about such eigenvalue problems in its generality; we will restrict therefore to special cases in the following, leaving a more complete investigation for later.

Having found DS's in finite gratings, defect modes will then be investigated. Different from DS's, which are non-translating states with vanishing Poynting quantity, a DM is a fully transmitted solution, and hence has nonzero Poynting quantity. Such DM will be obtained from a superposition of DS's at the same frequency. In fact, in the structures that we consider, there exist one so-called amplified DS with largely amplified field in the defect which closely resembles a DM. However, the non-translating property of a DS, and the translating property of a DM, also in the exterior uniform medium, make them very different, and a relation seems difficult to establish. The explanation for this apparent discrepancy is the coexistence of an attenuated DS at the same frequency which, when suitably superimposed with the amplified one, leads to the correct influx and trans-

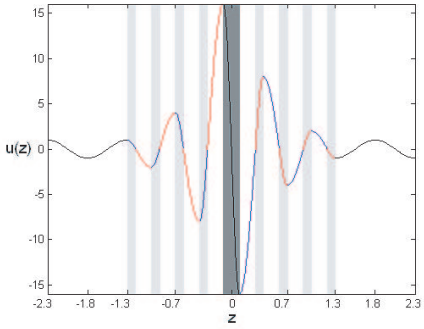

Figure 4.2: Defect mode profile of the defect grating structure in Figure 4.1 (right)

mittance properties while hardly changing the field profile in the defect region. This attenuated DS may be easily overlooked as being uninteresting in itself. Yet its contribution to the DM is essential: in exterior regions it is of the same order as the amplified state and together they can constitute a traveling wave; in the defect region, despite its small amplitude, the combination with the amplified state produces the correct value of the Poynting quantity.

Bragg gratings that have step-wise index changes caused by a periodic succession of materials with different index have been studied extensively [1,2]. In all cases the gratings can be viewed as one-dimensional versions of photonic bandgap materials or photonic crystals [3,4]. When in such a grating the periodicity is broken either in a geometric way, or by index changes, a 'cavity' is created in between two nearly completely reflecting mirrors. A Fabry-Perot cavity as described e.g. in Refs. [2,5-7] can be viewed as a result of such a 'defect' in a Bragg grating. The appearance of defect modes and the building up of a high intensity in the defect (growing with the number of periods in the supporting Bragg reflectors), has been investigated for linear and nonlinear structures by means of finite-element techniques [8,9]. The wavelength (frequency) of the defect mode depends sensitively on the refractive index in the cavity. Furthermore, according to systematic studies in Refs. [8] and [9], the width of the resonances can be narrowed - and the steepness of the transmission curve increased - by

extending the length of the cavity segment or by increasing the number of periods in the reflectors. These two properties of a DM explain the interest in structures which support DM's to design optical devices with various functionality. For instance, for sensor applications, the property can be used such that external influences on the defect region (temperature, stress, light) will affect the defect index; measuring the resulting change in the DF will correspond to the external effect. Another application is to exploit the amplified intensity to enhance the small nonlinear effects of nonlinear materials [9].

In section 4.2 we introduce a slightly novel way to characterize the optical properties of gratings; this will make it easier in the following to optically connect the gratings to the defect and surrounding regions by effective boundary conditions. Then in section 4.3 we construct DS's for various defect grating structures. In section 4.4, for symmetric structures consisting of two finite gratings surrounding a linear defect region, it is shown that a superposition of two coexisting DS's can produce a DM. In section 4.5 we will make several remarks about possible extensions of the methods.

4.2 Optical characterization of gratings

In this section we study the gratings that constitute important building blocks of the considered structures. We will introduce a novel way of describing the optical properties of gratings, or of any layered structure for that matter, which will allow to express the optical effect of the grating directly into a form, through effective boundary conditions, that allows a direct optical adjustment to surrounding media. We will only consider the TE-case, but the same method can be applied for TM polarization.

4.2.1 The Optical Transfer Matrix

The optical properties of any inhomogeneous interval $[0, L]$ are, for TE-polarization, completely determined by the connection of the field and its derivative at the end and at the beginning of the interval:

$$\begin{pmatrix} u \\ \partial_z u \end{pmatrix}_{z=L} = T(\omega) \begin{pmatrix} u \\ \partial_z u \end{pmatrix}_{z=0}$$

where the optical transfer map (or matrix) (OTM) T depends on ω. Since for linear materials there are precisely two independent solutions, the two boundary values at each of the two endpoints, and the observation that the amplitude of a solution is arbitrary, leads to the conclusion that three (real-valued) quantities are needed for a full characterization.

Although the OTM is closely related to the usual transfer matrix technique (TMT) for layered structures, see e.g. Refs. [10] and [11], and can be found for such structures from such TMT calculations, the OTM does not depend on the choice of base functions, and therefore makes it possible to describe in a direct way the connection between adjacent regions by continuity conditions at the endpoints, irrespective which method or base functions are used to calculate the OTM of the separate regions. This turns out to be very efficient and convenient in dealing with gratings in composite structures, as we shall see.

Restricting to frequencies inside the first BG of a linear grating, we will show that two of the basic quantities, denoted in the following by $\kappa^{\pm}(\omega)$, are the value of the quotient $\partial_z u/u$ at the edge (facet) of one (and any) period for the real valued attenuated and amplified independent solutions $G^{\pm}$; the notation $\kappa = \infty$ is used to denote the case when u vanishes at the period facet. The gain factor per period, denoted by g, is the third basic variable. The optical transfer properties of a grating with N periods are determined by the OTM which is then given by

$$T_N(\omega) = \frac{(-1)^N}{\kappa^- - \kappa^+} \begin{pmatrix} \kappa^- g^N - \kappa^+/g^N & -g^N + 1/g^N \\ \kappa^+\kappa^- \left(g^N - 1/g^N\right) & -\kappa^+ g^N + \kappa^-/g^N \end{pmatrix} \tag{4.2}$$

Note that $\det(T) = (-1)^N$, expressing area conservation in phase space. We will give the derivation of the OTM in the following section.

For frequencies inside the first BG we will give explicit formulas for the example of a linear grating with two layers; extension of the number of layers, or for arbitrary layered structures, composition of the matrices can be invoked. For smoothly varying index changes and or nonlinear materials, results of characterization of this OTM, and of the basic quantities by explicit variational expressions, will be published elsewhere.

4.2.2 Grating properties

Let n be the index of refraction that is periodic with period p. Then, according to Bloch's (Floquet) theorem for periodic structures, each solution

of

$$\partial_z^2 u + \omega^2 n^2(z) u = 0$$

can be written as a combination of two independent solutions that are of the form

$$u(z) = v(z)e^{iK(\omega)z}, \qquad v(z+p) = v(z)$$

where $K(\omega)$ describes the Bragg dispersion properties of the grating. For frequencies within the first BG, the value of K is given by $K(\omega) = \pi/p \pm i\rho(\omega)$, and the two corresponding real valued solutions are given by

$$G^{\pm}(\omega; z) = w^{\pm}(z)e^{\pm\rho z}, \quad w(z+p) = -w(z), \quad \rho > 0.$$

Since the quotient $\partial_z G/G$ is p-periodic, this value of this quotient is the same at each period-facet. Hence we can define real valued numbers associated with these solutions by

$$\kappa^{\pm}(\omega) := \frac{\partial_z G^{\pm}}{G^{\pm}} \text{ evaluated at (any) period-facet.}$$

Denoting by $g(\omega) := \exp(\rho(\omega)p)$ the 'gain-factor' per period (Floquet multiplier), we have $G^+(z+p) = -gG^+(z)$ and $G^-(z+p) = -G^-(z)/g$. The three quantities $g, \kappa^{\pm}$ can now be used to determine the OTM as follows. Any solution within the grating can be written as a superposition: $u = AG^+ + BG^-$. At the left facet of a period, say at $z = 0$, the solution and its derivative are given by:

$$\begin{aligned} u(0) &= AG^+(0) + BG^-(0) \\ \partial_z u(0) &= \kappa^+ AG^+(0) + \kappa^- BG^-(0), \end{aligned}$$

while after N periods, $z = Np$, these quantities are given by

$$\begin{aligned} u(Np) &= (-g)^N AG^+(0) + (-g)^{-N} BG^-(0) \\ \partial_z u(Np) &= \kappa^+ (-g)^N AG^+(0) + \kappa^- (-g)^{-N} BG^-(0). \end{aligned}$$

Eliminating the amplitude factors $AG^+(0), BG^-(0)$ leads to the OTM given in (4.2).

Calculation of the optical quantities

Consider as an example the case of a grating consisting of two layers with indices $n_{1,2}$ and width $\ell_{1,2}$, so that the period is given by $p = \ell_1 + \ell_2$; for notational convenience we use $k_{1,2} = \omega n_{1,2}$. Introducing phase parameters α, β, the solutions can be written down explicitly. For the 'amplified' solution we find:

$$G^+ = \begin{cases} \cos(k_1 z - \alpha) & \text{for } 0 \le z \le \ell_1 \\ \frac{\cos(k_1 \ell_1 - \alpha)}{\cos \beta} \cos(k_2 (z - \ell_1) - \beta) & \text{for } \ell_1 \le z \le p \end{cases}$$

which is a solution provided

$$k_1 \tan(k_1 \ell_1 - \alpha) = -k_2 \tan \beta$$
$$k_2 \tan(k_2 \ell_2 - \beta) = -k_1 \tan \alpha.$$

Having solved for α and β, the basic quantities can then be expressed in

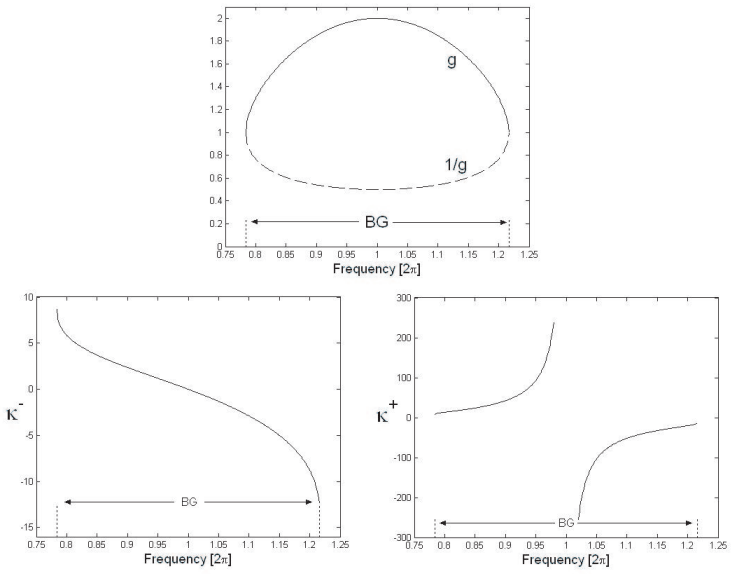

Figure 4.3: Plot of the gain factor $g(\omega)$, $\kappa^+(\omega)$ and $\kappa^-(\omega)$

the geometric and material properties of the grating trough the values of α

and β as follows:

$$g = -\frac{\cos(k_1\ell_1 - \alpha).\cos(k_2\ell_2 - \beta)}{\cos\alpha.\cos\beta}$$
$$\kappa^+ = k_1\tan\alpha, \quad \kappa^- = -k_2\tan\beta$$

Then an independent attenuated solution follows from reversibility:

$$G^- = \begin{cases} g\cos(k_1(\ell_1 - z) - \alpha) & \text{for } 0 \le z \le \ell_1 \\ -\frac{\cos(k_1\ell_1 - \alpha)}{\cos\beta}\cos(k_2\,(p - z) - \beta) & \text{for } \ell_1 \le z \le p \end{cases}$$

Quarter wave stack example

We present some graphical information about the relevant quantities for the case of a so-called quarter wave stack structure with two layers in Figure 4.3. Such a structure has the same optical path length in each layer since by design $n_1\ell_1 = n_2\ell_2 = 1/4$.

For indices $n_1 = 1.25$ and $n_2 = 2.5$, the band gap, determined by values ω for which $g > 1$, is the interval $2\pi \cdot [0.7836, 1.2163]$. Then, for the special ('design') frequency ω_0 such that $\omega_0 n_1\ell_1 = \pi/2$, a quarter 'wave length', it follows that the two basic solutions have at a period facet the boundary values

$$G^+(0) = 0, \partial_z G^+(0) = 1 \text{ and } G^-(0) = 1, \partial_z G^-(0) = 0$$

(when the low index layer is the first layer; else the signs are interchanged) corresponding to $\kappa^+(\omega_0) = 0$, $\kappa^-(\omega_0) = \infty$, while the gain factor is maximal $g = 2$.

For the design frequency, plots of the solutions G^+ and G^- are depicted over a distance of four periods, in which a gain of $2^{\pm 4}$ is visible, in Figure 4.4 below.

4.2.3 Effective Boundary conditions

The two basic solutions $G^\pm$ considered above are of no relevance for infinitely long gratings since then both are unbounded, and the only bounded solution is the vanishing field, the characteristic property of an infinitely long grating. When the grating is half-infinite, one solution is bounded inside the grating. Take as example the half-infinite grating at the left, say

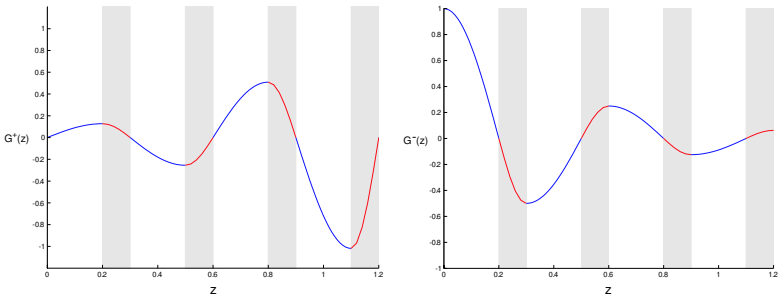

Figure 4.4: Plots of G^+ and G^- over four periods

$(-\infty, -L)$; then only the amplified solution G^+, that decays to zero at $-\infty$, is nontrivial and bounded. The optical effect of this half-infinite grating is then completely determined by the value κ^+. Stated differently, any field at the right should satisfy the boundary condition

$$\partial_z u = \kappa^+ u \text{ at } z = -L;$$

for obvious reasons we will call this an 'effective boundary condition' (EBC).

Remark 4 *The above formulation makes it possible to give a somewhat different interpretation to the value κ^+ which may also be more constructive in case when no explicit analytical solutions can be found, for instance for nonlinear gratings. In fact, the value of the coefficient κ^+ can be described in a variational way using the Helmholtz functional on the half-infinite interval. Specifying the amplitude at the end point, arbitrary for linear gratings, the characterization is :*

$$\kappa^+(\omega) = \inf \left\{ \int_{-L}^{\infty} \left\{ (\partial_z u)^2 - \omega^2 n^2 u^2 \right\} dz \,\middle|\, u(-L) = 1 \right\},$$

i.e. the value function of the Helmholtz functional is $\kappa^+ u(-L)$, see Ref. [12]. For nonlinear gratings the value of the amplitude has to be taken into account and appears nonlinearly in the result. This formulation makes it feasible to calculate the coefficient κ^+ numerically.

When the grating is finite, both basic solutions are bounded, and for optical communication with the two exterior sides the OTM-approach can

be applied. For instance, consider the configuration of a uniform medium at the left with index n_{left} and a finite grating of N periods between $[-M, -L]$. When we consider the transmission problem with a given influx from the left, the solution for $z < -M$ is given by

$$u(z) = Ae^{ik_{left}(z+M)} + re^{-ik_{left}(z+M)}$$

with A the influx amplitude and r the amplitude of the reflected wave. Then

$$\begin{pmatrix} u \\ \partial_z u \end{pmatrix}_{z=-L} = T_N(\omega) \begin{pmatrix} u \\ \partial_z u \end{pmatrix}_{z=-M} = T_N(\omega) \begin{pmatrix} 1 & 1 \\ ik_{left} & -ik_{left} \end{pmatrix} \begin{pmatrix} A \\ r \end{pmatrix}$$

from which we can solve $\partial_z u(-L)$ as function of A and $u(-L)$, leading to the effective boundary condition at $z = -L$.

A somewhat different interpretation is to look at the effect of influx from the left-most uniform exterior on the basic solutions in the finite grating. Taking the field in the uniform medium at the left that is consistent with the basic (amplified or attenuated) state in the grating, the state will be a standing wave $C\cos(k_0(z+M)+\theta)$ with $k_0\tan(\theta) = \kappa$, and so will be the state in the uniform medium to the right of the grating. The attenuated state will correspond to a very small amplitude state at the right. However, for the grating placed in air at both sides, an influxed wave $e^{ik_0 z}$ only from the left (no incoming wave from the right) will not be a standing wave: it will not be totally reflected and there is a small transmittance. Related to this is a slightly different effective bc at the grating end at $z = -L$. This will depend on the number of gratings: for increasing number of periods the presence of the uniform exterior becomes rapidly very small, see Figure 4.5 for the effective boundary value κ_N of the transmittance problem through the grating with N periods compared to the value κ^- for the half-infinite grating.

4.2.4 States and modes

In the following sections we will characterize special field distributions that may exist in defect grating structures. In section 4.3 we will investigate defect states DS, and in section 4.4 defect modes DM. The difference between the two is that a DS is a 'standing wave' while a DM is a traveling wave that is completely transmitted through the structure.

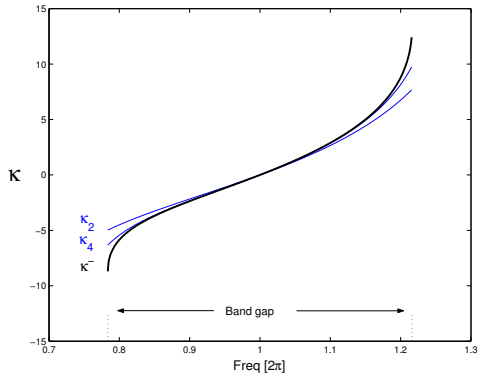

Figure 4.5: Graph of κ_N for $N = 2, 4$ and κ^-

As is well known, the Poynting vector can be used to distinguish clearly between standing waves and traveling (not necessarily completely transmitted) solutions.

In the one-dimensional case considered here, we will use the Poynting quantity which is related to the Poynting vector as being *the powerflow in the z-direction of the electromagnetic field.* For any solution u of the Helmholtz equation, the Poynting quantity is given by $P(z) := \mathrm{Im}\left[\frac{1}{\omega}\bar{u}\partial_z u\right]$, and is independent of z :

$$P(z) := \mathrm{Im}\left[\frac{1}{\omega}\bar{u}\partial_z u\right], \quad \partial_z P(z) = 0. \tag{4.3}$$

The relevance of this quantities becomes clear by investigating it for a uniform medium, say index n_0; with $k_0 = \omega n_0$, any solution consists of a superposition of a right and a left traveling wave $u = Ae^{ik_0 z} + Be^{-ik_0 z}$ and we find that at any position z :

$$P = n_0\left[|A|^2 - |B|^2\right].$$

In general, P measures the net flow of the power transported to the right and the left; our interest is that it clearly identifies a state as a solution for which $P = 0$ (then $|A| = |B|$ and the solution is a standing wave: $u = |A|\cos(k_0 z + \psi)$ for some ψ). A traveling wave, possibly superimposed

by a standing wave, will have $P \neq 0$, and so, in particular, any DM will have $P \neq 0$.

When investigating the so-called transmittance problem for an optical structure, one looks at a wave influxed from a uniform medium at the left, say, and investigates its transmittance through the structure into a uniform medium at the right, where no influx from the right into the structure is supposed. A DS cannot be obtained in that manner, since it has standing wave in the left region (meaning that an incoming wave $e^{ik_0 z}$ is compensated with a reflected wave of the same amplitude, forming together a standing wave) and just as well a standing wave in the 'outflux'-region at the right. This means that there is not only an outgoing wave to the right, but just as well a wave coming in from the right and hence a defect state cannot be 'produced' by light influxed from one side only.

4.3 Defect states in grating structures

In this section we consider various grating structures with defects; in each case we will employ effective boundary conditions for the defect region to replace the optical properties of the surrounding gratings. The interest is to find defect states, i.e. solutions with vanishing Poynting quantity P. In structures that contain at least one half-infinite grating, any nontrivial solution will have vanishing Poynting quantity and so any solution is a state.

4.3.1 Defect states between half-infinite gratings

When a defect region is introduced in an infinite grating, the defect separates a left and a right half infinite grating. The amplified state in the left grating can possibly be connected in the defect region to the attenuated state in the right one for suitable frequencies. Such 'resonant' frequencies will depend on properties of the gratings and of the defect region. The problem can be formulated as an eigenvalue problem on the defect region, say $[-L, L]$, when we use effective boundary-conditions at the defect boundaries:

$$\partial_z u = \kappa^+_{left}(\omega) u \text{ at } z = -L, \quad \partial_z u = \kappa^-_{right}(\omega) u \text{ at } z = L \qquad (4.4)$$

where we use obvious notation for the amplified/attenuated state in the left/right grating. If for some defect frequency there exists a field distribu-

tion inside the defect region that satisfies these two boundary conditions, a defect state is obtained.

Note that for this formulation it is not necessary that left and right gratings are the same. But it should be remarked that, even when the problem is linear, the eigenvalue problem is non-standard since the eigenvalue (ω) appears in a nonlinear way so that even methods for 'polynomial' eigenvalue problems [13,14] cannot be applied directly. Existence of a solution is therefore a nontrivial matter. When, in addition, the Helmholtz equation is nonlinear, bistable solutions can be expected to exist under certain circumstances [9]. We will show here that for some specific cases we can directly find the solution; more general results will be published elsewhere.

Consider the case of a linear defect region with constant index n_d. Then the general solution in the defect region is of the form

$$u = A\cos(\omega n_d z + \theta).$$

Satisfying the boundary conditions leads to the condition for ω

$$\omega n_d \tan(\omega n_d L - \theta) = \kappa^+_{left}(\omega) \text{ and } \omega n_d \tan(\omega n_d L + \theta) = -\kappa^-_{right}(\omega).$$

Eliminating θ leads to the equation for ω for arbitrary integer m :

$$2\omega n_d L = \arctan(\kappa^+_{left}(\omega)/\omega n_d) - \arctan(\kappa^-_{right}(\omega)/\omega n_d) + m\pi.$$

Since the right-hand-side is bounded, while the left-hand side is linear in ω, for suitable m there exists at least one solution that belongs to the band gap; the corresponding value of θ is then found from

$$2\theta = -\arctan(\kappa^+_{left}(\omega)/\omega n_d) - \arctan(\kappa^-_{right}(\omega)/\omega n_d) + m\pi$$

Hence we conclude that for a uniform defect region between arbitrary half-infinite gratings there always exists at least one DS.

In Figure 4.6 below we show an example for a quarter wave stack defect grating with low refractive index $n_1 = 1.25$ and high refractive index $n_2 = 2.5$. The defect layer between the two half infinite gratings has index $n_d = 2.5$ and twice as thick as the high index layer. The intersection between the function $f_1(\omega) = \arctan(\kappa^+_{left}(\omega)/\omega n_d) - \arctan(\kappa^-_{right}(\omega)/\omega n_d) + \pi$ and $f_2(\omega) = 2\omega n_d L$ gives the defect frequency $\omega = 1 \cdot 2\pi$.

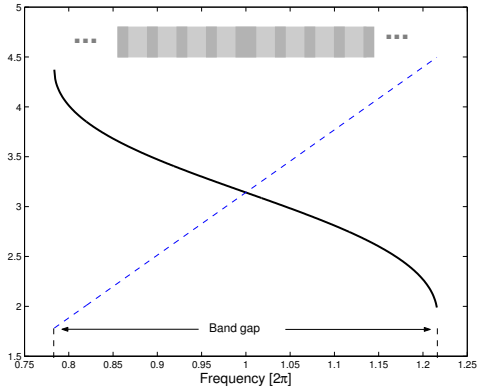

Figure 4.6: The graph of $f_1(\omega) = \arctan(\kappa^+_{left}(\omega)/\omega n_d) - \arctan(\kappa^-_{right}(\omega)/\omega n_d) + \pi$ (solid curve), and $f_2(\omega) = 2\omega n_d L$ (dashed line).

4.3.2 States for a single finite grating

Consider a finite grating, of N periods in the interval say $[-M, M]$; let $\kappa^{\pm}(\omega), g(\omega)$ be given, and take a uniform medium at both sides, index n_{left} for $z < -M$, n_{right} for $z > M$.

Then, for *each* ω in BG there is an increasing and a decreasing state which connect standing waves in the exteriors through the respective increasing and decreasing grating solutions $G^{\pm}$. Indeed, the total solution is of the form

$$u = \begin{cases} A\cos(\omega n_{left}(z+M) + \psi_{left}) & \text{for } z < -M \\ aG(z) & \text{for } -M < z < M \\ B\cos(\omega n_{right}(z-M) + \psi_{right}) & \text{for } z > M \end{cases}$$

Continuity of the field derivative leads to the two equations

$$\kappa(\omega) = -\omega n_{left}\tan(\psi_{left}) = -\omega n_{right}\tan(\psi_{right})$$

from which the values of ψ follow. For the amplitudes we then find

$$A\cos(\psi_{left}) = aG(-M), B\cos(\psi_{right}) = aG(M)$$

with $G(M) = (-g)^{\pm N}G(-M)$ corresponding to an amplitude amplification/attenuation g^N. In particular, when exteriors are identical, $B =$

$(-g)^N A$ for the amplified solution and $B = A/(-g)^N$ for the attenuated solution.

4.3.3 States in a defect grating

The result above for a single finite grating can now be used to investigate states in structures with a succession of possibly different finite gratings placed in air by composition of the OTM's. We will consider the case of one defect region $[-L, L]$ with two adjacent gratings in $[-M_{left,} - L]$ and $[L, M_{right}]$ only; for more defect regions between gratings, additional degeneracy conditions will have to be satisfied for a state to exist.

A defect state of the whole structure will couple in the defect region a decreasing or increasing state in the left grating to an increasing or decreasing state in the right grating. Suppose the left and right gratings are characterized by their values $\kappa^{\pm}$ and the gain factor g per period. Then with each possible combination of states in the separate gratings, a defect state of the whole structure is found for the frequency that solves an eigenvalue problem of the form shown in (4.1) on the defect region $[-L, L]$. Using obvious notation for the state S that corresponds to the different possible choices of the behaviour in the constituent gratings, we obtain the following four different possible states:

- S^{++}: the state that is amplified in both gratings;
- S^{+-}: the state that is amplified in the left grating and attenuated in the right grating;
- S^{-+}: the state that is attenuated in the left grating and amplified in the right grating;
- S^{--}: the state that is attenuated in both gratings.

We will denote the state S^{+-} by S^{+} in the following and call this the 'amplified' state since it has large amplitude inside the cavity compared to the exterior; likewise we will denote S^{-+} by S^{-} and call it the attenuated state since it has small amplitude in the defect region compared to the exterior. We will see in the next section that these two states can under specific conditions form a defect mode. The state S^{+} and S^{-} are solution of the eigenvalue problem on the defect region with boundary values

$$\text{for } S^{+} : \partial_z u = \kappa^{+}_{left}(\omega) u \text{ at } z = -L, \quad \partial_z u = \kappa^{-}_{right}(\omega) u \text{ at } z = L, \quad (4.5)$$

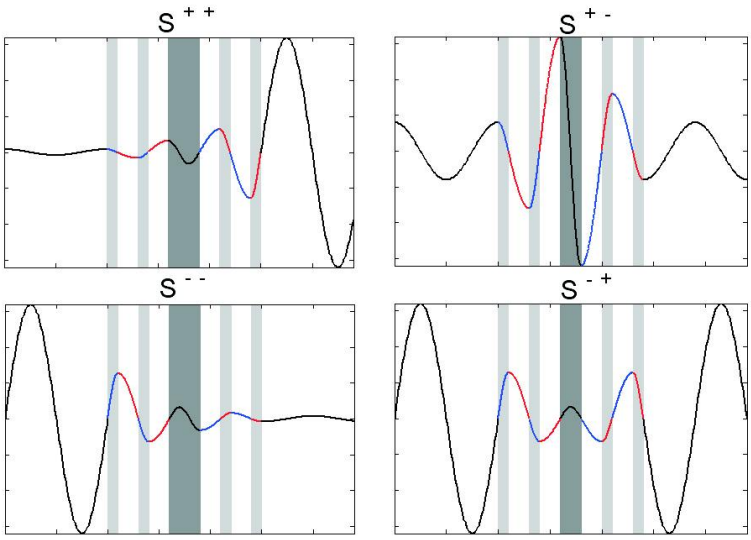

Figure 4.7: Illustration of four different possible states in a defect grating.

$$\text{for } S^- : \partial_z u = \kappa^-_{left}(\omega)u \text{ at } z = -L, \quad \partial_z u = \kappa^+_{right}(\omega)u \text{ at } z = L. \tag{4.6}$$

In general a defect frequency ω_+ of the amplified state will not coincide with a defect frequency ω_- of the attenuated state. For further use in the next section, we observe the phase difference of the solution over the defect-grating structure as follows. The amplified/attenuated state can be represented in the uniform exterior regions as (for $s = +$ or $s = -$)

$$S^s = \begin{cases} a_s \cos(\omega_s n_{left}(z + M_{left}) + \alpha_s) & \text{for } z < -M_{left} \\ b_s \cos(\omega_s n_{right}(z - M_{right}) + \beta_s) & \text{for } z > M_{right} \end{cases}$$

corresponding to a phase change of $\beta_s - \alpha_s$ over the complete structure; this phase change can also be found from the value of the Helmholtz functional.

4.4 Defect modes

We will now study the transmittance problem, and in particular solutions that are completely transmitted: defect modes.

The general transmittance problem is often studied by numerical methods, and by scanning the frequency range inside a band gap it is then

observed that defect modes can exist for certain resonant frequencies. Such a DM looks very similar to a defect state S^+ as characterized above. This is remarkable because the behaviour in the influx and outflux regions is completely different, and a defect mode can be created by one-sided influx, while a defect state cannot.

4.4.1 Defect mode decomposed into defect states

Consider a linear grating structure with one defect as considered above. If a defect mode exists for some defect frequency ω_d, its behaviour in the exterior regions is given by

$$M_d = \begin{cases} a_d \exp i(\omega_d n_{left}(z + M_{left}) + \alpha_d) & \text{for } z < -M_{left} \\ b_d \exp i(\omega_d n_{right}(z - M_{right}) + \beta_d) & \text{for } z > M_{right} \end{cases}$$

with real amplitudes a_d (which can be taken arbitrary) and b_d which satisfy (from Poynting conservation)

$$n_{left} a_d^2 = n_{right} b_d^2.$$

Now observe that, given a DM, the real and imaginary part of this mode are also solutions. Since these solutions are real, each has vanishing Poynting quantity. $\mathrm{Re}(M_d)$ and $\mathrm{Im}(M_d)$ are therefore two different defect states of the structure that exist at the same defect frequency ω_d. Moreover, each of these states has the same phase difference $\beta_d - \alpha_d$ over the total defect grating structure.

4.4.2 Defect mode as superposition of defect states

Now consider a defect grating structure for which we have identified four different DS's in subsection 4.3.3. We want to investigate under which conditions a DM exists in such a structure and how it can be obtained from a superposition of the two identified DS's S^+ and S^-; for definiteness, we normalize the amplitude of these waves at the left uniform exterior region and take $\alpha_+ = 0, \alpha_- = -\pi/2$, so that

$$S^+ = \cos(\omega n_{left}(z + M_{left})) \text{ for } z < -M_{left},$$
$$S^- = \sin(\omega n_{left}(z + M_{left})) \text{ for } z < -M_{left},$$

For later reference, we note that $S^+\partial_z S^- - S^-\partial_z S^+ = \gamma$ is a non-zero constant over the whole structure, in fact $\gamma = \omega n_{left}$.

In view of the results in the previous subsection, at least two accidental degeneracy conditions should be satisfied in order that a defect mode can exist. Restricting the further investigation to symmetric structures only, for which $n(z) = n(-z)$, we will now investigate the possibilities. For a symmetric structure it holds that

$$\kappa^+_{left} = -\kappa^-_{right} \text{ and } \kappa^-_{left} = -\kappa^+_{right},$$

and hence the Bc's are:

$$\text{for } S^+ : \partial_z u = -\kappa^-_{right}(\omega)u \text{ at } z = -L, \quad \partial_z u = \kappa^-_{right}(\omega)u \text{ at } z = L,$$
$$\text{for } S^- : \partial_z u = -\kappa^+_{right}(\omega)u \text{ at } z = -L, \quad \partial_z u = \kappa^+_{right}(\omega)u \text{ at } z = L.$$

Any solution in the defect region is of the form $u_d = A\cos(\omega n_d z + \theta)$, and hence

$$\left.\frac{\partial_z u_d}{u_d}\right|_{z=-L} = -\omega n_d \tan(-\omega n_d L + \theta), \left.\frac{\partial_z u_d}{u_d}\right|_{z=L} = -\omega n_d \tan(\omega n_d L + \theta).$$

In view of the Bc's for $S^\pm$ a first condition follows from the requirement that

$$\omega n_d \tan(-\omega n_d L + \theta) = -\omega n_d \tan(\omega n_d L + \theta)$$
$$\tan(\omega n_d L - \theta) = \tan(\omega n_d L + \theta)$$

from which we conclude that necessarily $\theta = 0$ or $\theta = \pi/2$. The two possible solutions in the defect region are therefore the symmetric and the skew-symmetric functions $\cos(\omega n_d z)$ and $\sin(\omega n_d z)$.

This leads to two cases depending on which defect solution will connect which state: for a solution with skew-symmetric amplified, and symmetric attenuated state we find the two conditions

$$\omega n_d \cot(\omega n_d L) = \kappa^-_{right}$$
$$-\omega n_d \tan(\omega n_d L) = \kappa^+_{right}$$

and for solution with symmetric amplified, and skew-symmetric attenuated state the conditions are:

$$-\omega n_d \tan(\omega n_d L) = \kappa^-_{right}$$
$$\omega n_d \cot(\omega n_d L) = \kappa^+_{right}$$

It is clear that for arbitrary grating the two conditions cannot be satisfied for the same ω, which means that only specific gratings can support a DM.

The case of a QWS is an example that can satisfy these conditions, at the design frequency ω_0 with $\omega_0 n_1 \ell_1 = \pi/2$, $\kappa^+_{right} = 0, \kappa^-_{right} = \infty$. Hence if the optical length of the defect region satisfies $\omega_0 n_d L = m\pi/2$ for some integer m, then for $m = odd$ we get we a skew-symmetric state S^+ and a symmetric state S^-, while for $m = even$ we get we a symmetric state S^+ and a skew-symmetric state S^-.

Each state has a standing wave at the influx region, but the phases of each will be different. Therefore a suitable complex combination will produce a pure influx wave from the left. Because of the normalization for

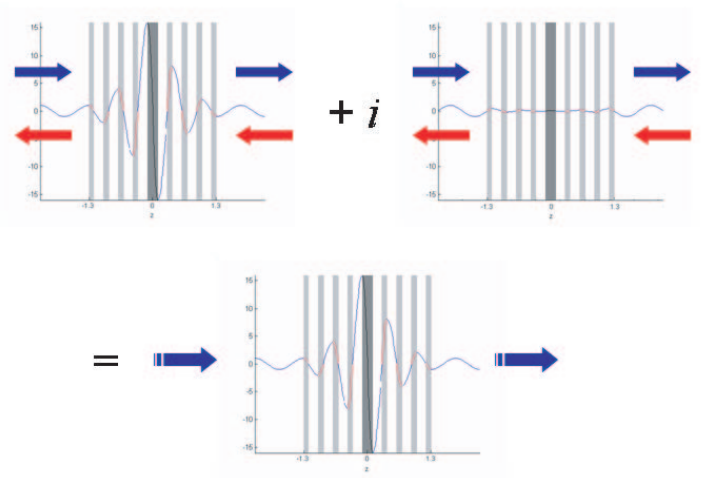

Figure 4.8: Construction of the defect mode from complex superposition of the 'amplified' and 'attenuated' states.

the states chosen above, we get for the specific complex superposition a purely incoming wave at the left:

$$u_M := S^+ + iS^- = \exp i(\omega_0 n_{left}(z + M)) \text{ for } z < -M.$$

The (skew-) symmetry of the states $S^\pm$ guarantee that their phase difference over the total structure is the same for both. Hence, the same

superposition produces a pure outflux wave at the right:

$$S^+ + iS^- = \exp i(\omega_0 n_{right}(z - M)) \text{ for } z > M.$$

It is interesting to see the importance of the attenuated state in the construction of this mode. In the exterior regions both constituent states have the same amplitude while in the defect region between gratings of N layers, the attenuated state has amplitude g^{-N} while the amplified state has amplitude g^N. Consequently, for large N, the contribution to the field profile of the attenuated state is hardly visible and the mode profile resembles the profile of the amplified state. Yet for the propagating property of the mode the contribution of the attenuated mode is essential, as seen by considering the Poynting quantity:

$$\begin{aligned} P\left(S^+ + iS^-\right) &= P(S^+) + P(S^-) + \mathrm{Im}\left(\frac{i}{\omega}S^+\partial_z S^- - \frac{i}{\omega}S^-\partial_z S^+\right) \\ &= 0 + 0 + \frac{1}{\omega}\left[S^+\partial_z S^- - S^-\partial_z S^+\right] = n_{left} \end{aligned}$$

since $P\left(S^{\pm}\right) = 0$ and $\frac{1}{\omega}\left[\, S^+\partial_z S^- - S^-\partial_z S^+\right] = n_{left}$ constant over the whole structure. See Figure 4.8 above for the illustration.

4.5 Remarks and conclusions

One dimensional grating structures as investigated in this paper are simple cases of two and three dimensional photonic structures. The mathematical methods, and the observed phenomena in this paper should therefore be helpful for a further investigation and understanding of these more-dimensional cases.

Concerning the mathematical methods, the use of the optical transfer matrix has proven to be fruitful to decompose the structure and to investigate the problems on successive intervals with effective boundary conditions replacing the optical effect of the adjacent intervals. However, the resulting boundary-value problem, and in particular the eigenvalue problem, is nonstandard since the eigenvalue (frequency) to be found appears in a nonlinear, non-algebraic way. Solving such problems is not easy since both a priori existence statements, as well as effective (iterative) solution methods, have still to be developed.

The optical phenomena found show an essential difference between the appearance of states and modes. In section 4.3 it is shown that states can be found as solutions of an eigenvalue problem. For the relatively simple cases to which we restricted ourselves, this eigenvalue problem could be solved by finding a solution of a transcendental equation for the frequency. No specific grating properties are required for their existence. However, in section 4 we showed that a mode, a full-transmitted traveling wave through the structure, corresponds to the existence of two different states, which requires the frequency to satisfy two such equations. Even for symmetric structures, these equations can only be satisfied simultaneously if an accidental degeneracy condition is satisfied, which means that the grating properties should be chosen appropriately. A quarter wavelength stack was shown to be an example that has the desired degeneracy properties, and defect modes were identified.

The findings in this paper can be useful for some applications of optical grating structures. For instance for the design of sensors, when the critical dependence of the defect frequency for a mode is to be used to detect changes in the optical properties in the structure. The existence of multiple states in a defect finite grating could have applications, for instance to construct an optical memory when light influx from both sides can control the change of the state.

Bibliography

[1] R. Kashyap. *Fiber Bragg Gratings*. Academic Press, 1999.

[2] N. Liu, Defect modes of stratified dielectric media, *Physical Review* **B 55**, 4097, 1997.

[3] J. D. Joannopoulos, R. D. Meade, and J. N. Winn. *Photonic Crystals: Molding the Flow of Light*. Princeton, 1995.

[4] S. G. Johnson and J. D. Joannopoulos. *Photonic Crystals: The Road from Theory to Practice*. Kluwer, 2002.

[5] A. Figotin and A. Klein, Localization of light in lossless inhomogeneous dielectrics, *Journal of the Optical Society of America* **A 15**, 1423, 1988.

[6] A. Figotin and A. Klein, Midgap defect modes in dielectric and acoustic media, *SIAM Journal on Applied Mathematics* **58**, 1748, 1988.

[7] S. Fan, J. N. Winn, A. Devenyi, J. C. Chen, R. D. Meade, and J. D. Joannopoulos, Guided and defect modes in periodic dielectric waveguides, *Journal of the Optical Society of America* **B 12**, 1267, 1995.

[8] A. Suryanto, E. van Groesen, M. Hammer, and H. J. W. M. Hoekstra, A finite element scheme to study the nonlinear optical response of a finite grating without and with defect, *Optical and Quantum Electronics* **35**, 313, 2003.

[9] A. Suryanto, E. van Groesen, and M. Hammer, Finite element analysis of optical bistability in one-dimensional nonlinear photonic band gap structures with a defect, *Journal of Nonlinear Optical Physics and Materials* **12**, 187, 2003.

[10] P. Yeh. *Optical Waves in Layered Media*. Wiley-Interscience, 1988.

[11] J. Lekner. *Theory of Reflection of Electromagnetic and Particle Waves*. Nijhoff, Dordrecht, 1987.

[12] E. van Groesen, Variational modelling for integrated optical devices, in *Proceedings of the 4th IMACS Symposium on Mathematical Modeling*, 76-82, TU Vienna, Austria, 2003.

[13] G. L. G. Sleijpen, J. G. L. Booten, D. R. Fokkema and H. A. van der Vorst, *BIT Numerical Mathematics* **36**, 595, 1996.

[14] G. L. G. Sleijpen, H. A. van der Vorst, and E. Meijerink, *Electronic Transactions on Numerical Analysis* **7**, 75, 1998.

Chapter 5

Pulse loading and radiative unloading of an optical defect grating structure: low dimensional modeling and numerical simulations

Abstract[†]. We present a low dimensional model for pulse loading and radiative unloading of an optical defect grating structure. This model describes accurately the process when a light pulse with spectral components confined to the band gap is incident towards a defect grating structure, including the radiative decay of the stored energy. The qualitative and quantitative aspects of the dynamics of each phase are given in terms of the defect states which define the leaky modes of the structure. We will show that both the loading and unloading phase of the process are mainly determined by a characteristic quantity which is the energy content of the amplified state. For a given structure, the result of the low dimensional model is compared with direct calculations using a FETD method.

Keywords: Defect grating structure, leaky modes, defect states, loading, radiative unloading, low dimensional model, FETD.

5.1 Introduction

The study of wave propagation through multilayer structures has been extensive in recent years with many contributions to the literature. A periodic arrangement of dielectrics is usually called a grating. A special property of such structures is the *band gap*: an interval of frequencies for which light can not propagate through the structure. This property of the grating has been exploited to make various devices. A grating embedded in an optical fiber (usually called a Fiber Bragg Grating (FBG)) is utilized to make

[†]This Chapter is submitted to Optics Communications.

sensor applications for various physical quantities, such as heat [6,7], strain [7,8], or concentrations of chemical substances [9]. Another application is to use the grating as a switch. If the refractive index of the grating is nonlinear (intensity dependent refractive index), a bistability phenomenon will occur: for sufficiently large intensity of the influxed electric field, there can be more than one output intensity, which can be utilized as a switch [10]. Another type of switching device uses two influx waves [11]: one wave acts as a pump and the other one as a probing wave with frequency inside the band gap, near the edge. Increasing the intensity of the incoming pump wave will shift the edges of the band gap [10,11], and this makes way for the probe wave to transmit through the grating structure.

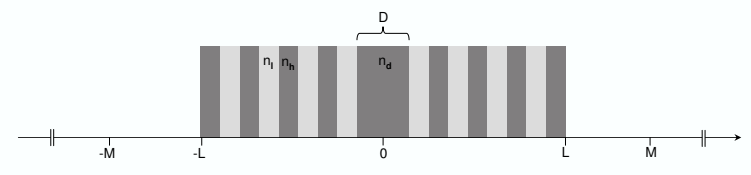

Figure 5.1: A symmetric quarter wave stack structure surrounded by air is considered as an example for the calculation in this paper.

All of the application devices above are based on a uniform grating structure. If we break the periodicity of the grating structure, say with one layer of a different material or a different geometry, the exceptional layer is called a defect layer, and the whole structure is called a defect grating structure. An example of such structure is illustrated in Figure 5.1. Due to this defect layer, there may be an additional resonant frequency inside the band gap. For this special frequency, the defect frequency, the electric field inside the grating is largely enhanced compared to the influxed intensity [10,11]. We can use this intensity enhancement for sensor purposes as well as for switching purposes. When the refractive index of the grating is nonlinear, frequencies near the defect frequency can be used for bistably controlled switching, where the threshold intensity needed to obtain bistability is reduced significantly [10].

The phenomena and applications described above are based on an influx wave with a single frequency. But in principle, switching and sensing with a defect grating structure can also be performed using time limited

influx (pulses), see e.g. [11,13]. In this paper, we will consider a time dependent problem for a defect grating structure. We will study the behavior of a pulse (which has many spectral components) incident onto a defect grating structure, for which all spectral components of the pulse are inside the band gap. See Figure 5.2 for the illustration.

We organize this paper as follows. In Section 5.2, we give a description of the Finite Element Time Domain method (FETD) that is used to directly solve the problem, and show the result of an example. In Section 5.3 we describe the defect states of a defect grating structure, and use energy arguments to derive the corresponding leaky mode of each state. Further we explain the loading and the unloading phase, a low dimensional model using the leaky modes in Section 5.4. In Section 5.5, we compare the result of the direct FETD calculation and the low dimensional model.

5.2 Finite Element Time Domain calculation

In this Section, we describe shortly the derivation for the direct calculation of the problem introduced in Section 5.1. Different from the analytical calculation that we have presented in [1], here we will use the Finite Element Time Domain (FETD) method. In the following Subsections, the approach for the Finite Element discretization of the spatial variable will be described, of which the use of transparent influx boundary condition is most important, followed by a Subsection for the time integration. At the end of this Section we will show the result for the example introduced in Section 5.1. For simplicity of exposition we will consider the TE-case; the TM case is similar.

5.2.1 Wave equation, weak formulation

Throughout this paper, we will use the space variable z and time t that are both dimensionless. We have scaled the 1-D Maxwell's equation with the following scaling: $z = \tilde{z}/\lambda$ and $t = \tilde{t} \cdot c/\lambda$ where $\tilde{z}$ and $\tilde{t}$ are the physical space and time variable, λ and c is the wavelength and speed of light in vacuum. Applying these, the electrical field E satisfies the two way wave equation

$$\mathcal{L}(E) \equiv \partial_z^2 E(z,t) - n^2(z)\partial_t^2 E(z,t) = 0. \tag{5.1}$$

For the purpose of numerical calculations, we restrict the computational domain to the interval $\Omega = [-M, M]$ that includes the full structure. This equation has to be equipped with boundary conditions. We assume that there are no incoming waves from the right, the boundary condition at the right should be transparent for any wave traveling to the right. The boundary condition at the left should provide the desired incident pulse $E_{in}(z,t)$, while being transparent for any wave travelling to the left that is reflected from the structure. Let $E_{in}(z,t) = F(z - t/n_0)$ be the pulse which is incident to the defect grating structure, the boundary conditions are then

$$\partial_z E + n_0 \partial_t E = 0 \text{ at } z = M \tag{5.2}$$

and

$$\partial_z E - n_0 \partial_t E = 2F'(-M - t/n_0) \text{ at } z = -M. \tag{5.3}$$

Applying the standard procedure for the Finite Element Method, we observe that solving the weak formulation

$$\begin{aligned}\mathcal{F}(E,v) \equiv \int_{-M}^{M} & n^2(z)\partial_t^2 E(z,t)v(z,t) + \partial_z E(z,t)\partial_z v(z,t) \cdot dz \\ & + n_0 \partial_t E(M,t)v(M,t) + n_0 \partial_t E(-M,t)v(-M,t) \\ & + 2F'(-M - t/n_0)v(-M,t) = 0\end{aligned} \tag{5.4}$$

where $v(z,t)$ is an arbitrary test function, is equivalent to solving (5.1), with (5.2) and (5.3).

5.2.2 Space discretization of the weak formulation, FEM

Projecting onto a finite dimensional space, we discretize the interval $\Omega = [-M, M]$ into grid points $z_j = -M + j \cdot \Delta z$, where $\Delta z = (z_{j+1} - zj), j = 1..N+1$, and we expand $E(z,t)$ and $v(z,t)$ in terms of nodal basis functions $\phi_j, j = 1..N+1$ at the grid points, writing $E(z,t) = \sum_{j=1}^{N+1} e_j(t)\phi_j(z)$ and $v(z,t) = \sum_{j=1}^{N+1} v_j(t)\phi_j(z)$. Substituting these into the weak form, and choosing ϕ_j to be standard 'tent' basis functions, results in a system of ordinary differential equation

$$\mathbf{M}\ddot{\mathbf{e}} + \mathbf{C}\dot{\mathbf{e}} + \mathbf{K}\mathbf{e} = \mathbf{f} \tag{5.5}$$

where $\mathbf{e} = [e_1, ..., e_{N+1}]^T$. The matrices $\mathbf{M}$, $\mathbf{C}$ and $\mathbf{K}$ have entries as follows

$$\mathbf{M}_{ij} = \int_\Omega n^2(z)\phi_i\phi_j dz, \ \mathbf{C}_{ij} = \int_{\partial\Omega} n_0 \phi_i \phi_j dz, \ \mathbf{K}_{ij} = \int_\Omega \partial_z\phi_i \partial_z \phi_j dz$$

and the vector of influx is given by $\mathbf{f} = [2F'(-M - t/n_0), 0, ..., 0]^T$.

5.2.3 Time integration

For the time discretization we use the following scheme at the discrete time level $t = t^n = n \cdot \Delta t$

$$\begin{aligned}
\ddot{\mathbf{e}} &= (\mathbf{e}^{n+1} - 2\mathbf{e}^n + \mathbf{e}^{n-1})/\Delta t^2 \\
\dot{\mathbf{e}} &= (\mathbf{e}^{n+1} - \mathbf{e}^{n-1})/2\Delta t \\
\mathbf{e} &= \beta \mathbf{e}^{n+1} + (1 - 2\beta) e^n + \beta \mathbf{e}^{n-1} \\
\mathbf{f} &= \beta \mathbf{f}^{n+1} + (1 - 2\beta) f^n + \beta \mathbf{f}^{n-1}
\end{aligned}$$

where e^n is the discrete time representation of e, namely, $e^n = e(n\Delta t)$. This scheme is called the Newmark-Beta time integration method [4,5,12] which is unconditionally stable for $\beta \geq 1/4$. Applying this to (5.5), we obtain an implicit scheme for the new time level $n + 1$ as follows

$$\begin{aligned}
\left[\mathbf{M} + \Delta t \mathbf{C}/2 + \beta \Delta t^2 \mathbf{K}\right] \mathbf{e}^{n+1} &= \left[2\mathbf{M} - (1 - 2\beta)\Delta t^2 \mathbf{K}\right] \mathbf{e}^n \\
&- \left[\mathbf{M} - \Delta t \mathbf{C}/2 + \beta \Delta t^2 \mathbf{K}\right] \mathbf{e}^{n-1} + \Delta t^2 \left[\beta f^{n+1} + (1 - 2\beta) f^n + \beta f^{n-1}\right]
\end{aligned} \tag{5.6}$$

5.2.4 Example

Consider a symmetric defect grating structure which consists of periodically alternating layers with high and low refractive indices (n_h and n_l respectively) and thicknesses d_h and d_l. All the layers are assumed to consist of linear dielectrics, lossless, and nondispersive. The defect layer has refractive index n_d and thickness D. An example of such a structure is illustrated in Figure 5.1.

The typical response of this structure for transmission experiments is well studied [2, 10, 11]. This structure functions as a resonator, a combination between mirror and cavity, similar to a *Fabry-Perot* etalon. For a certain frequency band, the gratings on the left and right of the defect layer depicted in Figure 5.1 act as mirrors, blocking almost all the incoming light: the bandgap region of frequencies with vanishing transmittance. The defect layer, on the other hand, acts as a cavity, allowing light with a certain frequency to tunnel through the structure. The presence of the

defect layer gives an additional resonance peak in the transmittance inside the bandgap. This peak has a very narrow band where the transmittance is non vanishing. The special solution with full transmittance is called the defect mode [2, 3].

Consider a pulse incident to the defect grating structure. Illustrated in Figure 5.2 (top), is the plot of the transmittance curve of the defect grating structure together with the spectrum of the pulse on the same frequency axis. The spectrum of the incident pulse (dashed) is chosen to lie inside the bandgap. Figure 5.2 (bottom) shows the initial condition of the problem, at $t = 0$.

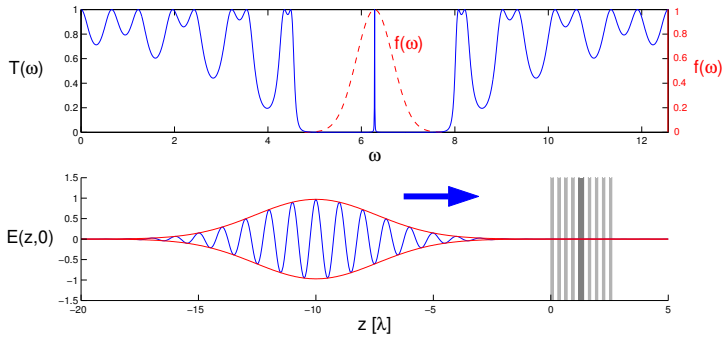

Figure 5.2: *Top*: The spectrum of the incident pulse F (dashed) together with the transmittance curve T of the defect grating structure (solid). All spectral components of the pulse lie inside the bandgap of the structure. *Bottom*: The initial situation, at $t = 0$, before the pulse is incident into the defect grating.

For the specific calculation to be presented, we took the typical defect grating configuration described in the introduction. Specifically the structure is placed in air ($n_0 = 1$), the defect layer has refractive index $n_d = 2.5$ and width $D = 1/(2n_d)$, and is surrounded by $N = 4$ grating periods with refractive indices $n_l = 1.25$ and $n_h = 2.5$, with width $d_l = 1/(4n_l)$ and $d_h = 1/(4n_h)$ respectively, see Figure 5.1. This configuration of the grating, known as a Quarter Wave Stack (QWS) structure, has defect frequency of $\omega_d = 2\pi$. The transmittance plot of the structure is shown in Figure 5.2. The chosen incoming pulse has a spectrum of Gaussian shape

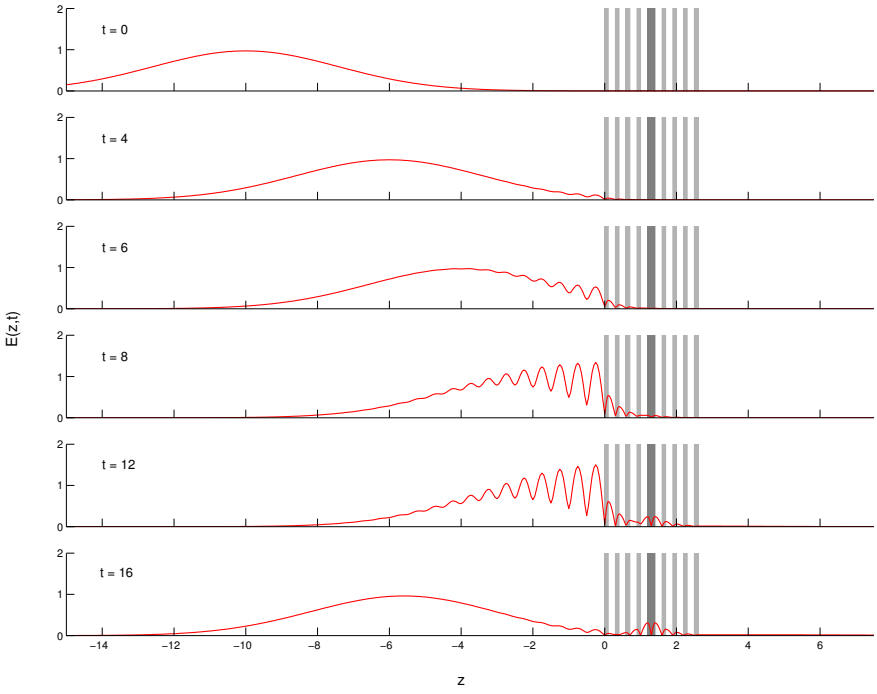

Figure 5.3: Reflection and loading phase of the pulse. Plotted is the envelope of the electric field versus distance at several instances.

centered around the defect frequency, specifically

$$\hat{F}(\omega) = e^{-(\omega-\omega_d)^2/\sigma^2} \tag{5.7}$$

and is practically confined in the band gap, for sufficiently small σ; for the following calculation we take $\sigma^2 = 0.3$. For the Newmark-Beta time integration scheme we take $\beta = 1/2$ for the calculation. The plots in Figure 5.2 refer to these choices.

Figure 5.3 shows the result of the FETD calculation for the envelope of $E(z,t)$), for various values of t. It can be seen that most part of the incoming pulse is reflected back, leaving only a small portion which is caught by the defect grating structure, and an even smaller part that is transmitted through the structure. These plots show the *loading* phase of the defect

grating structure. In Figure 5.4 we show plots of the *unloading* phase of the defect grating structure, after the process of *loading* has finished and the reflected pulse has almost left the defect grating structure. The simulation

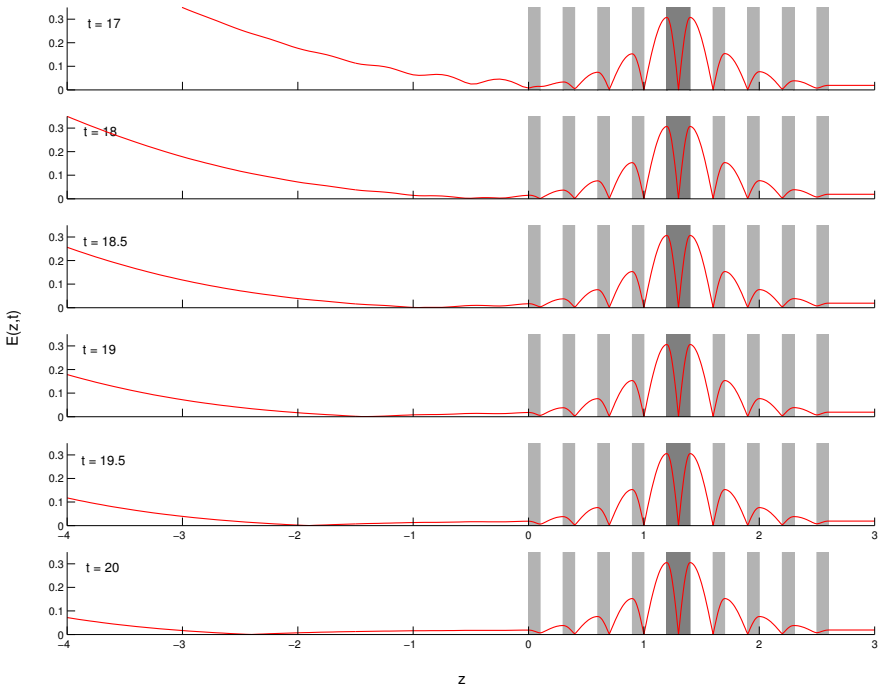

Figure 5.4: Unloading phase of the pulse. Plotted is the envelope of the electric field in the vicinity of the grating at several instances. After the pulse has reflected back to the left of the grating, the stored light inside the grating starts to radiate towards the exterior. (Note that in this plot the horizontal axis, vertical axis and the time scale is different than in Figure 5.3.).

shows that the electric field exists inside the grating for quite a long time duration after the major part of the pulse has been reflected back by the grating.

The plots of the electric field at increasing times show that, roughly

speaking, the loading phase is driven by the pulse (Figure 5.3). After a time determined by the time-length of the pulse (17 in the calculations, see Figure 5.3), the field inside the structure reaches its maximal amplitude. After a short time during which the reflected pulse interacts with the start of the radiative unloading, say $17 < t < 18.5$, the pure unloading phase shows the decrease of the field in the structure and radiation into the exterior at both sides.

From the results (see also Figure 5.8) we can see that the unloading phase develops much slower than the loading phase. The unloading phase (when structure and reflected pulse are disjoint) is independent of the pulse properties, but its duration and decay rate will depend on the specific configuration of the grating structure.

5.3 Defect states and leaky modes

Although quite straightforward, the use of FETD as above does not give much useful properties regarding the basic questions of the phenomenon. First, given a pulse and a defect grating, how much of the pulse goes inside the grating during the loading phase? And second, for a given grating configuration, can one describe the decay rate of the unloading phenomenon in terms of the grating properties? We will answer these questions by using a low dimensional model of the phenomena in this and the next Section.

In this Section we first describe the defects states of a symmetric structure. For the specific example described in Section 5.2.4 these states can be calculated explicitly using Transfer Matrix techniques, but we formulate the results for more general (defect) structures. Symmetry of the structure seems to be necessary to guarantee that there exists two states at the same defect frequency. The existence of two such states at the same frequency is equivalent to the property that there exists a pure defect mode i.e. a fully transmitted mode, see [2, 3].

These defect states are 'steady' states of the Maxwell equations, with standing wave behaviour inside and outside the structure. Practically this means that such a state can only exists when light is influxed from both sides so that the incoming light is superimposed with reflected light into a standing wave profile.

In the absence of this influxed light, these states cannot be static and are leaking towards the exterior. We will model these two leaky mode in

Section 5.3.2, and will show that the decay rate of the mode (the imaginary part of the frequency) is inversely proportional to a quantity that we will identify as the energy content of the state.

Using the leaky modes, we will model the loading and unloading of the structure by a pulse in the next Section 4.

5.3.1 Defect states

In [2, 3] we considered a linear defect grating structure for harmonic time dependent solution of the electric field. In there we have described two real valued steady states solutions of the Helmholtz equation

$$\partial_z^2 E_0 + \omega^2 n^2(z) E_0 = 0, \tag{5.8}$$

for the defect frequency $\omega = \omega_d$, which will result in the defect mode if superimposed in a certain way. These (steady) states are the *amplified* state S^+ and the *attenuated* state S^-. The *amplified* state S^+ is the electric field for frequency ω_d which satisfies

$$\omega_d^2 = \min_{E_0} \left\{ \int_0^L (\partial_z E_0)^2 dz \mid \int_0^L n^2 E_0^2 dz = 1,\ E_0(0) = 0 \right\}. \tag{5.9}$$

Then for this solution the complete boundary conditions are

$$E_0(0) = 0, \partial_z E_0(L) = 0, \tag{5.10}$$

and it can be extended to be skew-symmetric on $[-L, L]$. We call this the *amplified state* because for the specific defect grating structure considered here this solution is amplified from the exterior of the grating at the sides towards the cavity in the middle, see Figure 5.5 for the field profile. Note that for S^+ it holds that

$$\frac{1}{\omega_d^2} \int_{-L}^{L} (\partial_z S^+)^2 dz = \int_{-L}^{L} n^2 S^{+2} dz = 1. \tag{5.11}$$

For $\cos(\omega_d t)$ time dependence for this state, the corresponding magnetic field is $H = \frac{1}{\omega_d} \partial_z S^+ \sin(\omega_d t)$. The total electromagnetic energy for this state is given by

$$\begin{aligned} \mathcal{E} &= \frac{1}{2} \int_{-L}^{L} (n^2 E^2 + H^2) dz \qquad (5.12) \\ &= \frac{1}{2} \left[\cos^2(\omega_d t) \int_{-L}^{L} n^2 S^{+2} dz + \sin^2(\omega_d t) \int_{-L}^{L} \frac{1}{\omega_d^2} (\partial_z S^+)^2 dz \right], \end{aligned}$$

and because of the relation in (5.11) we can see that the time average electric and magnetic energy contributions are equal, this means that this state has *energy equipartition*. Further, the expression for the total electromagnetic energy in (5.12) simplifies to

$$\mathcal{E} = \int_{-L}^{L} n^2 (S^+)^2 dz.$$

This state is nonvanishing at the boundary, $S^+(L) \neq 0$ hence for this state we can define the normalized *energy content*

$$\mathcal{E}^+ = \frac{\int_{-L}^{L} n^2 (S^+)^2 dz}{S^+(L)^2}. \tag{5.13}$$

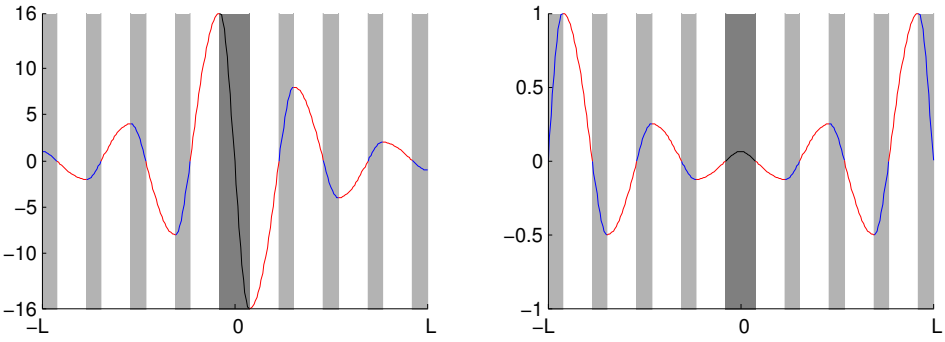

Figure 5.5: Field profile for the amplified state S^+ (left) and attenuated state S^- (right).

Besides the *amplified state*, there also exists an independent solution of the Helmholtz equation for the same frequendy ω_d. Being the critical point of (5.9), means that S^+ satisfies the Helmholtz equation with boundary condition in (5.10). Since $S^+(L) \neq 0$, there exist an independent solution S^- of the Helmholtz equation for the same frequency ω_d, with

$$S^-(L) = 0, \partial_z S^-(L) \neq 0.$$

Due to the symmetry of the structure, this solution is necessarily symmetric. Consequently $\partial_z S^-(0) = 0$ and we have that S^- is the solution of

$$\omega_d^2 = \min_{E_0} \left\{ \int_0^L (\partial_z E_0)^2 dz \mid \int_0^L n^2 E_0^2 dz = 1,\ E_0(L) = 0 \right\}.$$

We call this the *attenuated state* because this solution is decaying from the exterior of the grating at the sides towards the cavity in the middle, see Figure 5.5 for the field profile. Also for this state there is *energy equipartition*, and as above, we can define a normalized *energy content* but now normalized with respect to the derivative at the boundary

$$\mathcal{E}^- = \frac{\int_{-L}^{L} n^2 (S^-)^2 dz}{\frac{1}{\omega_d^2} \partial_z S^-(L)^2}.$$

Remark 1
These states S^+ and S^- state are real valued, hence they are non traveling solutions, and have vanishing *Poynting* quantity. Observe that we normalise the energy content for the attenuated state with the nonvanishing value of the derivative at the boundary. Actually, both states can also be expressed in terms of the the magnetic field instead of the electric field as above. Especially it is nice to combine the formulation of the (electric skew symmetric) amplified state in terms of the electric field, and the attenuated state by the magnetic field; this state is then magnetic skew symmetric also, and the variational characterization, now for the magnetic field Φ^-, is

$$\omega_d^2 = \min_{H_0} \left\{ \int_0^L (\frac{1}{n} \partial_z H_0)^2 dz \mid \int_0^L H_0^2 dz = 1,\ H_0(0) = 0 \right\}.$$

Note that since $\Phi^-(L) \neq 0$, the energy content is now given by

$$\mathcal{E}^- = \frac{\int_{-L}^{L} (\Phi^-)^2 dz}{\Phi^-(L)^2}$$

Remark 2
From energy equipartition it follows that we can define the energy content of the two states in an equivalent uniform way as the quotient of integrated local total energy density and the total energy at the boundary:

$$\mathcal{E} = \frac{\frac{1}{2} \int_{-L}^{L} \frac{1}{\omega_d^2} E_z^2 + n^2 E^2 dz}{\frac{1}{\omega_d^2} E_z(L)^2 + n^2 E(L)^2} \equiv \frac{\frac{1}{2} \int_{-L}^{L} H^2 + n^2 E^2 dz}{H(L)^2 + n^2 E(L)^2}.$$

This emphasizes the fact that the quotient relates properties of the internal fields to properties at its boundary where the structure interacts with the exterior.

Using these states as the properties of the defect grating, below we will model the unloading phase and later also the loading phase of phenomena observed in the previous Section. In the modeling, we will use an energy argument based on the energy conservation law.

5.3.2 Leaky modes

Above we formulated the two independent states inside the structure. Standing waves in the exterior should be added to obtain the state on the whole real line. We will now describe the leaky modes on the whole real line, for the amplified state with the electric field S^+, for the attenuated state with the magnetic field Φ^-. In the exterior, outward travelling waves should match with the decaying state in the interior.

Leaky mode for the amplified state

For the amplified state, if we denote the amplitude of the state in the interior by $A(t)$, the expression reads

$$E_{int}(z,t) = A(t)S^+(z)\cos(\omega_d t). \tag{5.14}$$

This interior behaviour should be connected to a travelling outgoing wave in the exterior. At the right exterior this is

$$\begin{aligned} E_{out}(z,t) &= A(t-n_0\tilde{z})S^+(L)\cos(k_o\tilde{z}-\omega_d t),\\ H_{out}(z,t) &= -n_0A(t-n_0\tilde{z})S^+(L)\cos(k_o\tilde{z}-\omega_d t), \end{aligned}$$

where $\tilde{z} = z - L$. For the left exterior we have also a travelling wave with amplitude $A(t)$, but due to the symmetry of the structure we will leave that out for simplicity.

Remark 3
This approximation of the fields solution in the interior of the defect grating is valid provided that $A(t)$ is slowly varying. This statement can be seen by substituting them to the wave equation (5.1) which gives the expression

$$\mathcal{L}(E_{int}) = n^2(z)S^+(z)\left(\partial_t^2 A - 2\partial_t A\sin(\omega_d t)\right),$$

for the residue. As a consequence, the ansatz (5.14) will be valid provided $|\partial_t A|$ is small. According to the result of the FETD calculation we can claim that this is true for the unloading phase.

The decay of the amplitude describes the leaky character of the mode. To find the decay rate, we use energy conservation which holds for all solutions of the 1-D Maxwell's equations

$$\partial_t \mathcal{W} - \partial_z \mathcal{P} = 0, \tag{5.15}$$

where $\mathcal{W} = \frac{1}{2}\left(n^2 E^2 + H^2\right)$ is the *electromagnetic energy density*, the sum of the electric energy density and magnetic energy density, and $\mathcal{P} = EH$ is the *power density*, also know as the Poynting quantity. The energy over the whole grating is obtained by integrating the electromagnetic energy density over the interval $[-L, L]$. Since the the electric and magnetic energy density are equal, we have the energy over the whole grating

$$\mathcal{E}_{int} = \int_{-L}^{L} \mathcal{W}_I dz = \mathcal{E}^+ (S^+(L))^2 A(t)^2 \cos^2(\omega_d t), \tag{5.16}$$

and assuming that $A(t)$ is constant over one period, then the time average is given by

$$\overline{\mathcal{E}_{int}} = \frac{1}{2}\mathcal{E}^+ S^+(L)^2 A(t)^2,$$

with $\mathcal{E}^+$ as given in (5.13). The exterior solution corresponds to an outflux

$$E_{out} H_{out} \,|_{-L}^{L} = -2n_0 S^+(L)^2 A(t)^2 \cos^2(\omega_d t),$$

with the time average

$$\overline{E_{out} H_{out}} \,|_{-L}^{L} = -n_0 S^+(L)^2 A(t)^2.$$

So the dynamics of the time averaged energy are, according to the conservation law (5.15)

$$\partial_t \{\overline{\mathcal{E}_{int}}\} = -n_0 S^+(L)^2 A(t)^2 \tag{5.17}$$

$$= -\frac{2n_0}{\mathcal{E}^+}\overline{\mathcal{E}_{int}}. \tag{5.18}$$

This differential equation has a solution which describes the exponential decay of the energy

$$\overline{\mathcal{E}_{int}}(t) = \overline{\mathcal{E}_{int}}(0) e^{-2\alpha^+ t}, \text{ with } \alpha^+ = \frac{n_0}{\mathcal{E}^+}. \tag{5.19}$$

The dynamic equation for the amplitude $A(t)$ can be derived further from (5.17)

$$\partial_t A(t) = -\frac{n_0}{\mathcal{E}^+} A(t),$$

and this shows that the amplitude $A(t)$ decays with a rate half of the decay rate of the energy, or

$$A(t) = A(0)e^{-\alpha^+ t}.$$

Leaky mode for the attenuated state

In a similar manner as for the amplified state, now for the leaky mode based on the magnetic attenuated state, we write the solution for the exterior

$$H_{int}(z,t) = B(t)\Phi^-(z)\sin(\omega_d t),$$

that is connected to travelling outgoing waves in the exterior at the right

$$\begin{aligned} E_{out}(z,t) &= -\frac{1}{n_0} B(t - n_0\tilde{z})\Phi^-(L)\sin(k_o\tilde{z} - \omega_d t), \\ H_{out}(z,t) &= B(t - n_0\tilde{z})\Phi^-(L)\sin(k_o\tilde{z} - \omega_d t). \end{aligned}$$

Because of the energy equipartition, the energy in the interior is

$$\mathcal{E}_{int} = \int_{-L}^{L} \mathcal{W}_I dz = \mathcal{E}^-\Phi^-(L)^2 B(t)^2 \sin^2(\omega_d t),$$

and the solution for the exterior allows outflux equal to

$$E_{out}H_{out}\,|_{-L}^{L} = -\frac{2}{n_0}\Phi^-(L)^2 B(t)^2 \sin^2(\omega_d t).$$

Hence the dynamics of the time averaged energy described from the conservation law (5.15) read

$$\partial_t\{\overline{\mathcal{E}_{int}}\} = -\frac{2}{n_0}\Phi^-(L)^2 B(t)^2 \tag{5.20}$$

$$= -\frac{2}{n_0\mathcal{E}^-}\overline{\mathcal{E}_{int}}. \tag{5.21}$$

This differential equation has a solution which describes the exponential decay of the energy

$$\overline{\mathcal{E}_{int}}(t) = \overline{\mathcal{E}_{int}}(0)e^{-2\alpha^- t}, \text{ with } \alpha^- = \frac{1}{n_0 \mathcal{E}^-} \tag{5.22}$$

The dynamic equation for the amplitude $B(t)$ can be derived further from (5.20)

$$\partial_t B(t) = -\frac{1}{n_0 \mathcal{E}^-} B(t),$$

and this shows that the amplitude $B(t)$ decays with a rate half of the decay rate of the energy, or

$$B(t) = B(0)e^{-\alpha^- t}.$$

5.4 Unloading and pulse loading

The leaky modes describe the unloading of the structure when there is a pure state initially, either the attenuated or the amplified state. When initially there is a superposition, the decay is determined by the averaged decay, weighted with the initial amplitudes. For example, for a combination of the amplified and the attenuated state as follows

$$\begin{aligned} E_{int}(z,t) &= \big[A(t)S^+(z) + B(t)S^-(z)\big]\cos(\omega_d t), \\ H_{int}(z,t) &= \big[A(t)\Phi^+(z) + B(t)\Phi^-(z)\big]\sin(\omega_d t), \end{aligned}$$

with $\Phi^\pm = \frac{1}{\omega_d}\partial_z S^\pm$, the dynamics of the time averaged energy, after following procedures as in the previous Section, is given by

$$\overline{\mathcal{E}_{int}}(t) = A(0)^2 e^{-2\alpha^+ t} + B(0)^2 e^{-2\alpha^- t}.$$

From this result it is seen that the slowest decaying mode will of course dominate the time asymptotic decay process; practically this will be the amplified state, and the decay can effectively be described taking into account only this single mode. See Figure 5.6 where the exact decay and a one-mode approximation are compared.

To model the loading of a structure by a pulse with a narrow spectrum around the defect frequency is a bit more involved. We reason as follows. Take the Lorentzian function with the characteristic width α

$$\widehat{L}(\omega) = \frac{1}{1 - i\frac{\omega - \omega_d}{\alpha}},$$

as a model for the spectral response around the defect frequency of the whole defect grating. This is motivated by the exponential decay behaviour in the unloading phase, which means that in the frequency domain it is represented by a Lorentzian function. For the parameter α, we take the same value as obtained for the unloading phase, i.e. the value from expression 5.19. For $F(t) = f(t)e^{-i\omega_d t}$ as the incoming signal of the pulse at $z = -L$, with $f(t)$ the envelope, the signal at the right grating end is

$$E(L,t) = \mathrm{Re}\left\{\int_{-\infty}^{\infty} \hat{F}(\omega)\widehat{L}(\omega)e^{-i\omega t}d\omega\right\},$$

or

$$E(L,t) = \frac{1}{2\pi}\,\mathrm{Re}\left\{\int_{-\infty}^{\infty} F(\tau)L(t-\tau)d\tau\right\}. \tag{5.23}$$

Since the Fourier transform of $\widehat{L}(\omega)$ is given by $L(t) = 2\alpha\pi e^{-\alpha t}e^{-i\omega_d t}H_v(t)$ where $H_v(t)$ is the Heaviside function, we can further evaluate the signal

$$E(L,t) = \alpha e^{-\alpha t}\cos(\omega_d t)\int_{-\infty}^{t} f(\tau)e^{\alpha\tau}d\tau.$$

Since $\alpha << 1$, we can approximate the integral as

$$E(L,t) \approx \alpha e^{-\alpha t}\cos(\omega_d t)\int_{-\infty}^{t} f(\tau)d\tau.$$

This formula for the signal gives a nice interpretation as follows. For small t the loading is dominated only by the pulse via the term $\alpha\int_{-\infty}^{t} f(\tau)d\tau$, and for large t, $e^{-\alpha t}$ shows the already known decaying behaviour of the unloading phase. For the example presented in Section 5.2.4, where we take the incoming spectrum of the pulse

$$\hat{F}(\omega) = e^{-(\omega-\omega_d)^2/\sigma^2},$$

we can calculate analytically the loading signal, and it is given by

$$E(L,t) = \left\{\alpha\pi e^{-\alpha T}\cdot\left[1+\mathrm{erf}(\frac{\sigma}{2}T)\right]\right\}\cos(\omega_d T), \tag{5.24}$$

where the shift of time $T = t - t_0$ is such that at $t = 0$ the whole pulse is at the left of the grating. From the expression above we can easily get the asymptotic behaviour of the signal for large and small t. For $t \gg 1$ we have that $[1 + \mathrm{erf}(\frac{\sigma}{2}T)] \to 2$ hence $E(L,t) \approx 2\alpha\pi e^{-\alpha T}\cos(\omega_d T)$, showing the already known exponential decay behaviour. For small t, $E(L,t) \approx \alpha\pi[1 + \mathrm{erf}(\frac{\sigma}{2}T)]\cos(\omega_d T)$. See Figure 5.7 for the comparison of this approximation with the FETD calculation.

5.5 Comparison of the low dimensional model with the FETD calculation

In this Section, we will compare results of the low dimensional model with the FETD calculation. First let us consider the unloading phase, for which we assume that initially there is light inside the defect grating, and nothing outside. More specifically the FETD scheme is used to solve the wave equation (5.1), with initial conditions

$$E(z,0) = \begin{cases} S^+(z) & \text{for} -L \le z \le L \\ 0 & \text{elsewhere} \end{cases}, \ \partial_t E(z,0) = 0.$$

In Figure 5.6 we show the result of the FETD calculation for the signal at the edge of the defect layer $z = -D/2$, together with a plot of the result of the low dimensional model. We can see that it is in very good agreement,

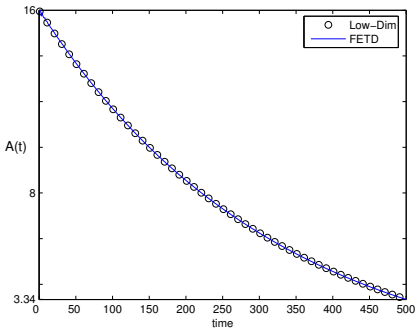

Figure 5.6: Result of the FETD calculation with the low dimensional model for the unloading phase, for $S^+(z)$ as the initial condition inside the grating. We ommited the harmonic oscillation with frequency ω_d from the FETD calculation and plotted together with $A(t)$ from the low dimensional model.

S^+ decays exponentially with decay rate α. Now for the loading phase, the function $E(L,t) \approx \alpha\pi[1+\mathrm{erf}(\frac{\sigma}{2}T)]\cos(\omega_d T)$ is the approximation of $E(L,t)$ for small t. To have the approximation at the defect edge $z = -D/2$ we have to multiply $E(L,t)$ with a certain number which represent the amplification at the defect layer. As described in [2], for N grating periods the *amplified* state has an amplification of $(-g(\omega_d))^N$, where $-g(\omega)$ is the

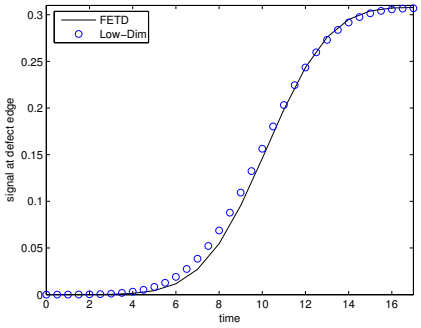

Figure 5.7: Result of the FETD calculation and of the low dimensional model, for the loading phase. We have omitted the harmonic oscillation with frequency ω_d from the FETD result and plotted together with $E(-D/2, t)$ from the low dimensional model.

amplification factor for one period of grating. Hence the signal at the defect edge is $E(-D/2, t) = (-g(\omega_d))^N \alpha\pi[1 + \mathrm{erf}(\frac{\sigma}{2}T)]\cos(\omega_d T)$, and we plot this function together with the signal from the FETD calculation in Figure 5.7. We can see that the agreement is good. For the complete loading and unloading signal at the defect edge $z = -D/2$, the FETD result is depicted in Figure 5.8 together with the result of the low dimensional model.

5.6 Conclusion

We considered pulse loading and unloading of a defect grating structure with a pulse that has its spectral components inside the band gap. We have solved the problem directly by using the Finite Element Time Domain (FETD) method. For representing the correct influx and outflux, the Finite Element Time Domain scheme is equipped with proper exact boundary conditions. The result shows that the remaining pulse inside the defect grating structure stays inside for times much longer than the width of the initial pulse.

Motivated by the result of the FETD calculation, we derived a low dimensional model to understand the important features of the loading phase and the unloading phase. Using this low dimensional model, we can

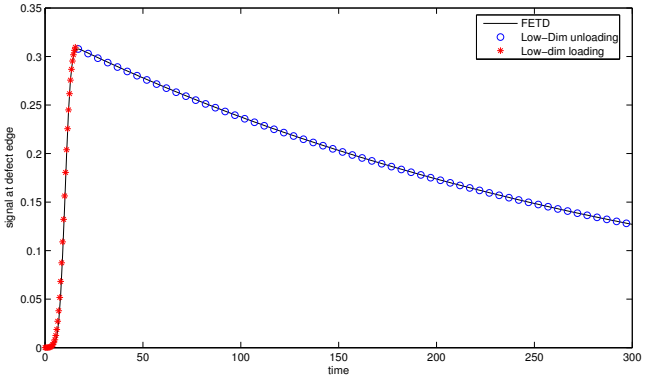

Figure 5.8: The complete loading and unloading signal at the defect edge $z = -D/2$ according to the FETD calculation and to the the low dimensional model. We have omitted the harmonic oscillation with frequency ω_d from the FETD calculation.

describe very simple, yet very accurately, the amount of light which penetrates the defect grating from a given influx pulse, and the decay rate of the unloading phase. The low dimensional model uses the two steady states of the defect grating, which are the basic fields that are used to describe the leaky modes. It is shown in Section 5.6, that the result of the low dimensional model is in very good agreement with the FETD calculation.

Acknowledgement
This research is supported by the KNAW (Royal Netherlands Academy of Arts and sciences) as part of Scientific Programme Indonesia-Netherlands, EPAM-Industrial Mathematics. The authors appreciate the fruitful discussions with M. Hammer.

Bibliography

[1] A. Sopaheluwakan and E. van Groesen, Calculation of pulse loading and radiative unloading of an optical defect grating structure, *Submitted to Photonics and Nanostructures*, 2006.

[2] E. van Groesen, A. Sopaheluwakan and Andonowati, Direct characterization of states and modes in defect grating structures, *Journal of Nonlinear Optical Physics and Materials* **13**, 155, 2004.

[3] E. van Groesen, A. Sopaheluwakan and Andonowati, in *Proceedings of the IEEE-LEOS Benelux Symposium*, 273, University of Twente, The Netherlands, 2003.

[4] S. D. Gedney, An unconditionally stable finite element time-domain solution of the vector wave equation, *IEEE Microwave and Guided Wave Letters* **5**, 332, 1995.

[5] V. F. Rodriguez-Esquerre, M. Koshiba and H. E. Hernandez-Figueroa, Finite-element time-domain analysis of 2-D photonic crystal resonant cavities, *IEEE Photonics Technology Letters* **16**, 816, 2004.

[6] N. Hirayama and Y. Sano, Fiber Bragg grating temperature sensor for practical use, *ISA Transactions* **39**, 169, 2000.

[7] M. G. Xu, J. L. Archambault, L. Reekie and J. P. Dakin, Discrimination between strain and temperature effects using dual-wavelength fibre grating sensors, *Electronics Letters* **30**, 1085, 1994.

[8] H. L. Lo, W. Jin, C. C. Chan, Y. Zhou and X. W. Wang, A fiber Bragg grating sensor for static and dynamic measurands, *Sensors and Actuators* **A 96**, 21, 2002.

[9] N. L. Dmitruk, O. I. Mayeva, S. V. Mamykin, O. B. Yastrubchak and M. Klopfleisch, Characterization and application of multilayer diffraction gratings as optochemical sensors, *Sensors and Actuators* **A 88**, 52, 2001.

[10] A. Suryanto, E. van Groesen, and M. Hammer, Finite element analysis of optical bistability in one-dimensional nonlinear photonic band gap structures with a defect, *Journal of Nonlinear Optical Physics and Materials* **12**, 187, 2003.

[11] P. Tran, Optical limiting and switching of short pulses by use of a nonlinear photonic bandgap structure with a defect, *Journal of the Optical Society of America* **B 14**, 2589, 1997.

[12] J. Jin. *The Finite Element Method in Electromagnetics*. Wiley-Interscience, 2002.

[13] Y. Liu and K. S. Chiang, Fiber-Bragg-Grating cavity sensor interrogated with a self-seeded Fabry−Perot laser diode, *IEEE Photonics Technology Letters*, **18**, 2153, 2006.

Chapter

6

Characterization and calculation of leaky modes in photonic crystal microcavities

Abstract[†]. We present a numerical study of a photonic crystal microcavity. Using Finite Element Method (FEM) as a calculation tool with Transparent Boundary Condition (TBC), plane waves and pulses are used to excite the resonant modes. For plane wave influx we can identify resonant modes by calculating the electric or magnetic energy contained in the photonic crystal microcavity over the whole band gap interval. Afterwards, using a pulse as influx, we can selectively excite resonant modes and calculate the quality factor by monitoring its decay. Alternatively, this process of unloading resonant modes can be viewed as (leaky) modes with complex valued frequency. We will characterize leaky modes variationally, and give an expression for the their quality factors in terms of the properties of the modes itself.

6.1 Introduction

Since the introduction in 1987 [1, 2], photonic crystals have attracted much attention. Photonic crystals are periodic dielectric structures that can inhibit an interval of frequency where no propagating field can exist. However, to exploit this phenomenon in a useful way, we must introduce defects in the structure. For example, if a series of rods are removed, the structure may act as a waveguides with low losses [3]. If a point defect is introduced in the structure, then localized resonant modes can exist. Such resonant modes are at the heart of photonic crystal devices, such as microcavities [4, 5], filters [6], etc. Important for applications is the so called quality

[†]This Chapter is to be submitted for publication.

factor (Q) of resonant modes. It is a measure for the confinement and field amplification of resonant modes. For example, for filter applications, modes with high Q value are needed because of their high selectivity.

Due to the absence of analytical solutions, numerical methods are required to solve the Maxwell equations. Finite Difference Time Domain (FDTD) calculations are commonly used with absorbing boundary condition or perfectly matched layer (PML) [7, 8, 9], or Finite Element Methods (FEM) with PML [5]. In this paper, we use FEM because the interface condition between two different materials are automatically satisfied in the formulation. The FEM scheme is used in combination with nonlocal Transparent Boundary Conditions (TBC) [10]. Such TBC's are formulated such that solutions in the computational domain can be connected smoothly to physical solutions in the exterior. Moreover, the FEM scheme plus TBC is more efficient than PMLs since no additional artificial computational domain is added, reducing the computational effort.

This paper is organized as follows. In Section 6.2 we start by describing briefly the finite element method and the transparent boundary condition used in this paper. In Section 6.3 we study the response of a photonic crystal microcavity under a plane wave influx. Then in Section 6.4 we use pulses as influx, to selectively excite resonant modes and to calculate the quality factor by monitoring its energy decay. In Section 6.5 we present the variational characterization of leaky modes (a solution of the Maxwell equations with complex valued frequency), and calculate their quality factor Q. In Section 6.6 we present integral expression to that describes the quality factor.

6.2 Computational approach

In this paper, we consider a photonic crystal microcavity that consists of 5×5 GaAs rods with refractive index $n_r = 3.4$, as shown in Figure 6.1. The rods have radius $0.2a$ where a is the lattice spacing. The cavity is formed by a single defect rod in the center of the photonic crystal , with radius $0.6a$.

We consider only TE polarization, where the electric field and magnetic field are $\mathbf{E} = (0, E_y, 0)$ and $\mathbf{H} = (H_x, 0, H_z)$. Throughout this paper we assume that the dimensions (scales) are normalized such that the speed of light in vacuum is equal to unity. For TE polarization we can

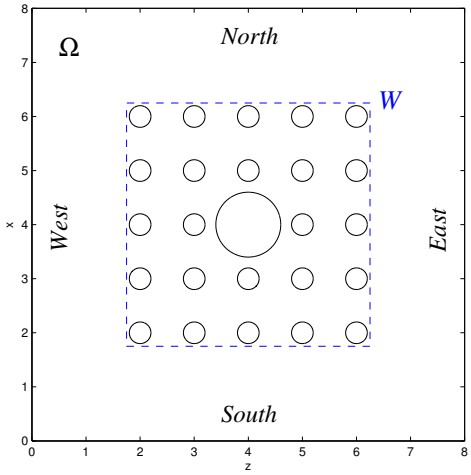

Figure 6.1: Plot of the computational domain.

reduce Maxwell equations into one wave equation for the component E_y only. Taking $e^{-i\omega t}$ as the time dependence for the fields, and writing $E_y = u(x,z)e^{-i\omega t}$, the wave equation simplifies to the Helmholtz equation

$$\Delta u + \omega^2 n^2(x,z)u = 0. \tag{6.1}$$

For the method of computation, we use a two dimensional FEM scheme with linear basis elements to solve the Helmholtz equation. For problems in integrated optics where scattering of the incoming light by the optical device towards the boundary of the computational domain is always present, the use of proper boundary conditions on the boundary of the computational domain is essential in obtaining the correct optical response from the structure. Boundary conditions have to represent the optical effect of the exterior of the computational domain, and take that into account in its formulation. Throughout this paper, we will assume that the photonic crystal microcavity investigated is embedded in a computational domain with uniform exterior. We use the Transparent Influx Boundary Condition formulation outlined in [10].

To arrive at the numerical scheme, we use the standard approach as

follows. Consider the following functional

$$\begin{aligned} \mathcal{K}(u) &= \iint_{\Omega} \left[(\nabla u)^2 - \omega^2 n(x,z)^2 u^2 \right] dxdz \\ &- \int_{\partial\Omega} \left[D^+(u)u + D^+(u^{in})u - D^-(u^{in})u \right] dl, \end{aligned} \tag{6.2}$$

where $D^{\pm}(u)$ is the Dirichlet to Neumann (DtN) operator with outgoing $(+)$ or incoming $(-)$ Sommerfeld boundary condition. Terms with $D^{\pm}(u^{in})$ take care of the correct treatment of a given influx u^{in} on the boundary. It can be shown that critical points of the functional $\mathcal{K}(u)$ (requiring the variational derivative to vanish) corresponds to solving the Helmholtz equation (6.1) in Ω with the Transparent Influx Boundary Condition (TIBC)

$$\partial_n u - D^+(u) = D^-(u^{in}) - D^+(u^{in}) \quad \text{on} \quad \partial\Omega.$$

In the absence of an influx field on some side of the boundary, the TIBC reduces to the Transparent Boundary Condition (TBC) $\partial_n u - D^+(u) = 0$. For more details on the TIBC and its implementation with the FEM scheme, readers can consult the reference [10]. The numerical scheme is obtained by approximating $u(x,z)$ as an expansion of chosen basis functions. More precisely, if we take the simplest piecewise linear elements, we want to find the solution expressed as a linear combination of 'tent' basis function $\{\phi_i(x,z)\}_{i=1}^N$

$$u(x,z) \approx \sum_{i=1}^{N} \tilde{u}_i \phi_i(x,z).$$

The basis functions ϕ_i are defined by piecewise linear interpolation between the nodal values $\phi_i(x_j, z_k)$, with the property

$$\phi_i(x_j, z_k) = \delta_{i,j,k}, \quad i = 1, .., N$$

where $\delta_{i,j,k}$ is the Kronecker delta and N is the number of nodal points. For the interior of Ω, the entries of the finite element stiffness (S) and mass (M) matrices are evaluated as follows

$$\mathrm{S}_{i,j} = \iint_{\Omega} \nabla\phi_i \nabla\phi_j ds \quad \text{and} \quad \mathrm{M}_{i,j} = \iint_{\Omega} n^2(x,z)\phi_i\phi_j ds.$$

6.3 Plane wave excitation

In this section, the response of the photonic crystal microcavity to a plane wave influx will be presented. A plane wave with unit amplitude is influxed from the Western boundary of the computational domain. For 1D structures, for example a defect grating structure, we can easily indicate defect modes by identifying sharp peaks in the band gap in the transmission curve. However, for problems in higher dimensions, the incoming field

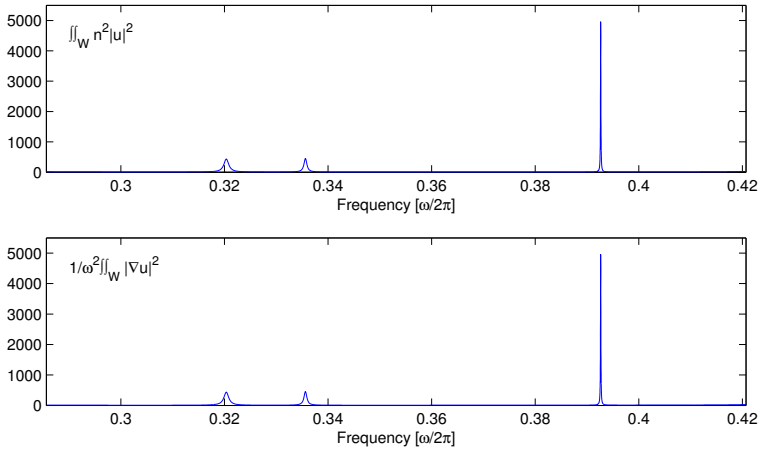

Figure 6.2: Energy versus frequency plot for normal incidence.

will scatter in arbitrary directions, hence it is difficult to define a proper definition for transmittance. In references [8, 9, 12], observation points are placed to monitor the response of the crystal to identify defect modes. A more robust approach is to calculate the electric and the magnetic energy contained in a region W covering the crystal, as illustrated in Figure 6.1. For TE polarization, the electric and magnetic energy content is defined as $\iint_W n^2|\mathbf{E}|^2 dxdz = \iint_W n^2|u|^2 dxdz$ and $\iint_W |\mathbf{H}|^2 dxdz = \frac{1}{\omega^2}\iint_W |\nabla u|^2 dxdz$ respectively. Considering frequencies only in the band gap range, we expect that there should be almost no energy that penetrates the crystal. Except if there are resonant modes, in which case there will be an energy build up around the cavity of the crystal. With this, it is possible to identify the resonant modes by looking at the electric and the magnetic energy content over the whole band gap interval. Using our own FEM based band

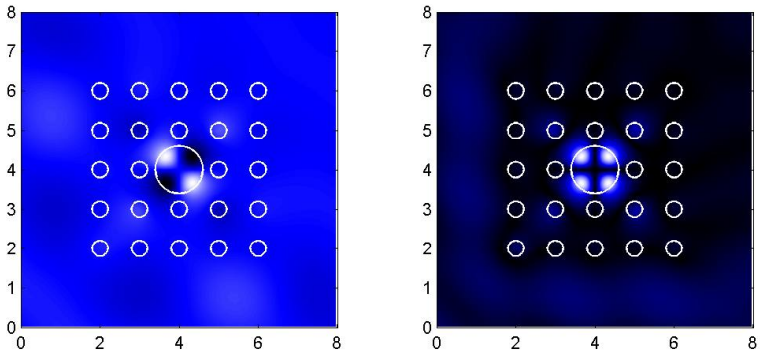

Figure 6.3: The electric field profile (real part), and the absolute value of the electric field of mode 1

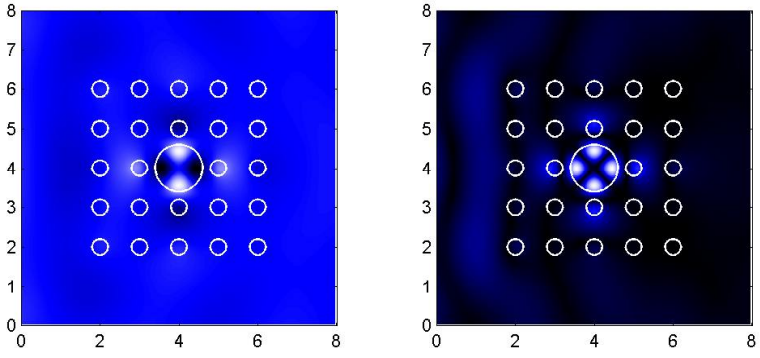

Figure 6.4: The electric field profile (real part), and the absolute value of the electric field of mode 2

structure solver, we found a band gap for the uniform crystal structure in the interval of $\omega = 2\pi[0.2856, 0.4207]$. We use the FEM scheme with TBC explained in Section 6.2, and discretize the computational domain in Figure 6.1 to a mesh structure with 781824 elements. Using these, a plane wave with unit amplitude is influxed to the structure. As reported in [4, 8, 11], we also found four resonant modes supported in this structure. First, for a plane wave with unit amplitude influxed from the Western boundary, the result is shown in Figure 6.2. We can identify three resonant modes from the sharp peaks in the energy versus frequency graph. The frequencies are $\omega_2/2\pi = 0.3201, \omega_3/2\pi = 0.3350$, and $\omega_4/2\pi = 0.3929$. We call these modes mode 2, mode 3 and mode 4 as indicated in the subscript indices in their frequency value. Additionally, a resonant mode with odd symmetry along the x axis is found when a plane wave under 45^o angle to the z axis is influxed. We call this mode 1, and it has frequency $\omega_1/2\pi = 0.2968$. The real part and the absolute value of the modes are shown in Figure 6.3-6.6.

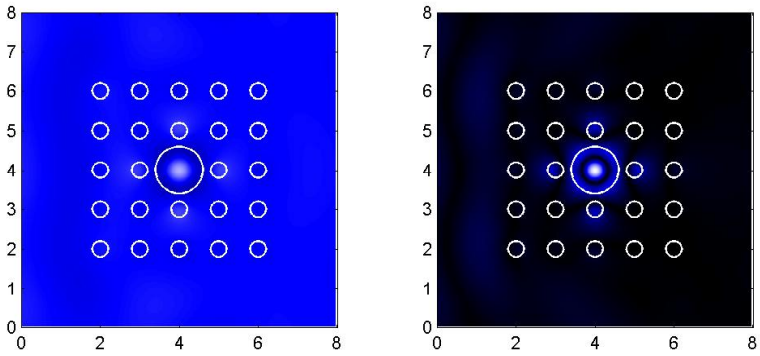

Figure 6.5: The electric field profile (real part), and the absolute value of the electric field of mode 3

6.4 Pulse excitation

In this Section, we use pulses to excite resonant modes. Choosing a certain spectral distribution of the incoming pulse, we can selectively excite any mode. So consider the following representation of a pulse, influxed

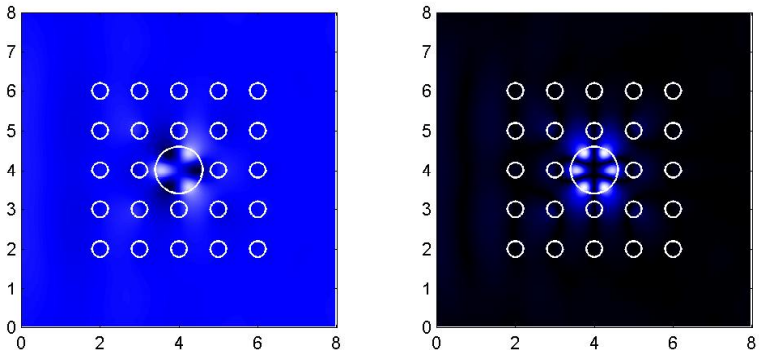

Figure 6.6: The electric field profile (real part), and the absolute value of the electric field of mode 4

horizontally from the Western boundary

$$E_y^{in}(x,z,t) = \int_{-\infty}^{\infty} \hat{f}(\omega) e^{i(\beta z - \omega t)} d\omega, \quad \text{where} \quad \beta = \omega n_0.$$

The function $\hat{f}(\omega)$ is the spectral distribution of the pulse. Here we take the following Gaussian function

$$\hat{f}(\omega) = e^{\frac{(\omega-\omega_0)^2}{\sigma^2}}$$

where ω_0 is the resonant frequency. The value of σ taken in the numerical calculation is such that only one resonant mode will be excited. Here we take $\sigma = 0.02$ for our calculation. To calculate the electric field E_y, we exploit the existing FEM plus TBC scheme. Let $u_\omega(x,y)$ be a solution for the Helmholtz equation (6.1) for incoming plane wave with amplitude one and frequency ω from the Western boundary. Then the overall electric field E_y is obtained by integrating all plane wave contribution with the weight function $\hat{f}(\omega)$

$$E_y(x,z,t) = \int_{-\infty}^{\infty} \hat{f}(\omega) u_\omega(x,z) e^{-i\omega t} d\omega.$$

We influx pulses to excite mode 2, 3 and 4, and we observe temporal the behaviour of the electric energy. We further calculated the electric energy

in domain W as a function of time, which shown that initially the crystal is loaded, after that the crystal unloads its energy into the exterior of the crystal. Figure 6.7 shows the calculation result.

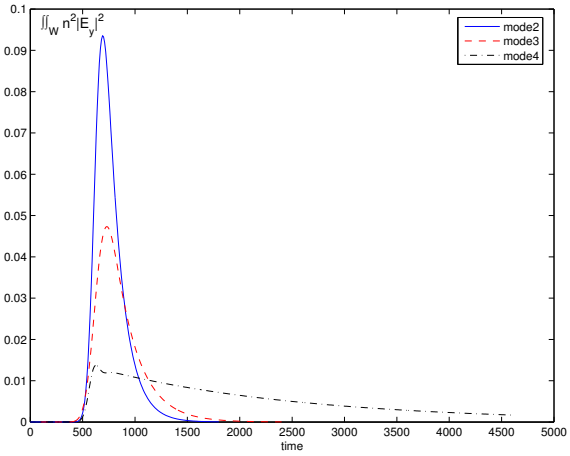

Figure 6.7: The electric energy content in the domain W as a function of time.

The decay of the resonant modes can be described by a quantity called the quality (Q) factor. The longer the mode 'stays' in the crystal, the higher its Q, and vice versa. Usually in the literature the quality factor of a certain resonant mode is determined in two ways. One way is to define the Q value using the frequency spectrum by

$$Q = \omega_0/\Delta\omega, \tag{6.3}$$

where ω_0 is the defect frequency and $\Delta\omega$ is the full width at half maximum of the peak frequency. Note that although we can use this definition with the quantities from Figure 6.2, we will not use this approach since it is not very accurate. A second way, is by observing the decay of the field or energy at some observation points [4, 7, 8]. In the following Section, we will use another approach to quantify the quality factor. We describe the decaying fields in the crystal as leaky modes, which are the solution of Helmholtz equation (6.1) with complex valued frequency, and the imaginary part of the frequency is then used as a measure of the quality.

6.5 Variational formulation for leaky modes

In the previous Section we have seen that the excited field in the crystal decays in time. Another way to view the phenomenon is by considering the decaying fields as leaky modes. Leaky modes are solutions of the Helmholtz equation (6.1) with boundary condition that describe only outgoing fields; as a consequence, the frequency will be complex valued. Expressing the frequency as $\omega = \omega_r + i\omega_i$, the imaginary part of ω will describe the decay in time. Below we will characterize leaky modes on a reduced domain shown in Figure 6.8. Depending on specific symmetry of the mode to

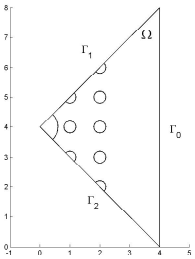

Figure 6.8: The reduced domain for the eigenvalue problem

be calculated, we will take homogeneous Neumann or Dirichlet boundary condition on the boundaries Γ_1 and Γ_2. On the boundary Γ_0 we will use an outgoing boundary condition to allow free flow to the exterior. The boundary condition on Γ_0 reads

$$\partial_n u - D^+(u) = 0. \tag{6.4}$$

Since the operator D^+ depends on ω itself, we arrive at an eigenvalue problem. We will describe some technical aspects in more detail. Neglecting the treatment of the (standard) Neumann or Dirichlet boundary condition on $\Gamma_{1,2}$, we consider the functional

$$\mathcal{L}(u) - \int_{\Gamma_0} D^+(u) u dx \tag{6.5}$$

with

$$\mathcal{L}(u) = \iint_{\Omega} \left[(\nabla u)^2 - \omega^2 n(x,z)^2 u^2 \right] dxdz.$$

Critical points produce the Helmholtz equation and the outflux condition (6.4). To describe the boundary term $\int_{\Gamma_0} D^+(u)udx$, we will use plane wave analysis in the exterior of the domain Ω. For a given Dirichlet value at Γ_0, say $u|_{\Gamma_0} = g(x) = \int_{-\infty}^{\infty} \hat{g}(k)e^{ikx}dk$, we can express the outgoing solution in the form of

$$u(x,z) = \int_{-\infty}^{\infty} \hat{g}(k)e^{i(kx+\beta(z-a))}dk \text{ where } \beta^2 + k^2 = \omega^2 n_0^2$$

Then

$$D^+(u) = \partial_n u = \partial_z u(x,a) = i\int_{-\infty}^{\infty} \sqrt{\omega^2 n_0^2 - k^2}\hat{g}(k)e^{ikx}dk, \tag{6.6}$$

and the boundary integral becomes (after applying Parceval's rule)

$$\int_{\Gamma_0} D^+(u)udx = 2\pi i \int_{-\infty}^{\infty} \sqrt{\omega^2 n_0^2 - k^2}\hat{g}^2(k)dk$$

We see that the boundary terms depend also on the eigenvalue being sought ω, in a nonlinear and a non-polynomial way. In all, we have a nonlinear eigenvalue problem for the eigenvalue ω. This can not be solved analytically, so we are going to solve this with FEM.

To our knowledge there is no method that is available to solve this type of nonlinear, non-polynomial eigenvalue problem directly. So to solve it we use a simple fixed point iteration scheme that will now be explained. To start with, we apply the standard FEM procedure and choose linear 'tent' functions as basis. The boundary integral will give a matrix which depends on ω, and we denote this by $\mathrm{B}(\omega)$. Then we arrive at a matrix eigenvalue system

$$(\mathrm{S} - \omega^2\mathrm{M} + \mathrm{B}(\omega))\vec{u} = 0 \tag{6.7}$$

where S and M are the stiffness and mass matrix. The eigenvalue problem (6.7) is solved by means of an iterative scheme. At the n-th iteration, the matrix $B(\omega)$ is set to be a constant matrix by substituting the value of ω obtained from the previous iteration. Then

$$(\tilde{\mathrm{S}} - \omega_n^2\mathrm{M})\vec{u} = 0 \text{ where } \tilde{\mathrm{S}} = \mathrm{S} + \mathrm{B}(\omega_{n-1}) \tag{6.8}$$

This iteration scheme is carried out until a certain stopping criterion is satisfied

$$\left|\frac{\omega_{n+1} - \omega_n}{\omega_n}\right| < \varepsilon.$$

As a initial value for the iteration, we use the resonant frequencies obtained from Section 6.3.

Characterization of mode 1 and 3

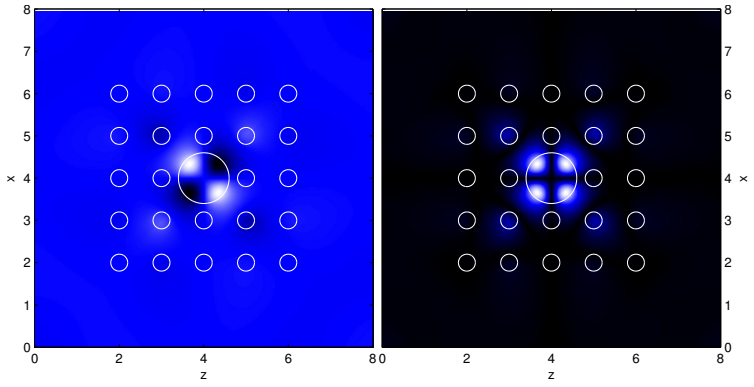

Figure 6.9: The electric field profile (real part), and the absolute value of the electric field of leaky mode 1

For these modes, both Γ_1 and Γ_2 are axis of symmetry, and hence $\partial_n u = 0$ at $\Gamma_{1,2}$. Without restrictions on the computing functions, these boundary conditions arise 'naturally' from the functional (6.5). The numerical experiment is carried out with 199616 elements and $\varepsilon = 1e-5$, and convergence of the iteration scheme is achieved after no more than 15 iterations. We obtained the leaky mode frequency for mode 1 $\omega_1/2\pi = 0.2968 - 2.2244e-4i$ and for mode 3 $\omega_3/2\pi = 0.3350 - 3.6920e-4i$. We show the profile of the field and its absolute in Figure 6.9 and 6.10.

Characterization of mode 2

For the characterization of mode 2, the boundaries $\Gamma_{1,2}$ are zero level sets. Restricting to functions vanishing at $\Gamma_{1,2}$ in (6.5) produces the correct formulation. Using the same procedure as above, we obtain the leaky mode frequency $\omega_2/2\pi = 0.3201 - 5.7204e-4$; the mode profile is shown in Figure 6.11.

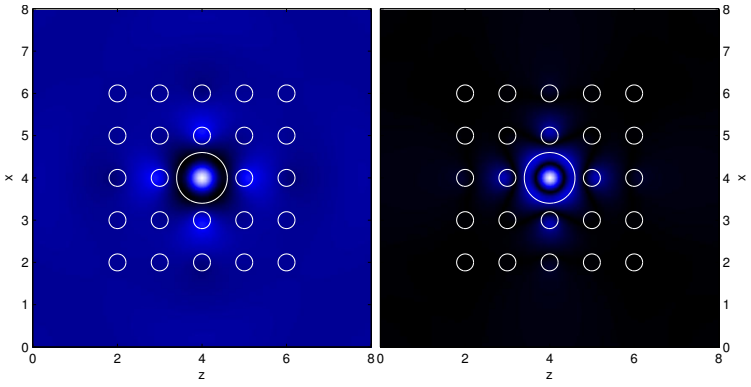

Figure 6.10: The electric field profile (real part), and the absolute value of the electric field of leaky mode 3

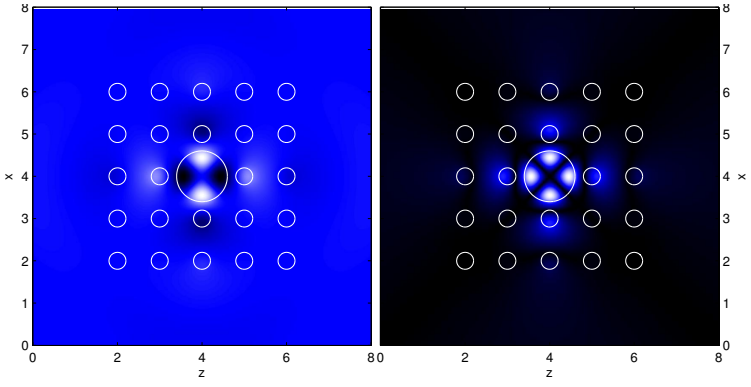

Figure 6.11: The electric field profile (real part), and the absolute value of the electric field of leaky mode 2.

Characterization of mode 4

For the characterization of mode 4, the boundary Γ_1 is a Dirichlet boundary, and Γ_2 is a Neumann boundary. Restricting to functions that vanishes at Γ_1 will produce the correct formulation from (6.5). Using the same procedure as above, we obtain the leaky mode frequency $\omega_2/2\pi = 0.3929 - 4.1147e-5$; the mode profile is shown in Figure 6.12. For this mode we observe the

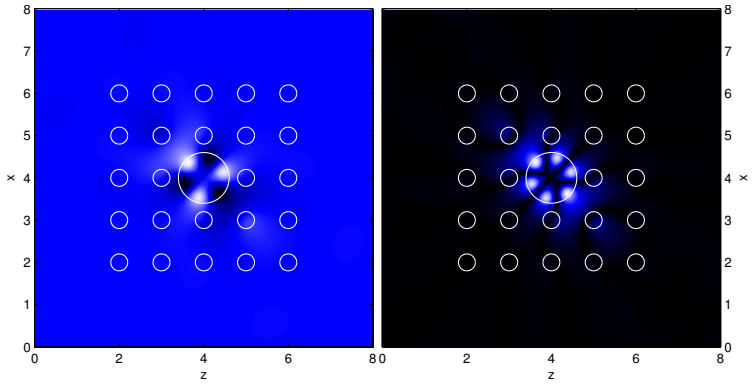

Figure 6.12: The electric field profile (real part), and the absolute value of the electric field of leaky mode 4

following fact. By interchanging the boundary condition, $u = 0$ on Γ_2 and the Neumann boundary condition on Γ_1, we actually have the same problem formulation, and the resulting eigenvalue should be the same, except now the field profile is the reflection with respect to the horizontal axis through the center of the crystal. This means that mode 4 is (doubly) degenerate.

Using these results, we can compare the leaky modes with the decaying resonant modes that were excited by the pulses from the previous Section. Note that the electric energy content of the modes in Ω

$$\iint_{\Omega} n^2 |\mathbf{E}|^2 dxdz = \iint_{\Omega} n^2 |u|^2 dxdz e^{2\omega_i t}$$

decays exponentially with factor $2\omega_i$. With the values of ω_i obtained from the characterization, we plotted $g(t) = E_0 e^{2\omega_i (t-t_0)}$ together with the electric energy plot in Figure 6.7 and it is shown in Figure 6.13. The constant

E_0 and t_0 were chosen such that at $t = t_0$, $g(t_0)$ coincides with the value of the electric energy.

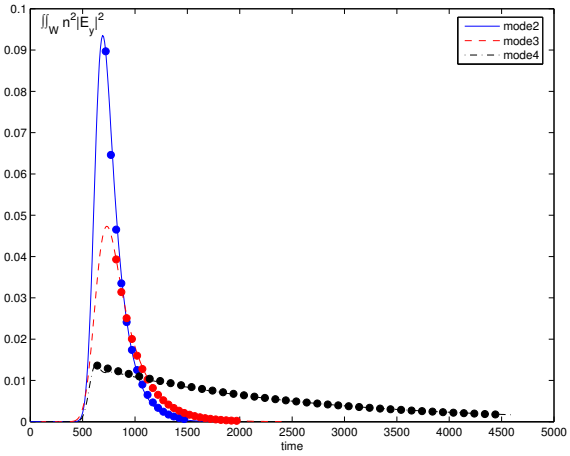

Figure 6.13: Comparison of the decay of the resonant modes from Section 6.4 (the solid, dash and dash-dot curves) and from the leaky mode characterization (the round, cross and diamond marker symbols).

6.6 Calculating the quality factor of leaky modes

Let $u(x, z)$ be a leaky mode characterized in the previous Section with frequency $\omega = \omega_r + i\omega_i$. Then as explained in the previous section, we observed that the electric energy content in Ω decays exponentially with factor $2\omega_i$. In references [8, 7, 12] it is stated the quality factor Q of a mode determines the decay of the energy in the form of $e^{-\frac{\omega_0}{Q}t}$, with ω_0 is the (real) resonance frequency. Using this definition for Q, it is straightforward to find Q as

$$Q = -\frac{\omega_r}{2\omega_i}. \tag{6.9}$$

which can then be used as a convenient definition. Using this definition, we find the Q values of the modes to be $667, 279, 453$ and 4774 for modes 1-4 respectively.

We can verify the accuracy of the results by observing the following fact for solutions of the Helmholtz equation (6.1). We multiply the equation with $\bar{u}$ and integrate over the domain Ω. Then after partial integrating the Laplacian term, and separating real and imaginary part, we will arrive at the following identity

$$\mathrm{Re}(\omega^2) = \frac{\iint\limits_{\Omega} |\nabla u|^2 - \int\limits_{\partial\Omega} \mathrm{Re}(\overline{u}\partial_n u)}{\iint\limits_{\Omega} n^2(x,z)|u|^2} \tag{6.10}$$

$$\mathrm{Im}(\omega^2) = \frac{-\int\limits_{\partial\Omega} \mathrm{Im}(\overline{u}\partial_n u)}{\iint\limits_{\Omega} n^2(x,z)|u|^2}. \tag{6.11}$$

Observe that these quotient expresses the real and imaginary part of the frequency in terms of the mode. This expression is useful to verify whether the calculation for the real and imaginary part of the frequency is accurate. If the calculation is accurate enough, then the above expression should hold. In our calculation we used this fact and the result satisfies these identities.

We can further combine (6.9) and (6.11) to arrive at the following expression

$$Q = \frac{\omega_r^2 \iint\limits_{\Omega} n^2(x,z)|u|^2}{\int\limits_{\partial\Omega} \mathrm{Im}(\overline{u}\partial_n u)}. \tag{6.12}$$

From this quotient we see that the quality factor is related to the mode, and it completely determines its value.

6.7 Conclusion

To conclude, we have presented a numerical study of photonic crystal microcavities. Using FEM with TBC as a calculation tool, resonant modes can effectively be excited by means of plane wave influxes. Using a pulse influx, modes can be excited selectively, and the decay of energy was monitored. This decaying process was alternatively seen as a leaky mode with complex valued frequency. Variational characterization for the leaky modes were given, where the imaginary part of the frequency leads immediately to the quality factor of the modes.

A final remark concerns the quality factor, observe that by defining Q as related to the energy, so by (6.9), this factor is completely determined by the expressions (6.12). That is to say, depend only on the leaky mode. In contrast, the definition (6.3) uses the full width at half maximum of the peak frequency, and hence depends on the crystal properties in a full neighborhood of the peak frequency. If the resonance would be described by a Lorentzian shape, these two definitions agree. Stated differently, for Lorentzian resonances, the quality factor can be estimated with (6.3) from a transmission plot.

Acknowledgement

This research is supported by EPAM-Industrial Mathematics of KNAW (Royal Netherlands Academy of Arts and Sciences) as a part of Scientific Programme Indonesia-Netherlands. The authors thank R. Stoffer for fruitful discussions.

Bibliography

[1] E. Yalonovitch, Inhibited spontaneous emission in solid-state physics and electronics, *Physical Review Letters* **58**, 2059, 1987.

[2] S. John, Strong localization of photons in certain disordered dielectric superlattices, *Physical Review Letters* **58**, 2486, 1987.

[3] A. Mekis, J. C. Chen, I. Kurland, S. Fan, P. R. Villeneuve, and J. D. Joannopoulos, High Transmission through Sharp Bends in Photonic Crystal Waveguides, *Physical Review Letters* **77**, 3787, 1996.

[4] P. R. Villeneuve, S. Fan, and J. D. Joannopoulos, Microcavities in photonic crystals: Mode symmetry, tunability, and coupling efficiency, *Physical Review* **B 54**, 7837, 1996.

[5] J. K. Hwang, S. B. Hyun, H. Y. Ryu and Y. H. Lee, Resonant modes of two-dimensional photonic bandgap cavities determined by the finite-element method and by use of the anisotropic perfectly matched layer boundary condition, *Journal of the Optical Society of America* **B 15**, 2316, 1998.

[6] J. C. Chen, H. A. Haus, S. Fan, P. R. Villeneuve, and J. D. Joannopoulos, Optical filters from photonic band gap air bridges, *Journal of Lightwave Technology* **14**, 2575, 1996.

[7] H. Y. Ryu, J. K. Hwang and Y. H. Lee, The smallest possible whispering-gallery-like mode in the square lattice photonic-crystal slab single-defect cavity, *IEEE Journal of Quantum Electronics* **39**, 314, 2003.

[8] S. Guo and S. Albin, Numerical techniques for excitation and analysis of defect modes in photonic crystals, *Optics Express* **11**, 1080, 2003.

[9] K. B. Chung and S. H. Kim, Defect modes in a two-dimensional square-lattice photonic crystal, *Optics Communications* **209**, 229, 2002.

[10] J. B. Nicolau and E. van Groesen, Hybrid analytic-numeric method for light through a bounded planar dielectric structure, *Journal of Nonlinear Optical Physics and Materials* **14**, 161, 2005.

[11] J. M. Lopez-Alonzo, J. M. Rico-Garcia and J. Alda, Photonic crystal characterization by FDTD and principal component analysis, *Optics Express* **12**, 2176, 2004.

[12] T. Xu, S. Yang, S. V. Nari and H. E. Ruda, Confined modes in finite-size photonic crystals, *Physical Review* **B 72**, 045126, 2005.

Chapter 7

Conclusions and recommendations

We have presented a study on the characterization of localized states in one and two dimensional optical resonator structures. Below we conclude this thesis by extracting important findings and mention some possibilities for directly related future research.

An extremal characterization of the first band gap edges of one dimensional photonic crystals (gratings) has been presented. Using the formulation it is possible to handle gratings with step index variation, smooth index variation and also nonlinear gratings. In our approach we aim to obtain the band gap edges and fields simultaneously, so the extremal characterization (minimum or maximum) is in the form of an eigenvalue problem. We show that the extremum property is useful, that we can approximate, or give bounds to the band gap edges, by using a simple 'suitable' trial function with low degrees of freedom. The word 'suitable' here means that the trial function has only approximately to satisfy the Helmholtz equation and the boundary conditions. By using trial functions with higher degrees of freedom, a superposition of local basis 'tent' function (Finite Element Method), the accuracy of the band gap edges calculation increased. We have also extend the characterization to accommodate structures with nonlinear index. An extension of the extremal characterization of the band gap edges for photonic crystal structures with higher space dimensions would be interesting to investigate in the future.

When the grating is finite and the periodicity of the structure is broken by a defect layer, then localized states with frequency in the band gap may exist. Direct characterization of states and modes for symmetric defect grating structures has been presented. Defect states are defined

as non-propagating solutions of the Helmholtz equation. These states have been characterized by exploiting the use of an effective boundary condition, such that the problem of finding the frequency of the defect states reduces to solving the Helmholtz equation in defect layer with these boundary condition. The resulting problem is a nonlinear eigenvalue problem, since the frequency dependence appear in the boundary condition in a nonlinear and non-algebraic way. For the simple one dimensional system that has been considered, the defect frequency was found by solving a transcendental equation for the frequency. Defect modes, are defined as propagating, fully transmitted solutions of the Helmholtz equation for the defect grating structure. We have shown that a defect mode is infact a simple complex superposition of the defect modes. An investigation of the existence of defect states in non-symmetric structures, and for nonlinear structures, is a completely open, challenging topic for future research.

Further we considered a time dependent phenomenon for the symmetric defect grating structure, the more realistic scenario with time limited influx. We considered a pulse with spectral components inside the bandgap. We developed a Finite Element Time Domain (FETD) scheme to simulate the problem, where we used Finite Element Method to handle the space discretization and Newmark scheme for the time discretization. Essential for the numerical scheme is the use of exact time domain Transparent Influx Boundary Condition (TIBC). We showed that the defect grating is loaded in a relatively short time (proportional to the duration of the influx pulse), and the 'trapped' field stays inside the defect grating much longer. The loaded field then decays in time and unloads its energy toward the exterior of the structure. We have developed a low dimensional model for the loading and the unloading phenomenon, where we assumed that it is sufficient to consider only a single frequency component to describe the phenomenon. Using this model we are able to quantify the build up of the field during the loading phase and the decay of the field during the unloading phase in terms of the energy content of the field. This provides a direct relation with the quality factor (Q) of the decaying field. A further extension of the study would be by considering non-symmetric defect grating structures, or nonlinear defect grating structure, investigating switching behaviour between nonlinear defect states in time domain.

With the same ideas as for time domain defect grating structures, we studied a finite two dimensional photonic crystal with defect. The same as

for the one dimensional defect grating, for the two dimensional structure defect modes can also exist. We used a two dimensional Finite Element Method as calculation tool, equipped with Transparent Influx Boundary Condition (TIBC). We have characterized the leaky (defect) modes of the structure, and the use of the TIBC leads to a nonlinear eigenvalue problem. Prescribing symmetries in the structure, we reduce the computational domain and we obtain several modes. The nonlinear eigenvalue problem was solved by using a fixed point iteration scheme. Using the properties of the mode, we were able to describe the decay of the leaky modes as well as the quality factor (Q). A direct method to solve the nonlinear eigenvalue problem would be a very interesting topic for further research.

Summary

This thesis deals with the characterization of localized states of resonant optical structures. We restrict ourself to one and two dimensional photonic crystal structures.

A photonic crystal structure is an optical structure with a periodic arrangement of refractive indices. It is widely known that such structures may have a certain frequency range where the propagation of light is forbidden. The first topic in this thesis is about the simplest case of a photonic crystal structure, namely it is the infinite one dimensional grating. We have developed a variational characterization that gives directly the band gap edges of the first band gap. The numerical implementation of the characterization is done using the Finite Element Method (FEM). To illustrate the method, we study a grating that is build from two different materials. For this specific type of grating, explicit solutions are available for linear materials, and hence it is possible to compare results. The characterization of the band gap edges can also be used for grating structures with smooth index variation, or even for nonlinear index variations.

When we consider a finite grating structure of which the periodicity is broken by a defect layer, localized defect states may exist. The feature of these localized states is that their frequency lies inside the band gap, and that the field is largely enhanced or attenuated; a complex superposition of the two states provides the full transmission mode. For application purposes it is important to be able to identify the defect frequency. We have derived a direct characterization of the defect frequency and these localized states, without having to 'scan' the whole band gap range. The characterization exploits the use of a so-called effective boundary condition; the problem of

finding the defect frequency then becomes the problem to solve a nonlinear eigenvalue problem for the defect layer only.

Different from the usual time harmonic investigation of transmittance, we also studied time limited influx, in particular when a pulse with spectral components inside the bandgap is influxed to the defect grating structure. We developed a Finite Element Time Domain (FETD) scheme to solve this, where the use of exact time domain Transparent Influx Boundary Condition (TIBC) is essential. Two different phases can be identified in the process, namely a loading and an unloading phase. We have developed a low dimensional model for the loading and the unloading phenomenon, where we assumed that it is sufficient to consider only a single mode to describe the phenomenon. Using this model we are able to quantify the build up of the field during the loading phase and the decay of the field during the unloading phase in terms of the energy content of the field inside the structure. This provides a direct relation between the quality factor and the decaying field.

The above mentioned study on the time dependent phenomenon for the defect grating structure is extended to two dimensional photonic crystal structures. For the two dimensional photonic crystal structure resonant modes may also exist. We use a two dimensional Finite Element Method as calculation tool, equipped with Transparent Influx Boundary Condition (TIBC). We study pulses as influx, with the spectral components centered around each defect frequency. The excited modes decay in time and leak their energy towards the exterior. We modeled this decay with a leaky mode, a decaying solution of the Helmholtz equation with only one (complex valued) frequency component. We characterized the leaky modes of the structure; the use of the TIBC leads to a nonlinear (non-polynomial) eigenvalue problem. The nonlinear eigenvalue problem was solved by means of a fixed point iteration scheme. Using the properties of the mode, we are able to describe the decay of the leaky modes as well as the quality factor.

Samenvatting

Dit proefschrift houdt zich bezig met de karakterisering van gelokaliseerde toestanden van resonante optische structuren. Daarbij beperken we ons tot één- en tweedimensionale fotonische kristalstructuren.

Een fotonische kristalstructuur is een optische structuur met een regelmatige plaatsing van materialen met verschillende brekingsindex. Het is algemeen bekend dat dergelijke structuren een frequentieinterval (band gap) hebben waarvoor geen lichtvoortplanting kan plaatsvinden. Het eerste onderwerp in dit proefschrift behandelt een eenvoudig fotonische kristal, namelijk de oneindig lange eendimensionale grating. Wij presenteren een variationele karakterisering voor de randen van de eerste band-gap. De numerieke implementatie van de karakterisering is uitgevoerd met behulp van de Eindige Elementen Methode (EEM). Als illustratie bestuderen we een grating die bestaat uit twee lagen van verschillend materiaal. Voor dit type van gratings met lineaire materiaaleigenschappen is een expliciete oplossing beschikbaar waardoor het mogelijk is om de oplossingen te vergelijken. De karakterisering van de randen van de bandgap kan ook gebruikt worden voor structuren met een continu veranderende index, en zelfs voor niet-lineaire materialen.

Wanneer wij een eindige gratingstructuur beschouwen waarvan de periodiciteit gebroken wordt door een zogenaamde defectlaag, kan een gelokaliseerde defecttoestand ontstaan. De eigenschap van deze defecttoestanden is dat de frequentie ervan in de band-gap ligt, en dat het veld ervan sterk vergroot of sterk verkleind is. Het blijkt dat een complexe superpositie van die twee toestanden precies een volledig doorgelaten toestand (mode) oplevert. Voor verschillende toepassingen is het belangrijk om de defectfre-

quentie uit te kunnen rekenen. Wij hebben een directe karakterisering van de defectfrequentie en van de gelocaliseerde toestanden gevonden waardoor het niet meer nodig is om de hele band-gap te 'scannen'. De karakterisering maakt gebruik van zogenaamde effectieve randvoorwaarden; het probleem om de defectfrequentie te vinden wordt dan vervangen door het probleem om de oplossing van een niet-lineair eigenwaardeprobleem te vinden dat gedefinieerd is voor alleen maar de defectlaag.

Naast het gebruikelijke onderzoek van tijdharmonische signalen, is ook het geval van in de tijd beperkte influxsignalen bestudeerd, in het bijzonder influxsignalen waarvan de spectrale componenten binnen de band-gap liggen. We hebben een Tijd Domein Eindige Elementen (TDEE) schema ontwikkeld; het gebruik van exacte tijd domein Transparante Influx Rand-Voorwaarden (TTRV) is daarvan een belangrijk onderdeel. Twee verschillende fasen kunnen onderscheiden worden in het tijdsgedrag, met name de ladings- en de ontladings fase. We hebben een laagdimensionaal model ontwikkeld voor dit ladings- en ontladings gedrag; daartoe hebben we aangenomen dat het voldoende is ons te beperken tot een beschrijving met n mode. Met dit model kunnen we de opbouw van het veld tijdens de ladings fase, en het verval van het veld tijdens de ontladings fase kwantificeren met de energieinhoud van het veld in de structuur. Dit geeft een direkt verband tussen de kwaliteitsfactor en de afname van het veld.

De bovengenoemd studie van het tijdafhankelijk gedrag van een defectgrating is uitgebreid tot tweedimensionale fotonische kristal structuren. Ook voor tweedimensionale fotonische kristalstructuren kunnen resonante toestanden bestaan. Om de berekeningen uit te voeren gebruiken we een tweedimensionale Eindige Elementen Methode met Transparante Influx Rand- Voorwaarden (TTRV). Als influx bestuderen we pulssignalen waarvan de spectraalcomponenten in de omgeving van de defect frequencies liggen. De daardoor in de struktuur opgewekte toestand vervalt in de tijd door het wegstromen van energie uit de struktuur. Wij modeleren dit verval met een zogenaamde leaky mode, een in de tijd uitdovende oplossing van het Helmhotz vergelijking met n (complexwaardige) frequentie. Wij hebben deze leaky modes theoretisch gekarakterizeerd; het gebruik van de TTRV leidt dan tot een niet-lineair (niet-polynomiaal) eigenwaardeprobleem. Dit niet-lineaire eigenwaardeprobleem is opgelost met een vaste punt iteratieschema. De eigenschappen van deze leaky modes geven zowel het verval in de tijd alsook de kwaliteitsfactor.

Acknowledgements

This thesis is the result of a research project which was conducted at the research group Applied Analysis and Mathematical Physics (AAMP), University of Twente. Here I would like to express my sincere thanks to those who have contributed in accomplishing the research reported in this thesis. This thesis could not have been completed without their help and support, for which I am very grateful.

I am much indebted to my promotor and supervisor Brenny van Groesen, for the opportunity to conduct research in the AAMP group, as well as for his dedication in guiding me during the entire Ph.D. project. I also would like to thank the members of the graduation committee: Erik Fledderus, Hugo Hoekstra, Remco Stoffer, Andonowati, Yong Hee Lee and Klaus Boller, for their willingness to be in the graduation committee, as well as for the constructive suggestions and critical comments on this thesis.

I would like to acknowledge the funding of this research by the KNAW (Royal Dutch Academy of Arts and Sciences) under the programme of Extended Programme in Applied Mathematics-Industrial Mathematics of KNAW (Royal Dutch Academy of Arts and Sciences), which made this research possible.

The fruitful discussion during the bi-weekly "optics meeting" is very much appreciated. I am grateful to the staff members (and former) of the group: Stephan, Manfred (also for the many discussion on optics and suggestions for my work), Chris, Gerard, Frits and Debby for making my study in the group very enjoyable. Thanks to Jaqueline for the friendship and the many discussion on transparent boundary condition, without it Chapter 2 and 6 of this thesis would have not existed. I would like to

thank former members of the group, Agus Suryanto (for many discussion during the initial phase of my Ph.D.), Helena, Kiran, Hadi for the friendship and fun times during the Ph.D. period.

I also would like to thank Natanael to whom I went to discuss about general mathematics, and light everyday conversation about life in The Netherlands. I wish to express my thanks to my office mates: Vijaya Ambati, Christiaan Klaij (also for the TEXtemplate), Domokos, and Mikhail Tchesnokov, for the fun and 'serious' office hours. Also thanks to Davit, Pablo, Alyona, Maks, Fedderik, Arek, Joris, Vita, Lars, Sander, Tim, Ivan and Lie for the friendship. Thanks to Marielle and Diana for helping me with many administration stuffs.

I am very grateful to all member of Indonesian Student Association in Enschede whom I can not name one by one, which made my stay in Enschede enjoyable. Many thanks are due to my father and mother in Jakarta, and Papa Zamah and Mama Ully in Lampung, for their invaluable support and prayers. Also to De Tia and Aree in Groningen, and my brothers and sisters in Lampung for their support. Finally, my special gratitude is directed to my beloved wife Fitri for her love, patience, prayers, understanding and support. With you I will sail the next chapters of life ...

Enschede, November 10^{th}, 2006.

List of publications

- E van Groesen and A. Sopaheluwakan, Extremal characterization of bandgaps in nonlinear gratings, *Journal of Nonlinear Optical Physics and Materials* **12**, 135-148, 2003.
- E. van Groesen, A. Sopaheluwakan and Andonowati, Direct characterization of defect states and modes in defect grating structures, *Journal of Nonlinear Optical Physics and Materials* **13**, 155-173, 2004.
- E. van Groesen, A. Sopaheluwakan and Andonowati, Full transmission modes and steady states in defect gratings. In R.M. de Ridder, G. Altena, D.H. Geuzebroek and R. Dekker (Eds.), *Proceedings IEEE/LEOS Benelux Chapter Symposium, University of Twente, The Netherlands*, 273-276, 2003. ISBN 90-365-1190-x.
- J.B. Nicolau, A. Sopaheluwakan and E. van Groesen, On an application of a 2D transparent-influx boundary conditions for photonic crystals, in X. Letartre (Ed.), *Proceedings of the 13th International Workshop on Optical Waveguide Theory and Numerical Modeling, Grenoble, France*, 2005.
- A. Sopaheluwakan and E. van Groesen, A simple low-dimensional model and efficient FEM calculations to determine the quality of photonic crystal cavities, in A. Melloni (Ed.), *Proceedings of the 15th International Workshop on Optical Waveguide Theory and Numerical Modeling, Varese, Italy*, 2006.
- A. Sopaheluwakan and E. van Groesen, Calculation of pulse loading and radiative unloading of an optical defect grating structure, *submitted Photonics and Nanostructures*, 2006.
- A. Sopaheluwakan and E. van Groesen, Pulse loading and radiative unloading of and optical defect grating structure: low dimensional modeling and numerical simulations, *submitted Optics Communications*, 2006.

- A. Sopaheluwakan and E. van Groesen Characterization of resonant states in photonic crystal microcavities, *to be submitted for publication.*

About the author

Ardhasena Sopaheluwakan was born in Jakarta, Indonesia, on February 1st, 1976. After completing his secondary education at Sekolah Menengah Atas Negeri 3 (SMAN3) Bandung in 1994, he continued his study at the Bandung Institute of Technology (ITB), Indonesia, from which he obtained his bachelor's degree in Mathematics in 2000 on the subject of "Wave groups solutions of the Kadomtsev-Petviashvili equation" under the supervision of Prof. dr. Edy Soewono. Then he joined the Center of Mathematics (P4M-ITB) as a research staff, to work in a research consortium between ITB and oil and gas companies on Optimization on Gas and Oil Transmission and Distribution Pipeline Network (OPPINET).

In December 2001 he started to study at the Department of Applied Mathematics, University of Twente, The Netherlands, as a Master's student. After finishing his Master's thesis on "Defect states and defect modes of 1D Photonic Crystals" under the supervision of Prof. dr. Brenny van Groesen, he received his Master's degree in Engineering Mathematics in December 2003.

Afterwards, he started his Ph.D. research in the Applied Analysis and Mathematical Physics group, Department of Applied Mathematics, and was affiliated with MESA+ Institute for Nanotechnology. With supervision from his promotor Prof. dr. Brenny van Groesen, in December 2006 he finished his doctoral studies. The results of his Ph.D. research are presented in this thesis.